CD8 Receptor-Targeted Lentiviral Vectors –
an Approach for the *in vivo* Generation of
Chimeric Antigen Receptor
(CAR) T Cells

Dissertation von
Anett Pfeiffer, M. Sc.
aus Görlitz

Pfeiffer, Anett: CD8 Receptor-Targeted Lentiviral Vectors – an Approach for the *in vivo* Generation of Chimeric Antigen Receptor (CAR) T Cells

Darmstadt, Technische Universität Darmstadt

Jahr der Veröffentlichung der Dissertation auf TUprints: 2018

URN: urn:nbn:de:tuda-tuprints-77188

Tag der mündlichen Prüfung: 10.08.2018

Summary

Gene therapeutic applications have gained substantial significance in modern medicine, especially for the treatment of cancer diseases. Genetically engineered T cells that express a chimeric antigen receptor (CAR) have been shown to mediate impressive anti-tumoral efficacy in patients suffering from B cell malignancies. In 2017, the first CAR T cell product was approved in the United States (U.S.). However, cell selective gene delivery still represents a big hurdle, making *ex vivo* gene delivery indispensable that is accompanied by complex efforts and high costs due to the personalized treatment. Receptor-targeted lentiviral vectors mediate selective gene delivery into a certain cell type and represent a powerful tool for the *in vivo* gene transfer. This thesis investigates the *in vivo* generation of CAR T cells in small animal models using a CD8-targeted lentiviral vector (CD8-LV).

CD8-LV has been generated before by pseudotyping lentiviral vectors with modified Nipah virus glycoproteins displaying an anti-human CD8-targeting domain. In this thesis, selective *in vivo* reporter gene delivery into CD8$^+$ lymphocytes was demonstrated upon systemic administration of CD8-LV into mice engrafted with human peripheral blood mononuclear cells (PBMC). Thereby, reporter gene expression exclusively within the CD8$^+$ cells proved the highly selective targeting of CD8-LV. *In vitro* generation of CAR T cells upon transduction of PBMC with CD8-LV transferring a CD19-specific chimeric antigen receptor was shown, and functionality of these generated CAR T cells was demonstrated. They selectively expanded upon antigen stimulus and specifically killed CD19$^+$ target tumor cells *in vitro*. CD8-LV(CAR) administration into mice resulted in the *in vivo* generation of CAR T cells with remarkably high frequencies of CAR-positive cells. Higher frequencies of transgene-positive and CD8-positive cells compared to reporter gene transfer indicated selective CAR T cell expansion *in vivo*. Importantly, functionality of *in vivo* generated CAR T cells was demonstrated when CD19$^+$ target cells had been eliminated. Moreover, CD19$^+$ cells were identified as antigen stimulus triggering antigen-specific CAR T cell proliferation. Phenotype analysis of CAR T cells by surface marker analysis revealed the presence of diversely differentiated CAR T cells, which is highly preferable in terms of generating a pool of CAR T cells with various effector functions and proliferative capabilities. Furthermore, anti-tumoral efficacy was evaluated in xenograft mice engrafted with human tumor cells. Although tumor outgrowth was not prevented, these CAR T cells demonstrated killing activities against CD19$^+$ B cells and emigrated to various organs. Showing organ-specific subset distribution of diversely differentiated CAR T cells, highest levels of effector CAR T cells were observed at the tumor site.

This thesis highlights the potential of CD8-LV to genetically engineer CD8 T cells *in vivo*. Selective gene transfer and functionality of *in vivo* generated human CAR T cells represent encouraging data to build on for further investigations in translational research. Pursuing receptor-targeted LVs for clinical application as an alternative approach of CAR T cell generation opens up an attractive possibility to tremendously simplifying CAR T cell therapy. In conclusion, CD8-LV represents a promising tool for the *in vivo* CAR T cell generation with the potential to transform personalized CAR T cell therapy into a broad applicable treatment option.

Zusammenfassung

Gentherapeutische Anwendungen gewinnen zunehmend an Bedeutung in der modernen Medizin, im Besonderen auch in der Krebstherapie. Genetisch veränderte T-Zellen, die einen chimären Antigen-Rezeptor (CAR) exprimieren, haben beeindruckende anti-tumorale Wirksamkeit in Patienten gezeigt, die an B-Zell Erkrankungen litten. Dies führte 2017 zur Marktzulassung der ersten CAR-T-Zell-Therapie in den Vereinigten Staaten von Amerika. Eine der größten Herausforderungen der Gentherapie bleibt jedoch der zielgerichtete Gentransfer, sodass eine *ex vivo* Manipulation der Zellen noch immer unerlässlich ist. Diese personalisierte Behandlung ist mit hohem Aufwand und Kosten verbunden. Rezeptor-targetierte Vektoren vermitteln selektiven Gentransfer in einen bestimmten Zelltyp und könnten einen alternativen Ansatz zur derzeitigen Behandlung eröffnen. Diese Arbeit zeigt die *in vivo* Generierung von CAR-T-Zellen in Kleintiermodellen mittels eines CD8-targetierten lentiviralen Vektors (CD8-LV).

Der CD8-LV wurde bereits zuvor generiert, wobei der lentivirale Vektor mit modifizierten Glykoproteinen des Nipah Virus pseudotypisiert und eine Targeting-Domäne gegen den humanen CD8 Rezeptor präsentiert wird. In der vorliegenden Arbeit wurde zuerst der selektive Reportergentransfer in CD8$^+$ Zellen *in vivo* nachgewiesen. Dazu wurden humane Immunzellen in Mäuse transplantiert und der Vektor systemisch injiziert. Die Expression des Reportergens, ausschließlich in den Zielzellen, wies einen hoch selektiven Gentransfer nach. *In vitro* Studien zeigten die Generierung von CAR-T-Zellen mittels CD8-LV, der einen CD19-spezifischen CAR in CD8 T-Zellen transferierte. Des Weiteren wurden die Funktionalität der CAR-T-Zellen gezeigt, wie zum Beispiel die selektive Expansion nach Antigen-Stimulus und die spezifische Eliminierung von CD19$^+$ Tumorzellen. Nach Injektion von CD8-LV(CAR) konnte die *in vivo* Generierung von CAR-T-Zellen nachgewiesen werden, wobei ein bemerkenswert hoher Anteil der CD8 T-Zellen CAR-positive Zellen waren. Dabei war der prozentuale Anteil von transgen-exprimierenden Zellen sowie von CD8-positiven Zellen im Vergleich zum Reportergentransfer erhöht, was darauf hindeutete, dass eine selektive Expansion der CAR-T-Zellen stattgefunden hatte. Diese CAR-T-Zellen eliminierten CD19$^+$ Zellen, was darauf hindeutete, dass *in vivo* generierte CAR-T-Zellen funktional waren. Die Phänotypisierung anhand von Oberflächenmarkern zeigte die Generierung von CAR-T-Zellen mit unterschiedlichem Differenzierungsgrad. Dies ist gerade in Bezug auf die klinische Wirksamkeit von CAR-T-Zellen erwünscht, da unterschiedlich ausdifferenzierte CAR-T-Zellen einerseits wichtige Effektor Funktionen erfüllen als auch proliferatives Potential besitzen. Die anti-tumorale Wirksamkeit wurde in Mäusen überprüft, die humane Tumorzellen transplantiert bekamen. Obwohl das Tumorwachstum

nicht verhindert wurde, eliminierten die CAR-T-Zellen die CD19$^+$ B-Zellen und wanderten in verschiedene Organe aus. Dabei wurde eine Organ-spezifische Verteilung von Subtypen beobachtet, wobei der größte Anteil der Effektor CAR-T-Zellen beim Tumor gefunden wurde.

Diese Arbeit zeigt das Potential von CD8-LV CD8 T-Zellen *in vivo* genetisch zu verändern. Selektiver Gentransfer und funktionale *in vivo* modifizierte Zellen stellen vielversprechende Daten dar, auf denen in der translationalen Forschung weiter aufgebaut werden kann. Der Ansatz Rezeptor-targetierte lentivirale Vektoren in der klinischen Anwendung zu nutzen, bietet einen neuen Weg CAR-T-Zellen herzustellen und würde eine attraktive Möglichkeit eröffnen die CAR-T-Zell-Therapie wesentlich zu vereinfachen. Der CD8-LV stellt ein sehr vielversprechendes Instrument für die *in vivo* Herstellung von CAR-T-Zellen dar und birgt das Potential die personalisierte CAR-T-Zell-Therapie zu revolutionieren und eine breit anwendbare Therapiemöglichkeit zu schaffen.

Table of Content

1   Introduction

The immune system is the host's defense to protect from harmful pathogens. Distinguishing between foreign and self is a critical task to prevent diseases. Especially when it comes to cancer progression, the immune system fails to discriminate between healthy and malignant cells. Current state-of-the art cancer therapies aim in empowering the patient's immune system to fight cancer. So called cancer immunotherapies, using several different strategies, have led to dramatic clinical success in cancer patients whose conditions were considered untreatable. Among others, a promising therapy involves engineering the patient's own T cells to express a chimeric antigen receptor (CAR) sensitizing the immune system to recognize and eliminate cancer cells. Clinical success was so remarkable that the U.S. Food and Drug Administration (FDA) approved the first CAR T cell therapy in 2017, making this therapy available for patients in need.

1.1   T lymphocytes

T cells represent, besides B cells, major key players in the adaptive immune system mediating specific and long-lasting immune response against harmful pathogens, foreign agents as well as malignant, tumorigenic cells. Once selected for being unresponsive to self-antigens, naïve T cells circulate through secondary lymphoid organs and get activated upon antigen encounter which mediates an antigen-specific immune response (Chaplin, 2010; Murphy et al., 2012). Effector T cells are generated in large numbers to clear pathogens distributed anywhere in the periphery. Upon clearance, T cell numbers are reduced and long-lasting immunity is implemented by the surviving memory T cells (Kaech et al., 2002; Sallusto et al., 2004; Farber et al., 2014).

1.1.1   T cell receptor-mediated activation

To induce T cell activation, naïve T cells need to encounter their cognate antigen via T cell receptor (TCR)-mediated binding of the antigen that is presented by a major histocompatibility complex (MHC) on professional antigen-presenting cells (APCs) such as dendritic cells (DCs). The TCR consists of two chains, the alpha and beta chain, which are linked via disulfide bridges (Meuer et al., 1983; Wang and Reinherz, 2012; Reinherz, 2014). Each chain consists of one constant and one variable immunoglobulin (Ig) domain, which in turn contains three hypervariable complementarity determining regions dedicated to bind the antigen (Davis and Bjorkman, 1988; Katayama et al., 1995). The TCR is associated with the CD3 receptor consisting of three heterodimers CD3 γε, CD3 δε and

CD3 ζζ. Building a complex structure, the TCR-CD3 complex consists of in total four heterodimers. Since the cytosolic domains of the TCR are too short, those of CD3 mediate intracellular signaling via their immunoreceptor-tyrosin-based activation motifs (ITAM) (Weiss and Stobo, 1984; Irving and Weiss, 1991). Upon receptor-ligand interaction, clustering of intracellular signaling domains results in phosphorylation of ITAMs activating a kinase cascade with several mediators involved, such as src and syk kinases, activating various downstream signaling pathways (Irving and Weiss, 1991; Letourneur and Klausner, 1991; Chan et al., 1992; Iwashima et al., 1994; Minguet et al., 2007). For productive T cell activation, three signals are required, the first signal being provided by antigen recognition. For full activation, co-stimulatory receptor binding (signal 2) and interleukin-2 (IL-2) (signal 3) are just as much required (Smith-Garvin et al., 2009). T cell activation is characterized by several intrinsic changes mediated by the activation of transcription factors which regulate gene expression of T cell activating genes such as IL-2 (Serfling et al., 2000). Furthermore, differential surface receptor expression, increased metabolic activity, production of various cytokines and subsequent clonal expansion or differentiation comes along with T cell activation (Savignac et al., 2007; Smith-Garvin et al., 2009; Almeida et al., 2016).

1.1.2 Subsets of T cells

Dependent on the expression of CD4 or CD8 co-receptors, two types of T cells are distinguished – CD4$^+$ T helper cells and CD8$^+$ cytotoxic T cells conducting different effector functions. While CD4 T cells are mainly professional cytokine producing cells helping other immune cells to actively participate in the immune response, CD8 T cells directly execute killing activities against infected cells. Upon antigen binding, calcium dependent release of lytic granules triggers apoptosis-induced cell death of target cells in which both perforin and granzymes are crucial for effective cell killing. Immediate action and elimination of infected cells make CD8 T cells highly critical to prevent disease outbreak and to limit infections.

CD4 and CD8 T cells can be further distinguished. Dependent on their status of differentiation, subset phenotypes are categorized into naïve T cells (T_N), effector T cells (T_{Eff}) and memory T cells. Thereby, additional subtypes exist for memory T cells, namely the central memory T cells (T_{CM}) and the effector memory T cells (T_{EM}). In 2011, Gattinoni et al. discovered an intermediate phenotype, the stem cell-like memory T cell (T_{SCM}) (Gattinoni et al., 2011). The degree of differentiation not only affects the capacity of self-renewal, proliferation and effector function but also correlates with the differential expression of surface molecules. The combinatorial expression of surface markers is

typically used to identify the phenotype of a T cell. Common markers for the identification of CD8 subtypes are depicted in Figure 1. T_N cells represent the least differentiated phenotype which have not yet encountered their antigen and are characterized by a high self-renewal capacity. High expression levels of lymph node homing receptors CD62L, CD45RA and C-C chemokine receptor 7 (CCR7) dedicates them to recirculate between blood and secondary lymphoid organs to enhance the chance of antigen encounter. Upon binding to their cognate antigen, T_N cells produce high levels of IL-2 and differentiate into T_{Eff} cells (Butcher et al., 1999; van Stipdonk et al., 2001; Berard and Tough, 2002; van den Broek et al., 2018). T_{Eff} cells own the capability of invading into peripheral tissue and producing various cytokines such as IL-2, interferon gamma (IFN-γ) and tumor necrosis factor alpha (TNF-α). This allows immediate cytotoxicity towards infected cells. However, being highly differentiated, they have a low proliferative capability and die off rapidly upon antigen clearance (Podack and Kupfer, 1991; Haring et al., 2006).

	T_N	T_{SCM}	T_{CM}	T_{EM}	T_{Eff}
CD62L	+	+	+	-	-
CD45RA	+	+	-	-	+
CD45RO	-	+	+	+	-
CCR7	+	+	+	-	-
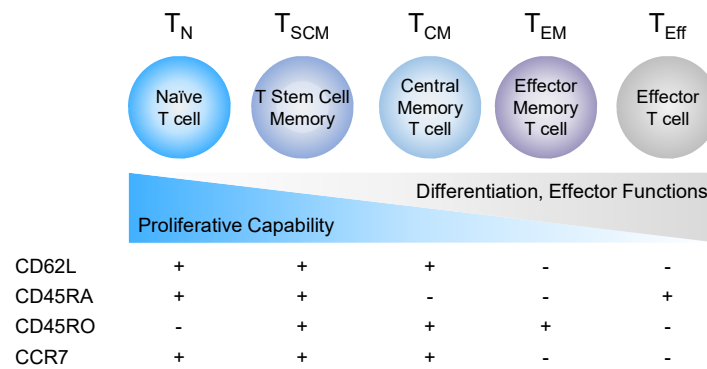
Figure 1: The different CD8$^+$ subsets
T cell subtypes are distinguished according to their differentiation status. Degree of differentiation from lowest to highest (left to right), with least differentiated T_N (highest proliferative capability) and highest differentiated T_{Eff} (lowest proliferative capability). Effector functions inversely correlate with proliferative capability. Each subtype is characterized by a differential expression of the surface markers CD62L, CD45RA, CD45RO and CCR7. T_N, naïve T cell; T_{SCM}, stem cell memory T cell; T_{CM}, central memory T cell; T_{EM}, effector memory T cell; T_{Eff}, effector T cell. Modified from (Golubovskaya and Wu, 2016).

In contrast, memory T cells provide long lasting immunity. With a certain capability of self-renewal and high expression of anti-apoptotic proteins they survive the absence of antigen in a quiescent state, even for years (Lau et al., 1994; Hammarlund et al., 2003). While T_{CM} represent early differentiated progenitors with higher self-renewal capacity and expression of lymph node homing receptors, T_{EM} confer more rapid effector functions and, due to the lack of CD62L expression, are able to invade into peripheral tissue (Sallusto et al., 2004). T_{SCM} are antigen-experienced and acquire rapid effector functions following TCR stimulation. However, they also possess a strong naïve-like phenotype being unique in combining the most characteristic properties of T_N and T_{Eff} (Gattinoni et al., 2011; Lugli et al., 2013). To ensure a sufficient pool of memory and naïve T cells, cytokines such as

IL-7 and IL-15 provide homeostatic proliferation stimuli conferring T cell proliferation without differentiation (Schluns et al., 2000; Boyman et al., 2009).

1.2 Cancer Immunotherapy

Strengthening the immune system to fight cancer has become an indispensable pillar of current cancer therapies. Traditional cancer treatments such as surgery, radio- and chemotherapy, which unspecifically eliminate rapidly growing cells, paved the way for clinically relevant success in anti-cancer therapies. However, recurrences of aggressive tumors, metastases and complex tumor entities require more effective therapies. The combination of conventional therapies accompanied by immunotherapies resulted in impressive clinical success of end-stage-cancer patients, some of which became tumor-free upon treatment. Several different strategies have been developed, including cancer vaccines, oncolytic viruses, immune checkpoint inhibitors and cell therapies such as allogeneic and autologous T cell transfer (Farkona et al., 2016; Oiseth and Aziz, 2017).

1.2.1 Cell therapies

Adoptive T cell transfer is meant to enhance the number of functional tumor-specific T cells in the cancer patient. In tumor-infiltrating lymphocyte (TIL) therapy, tumor-specific T cells are obtained from resected tumor fragments and expanded *ex vivo* under reactivating cytokine conditions before they are infused back into the patient (Dudley et al., 2010). TIL therapy has demonstrated clinical success in end-stage melanoma patients, however, failed to induce anti-tumoral effects in other cancer types (Dudley et al., 2002; Rosenberg et al., 2008; Yee, 2013; Hinrichs and Rosenberg, 2014). The lack of tumor-specific T cells due to tumor tolerance was of major hindrance and resulted in the development of new therapeutic approaches using genetically engineered T cells. Introducing TCR genes provides flexibility in targeting cancer associated antigens. For this purpose, tumor-specific T cells are screened *ex vivo* from patients with natural anti-tumor activities and TCR genes are isolated. These can be engineered further to increase affinity before they are transferred into the lymphocytes via retro- or lentiviral gene delivery (Hughes et al., 2005; Presotto et al., 2017). Mediating newly established tumor-specific immune response, TCR-engineered T cells induced cancer regression in melanoma patients (Morgan et al., 2006; Robbins et al., 2011). However, TCR-mediated tumor antigen recognition relies on MHC-dependent tumor antigen presentation, which is often downregulated in cancer cells, a common evasion mechanism of tumor cells limiting TCR T cell therapy (Garrido et al., 2016).

CAR-engineered T cells circumvent this obstacle by recognizing antigens in a MHC-independent manner. CAR T cell therapy is highly effective in B cell malignancies, as demonstrated by high response rates, e.g. up to 88% in acute lymphoblastic leukemia (ALL) patients treated with CD19 CAR T cells (Davila et al., 2014; Maude et al., 2014). Given this tremendous clinical success, the FDA approved two CAR T cell therapies by the end of 2017. Novartis' Kymriah™ was the first approved CAR T cell therapy for relapsed/refractory (r/r) B-cell ALL for young adults and for r/r diffuse large B-cell lymphoma (DLBL) for adult patients. Kite Pharma got Yescarta™ approved by the FDA for the treatment of end-stage patients suffering from large B-cell lymphoma. CAR T cell therapy represents a breakthrough therapy and was recently celebrated as Advance of the Year in the annual report 2018 of the American Society of Clinical Oncology (ASCO), highlighting its clinical relevance for future cancer therapies.

1.3 CAR T cell therapy

1.3.1 Structure of CARs

CARs are artificial receptors that combine the specificity of an antibody and the intracellular signaling machinery of a T cell receptor (Figure 2). The extracellular domain confers antigen specificity via the incorporation of a single chain variable fragment (scFv) that is derived from an antibody and mediates MHC-independent antigen recognition (Kuwana et al., 1987; Gross et al., 1989; Eshhar et al., 2001). As scFvs are exchangeable, any desired antigen can be targeted, simply limited by the availability of scFvs. Recently, also designed ankyrin repeat proteins (DARPins), which are poorly immunogenic and can be generated by a selection process to any kind of antigen, were used as targeting domains for CARs (Stumpp and Amstutz, 2007; Hammill et al., 2015; Siegler et al., 2017). The hinge domain links the targeting domain and the transmembrane domain (TM), providing scFv flexibility. Parts of several different Ig-like domains such as IgG1, IgG4 and the extracellular CD8 domain have been successfully used (Moritz and Groner, 1995; Zhao et al., 2009; Hombach et al., 2010; Jonnalagadda et al., 2015). Dependent on the size of the targeted antigen, the distance between tumor and CAR T cell can vary. Thereby, the length of the hinge domain can affect proper tumor antigen recognition and CAR T cell effector functions (Hombach et al., 2007; Hudecek et al., 2015). The TM domain is typically derived from membrane-spanning domains of CD4, CD8 or CD28 (Kahlon et al., 2004; Pulè et al., 2005; Milone et al., 2009). The intracellular domain provides crucial signaling domains, ensuring CAR T cell activation upon antigen

encounter. Over the years, CAR design evolved and meanwhile different generations of CAR structures can be distinguished (Figure 2).
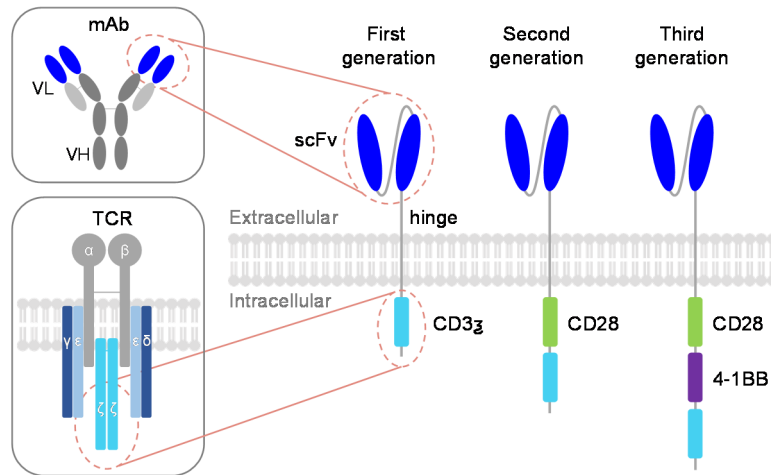
Figure 2: Scheme of the structure and design of CARs
CARs are artificial proteins that combine the intracellular signaling domain of the T cell receptor (TCR) with an extracellular binding domain that is usually an antibody-derived scFv. The hinge domain links the targeting domain to the transmembrane domain, which is fused to the intracellular signaling domain. First generation CARs contain CD3ζ, second generation and third generation CARs additionally contain one or two co-stimulatory domains, such as CD28 or 4-1BB. mAB, monoclonal antibody; scFv, single chain variable fragment; VH, variable heavy chain; VL, variable light chain.

While first generation CARs incorporate a single CD3ζ activation domain, second generation CARs harbor an additional co-stimulatory domain such as CD28, 4-1BB, OX40 and others (Finney et al., 2004; Imai et al., 2004; Kowolik et al., 2006). The usage of different co-stimulatory domains confers individual properties to the CAR T cells. While the CD28 co-stimulatory domain confers rather immediate effector functions, but also augments exhaustion in CAR T cells, the 4-1BB domain has been shown to mediate longer persistence of CAR T cells (Maude et al., 2014; Lee et al., 2015). Third-generation CARs consist of one activation and two co-stimulatory domains. Although preclinical studies demonstrated superior CAR T cell expansion, these CARs did not outperform second-generation CARs in clinical trials so far, but rather were associated with toxicities (Morgan et al., 2010; Till et al., 2012).

1.3.2   CD19-specific CAR T cells against B cell malignancies

Several clinical trials have been performed to investigate the clinical potential of CAR-engineered T cells against various cancer types (Hartmann et al., 2017). However, the most remarkable success in CAR T cell therapy was achieved with second generation CARs targeting the CD19 antigen in B cell malignancies. End-stage patients suffering from chronic lymphocytic leukemia (CLL) or ALL with no further treatment options were enrolled in CD19 CAR clinical trials. Meanwhile, one can look back at several clinical trials

providing comprehensive data sets for the treatment of B cell malignancies with CD19 CAR T cells.

The first trial was performed using T cells engineered with first generation CARs (Jensen et al., 2010). Although anti-tumoral effects were only temporary, lessons were learned about beneficial structures of CARs and lymphodepletion. As already seen in TIL therapies, pre-conditioning prior to T cell transfer depletes cytokine sinks and regulatory T cells resulting in beneficial engraftment and enhanced efficiency of the transferred cells (Dudley et al., 2005; Brentjens et al., 2011).

Clinical trial investigations implicated major advantages of the usage of second generation over first generation CARs. Long-term anti-tumoral effects were observed with second generation CARs and clearly correlated with efficient proliferation and persistence of the CAR T cells (Kalos et al., 2011; Porter et al., 2011). However, first signs of toxicities appeared. Some patients developed symptoms of systemic inflammatory reactions indicated by high fever, nausea, tachycardia, hypotension and dyspnea (Brentjens et al., 2011; Porter et al., 2011; Kochenderfer et al., 2015). Although never observed in pre-clinical models, several patients enrolled in different studies showed symptoms of cytokine release syndrome (CRS), which is categorized into grade 1-4, ranging from mild to severe CRS. Being a direct effect of T cell proliferation and large numbers of activated T cells, high amounts of IFN-γ, IL-6 and TNF-α can cause severe, life-threatening CRS with the need for intensive care (Kochenderfer et al., 2012; Grupp et al., 2013; Davila et al., 2014; Lee et al., 2015). Treatment with corticosteroids and the IL-6 receptor-blocking monoclonal antibody tocilizumab usually used for the treatment of rheumatoid arthritis have been shown to be effective in reversing severe CRS (Grupp et al., 2013; Davila et al., 2014; Lee et al., 2014; Maude et al., 2014). Meanwhile, inpatient treatment and improved guidelines for early treatment suggest these side effects to be manageable. Along with efficient tumor cell elimination, B cell depletion was observed in patients. B cells also express the CD19 antigen. Therefore, B cells are targeted as well by CD19 CAR T cells, known as on-target/off-tumor toxicity. Despite being a side effect of the treatment, B cell depletion upon CD19 CAR T cell treatment serves as useful pharmacodynamic marker of CAR T cell persistence. The absence of B cells, however, requires immunoglobulin replacement therapy, but represents a tolerable and manageable side effect (Kochenderfer et al., 2012; Maude et al., 2014).

With market authorization of Kymriah™ and Yescarta™ in the U.S., CAR T cell therapy is available for patients. However, along with market access, the highly personalized manufacturing process faces hurdles never met with conventional commercially available off-the-shelf drugs.

1.3.3 Manufacturing of CAR T Cells

Generating CAR T cells begins with the collection of PBMC from the patient, a process termed leukapheresis. Prior to activation of the T cells, T cells are isolated, and a T cell selection process such as magnetic separation of CD3$^+$ cells or even the separation of CD4$^+$ and CD8$^+$ cells may be included. Different activation protocols are available and applied in clinical trials (Wang and Rivière, 2016). While cell-based T cell activation by DCs or artificial APCs require human leukocyte antigen (HLA)-matched cell lines and hinders broad applicability, usage of beads covalently coupled with αCD3 and αCD28 antibodies together with IL-2 represents a standardized method of T cell activation. Engineering T cells with the CAR transgene often relies on retro- or lentiviral gene transfer. Following gene transfer, a process of T cell expansion generates high numbers of CAR T cells. According to different protocols, this procedure may take between ten days up to three weeks until CAR T cells are finally prepared for re-infusion into the patient (Dai et al., 2016).

1.3.3.1 Drawbacks of an e*x vivo* manufactured personalized CAR T cell product

Several protocols with varying expansion times and cytokine treatments to generate CAR T cell products are currently available among different centers. So far, it is still under discussion which procedure generates the most efficient CAR T cell product. It is known, however, that longer expansion times can favor T cell exhaustion impeding anti-tumoral functions of CAR T cells. Therefore, shorter manufacturing processes are desired to generate more efficient products (Gattinoni et al., 2012). Furthermore, the differentiation status, which is highly influenced by *ex vivo* culture conditions, is discussed to influence anti-tumoral potency. Often, *ex vivo* manipulation favors T cell differentiation and efforts are ongoing to prevent CAR T cell differentiation during *ex vivo* manufacturing. The addition of homeostatic cytokines (IL-15 and IL-7) during the expansion process is known to favor the maintenance of less differentiated CAR T cells (Klebanoff et al., 2004; Cieri et al., 2013). Meanwhile, CAR T cell products generated from T$_N$, T$_{SCM}$ and T$_{CM}$ cells are under investigation to mediate more efficient anti-tumoral effects (Wang et al., 2012; Casati et al., 2013; Xu et al., 2014; Sabatino et al., 2016).

The generation of an individualized medicinal product makes CAR T cell manufacturing a complex process that faces logistic challenges never met with commercially off-the-shelf drugs. CAR T cell generation currently represents a highly labor-intensive process with the need for well-equipped, good manufacturing practice (GMP)-certified facilities as well as highly skilled staff. During *ex vivo* cell manipulation, separate machines for cell

preparation, activation, transduction, expansion and final formulation are required. Transfer between the machines and the included washing steps require cell handling in open systems with the risk of contamination (Levine et al., 2017). Closed systems such as the CliniMACS Prodigy® combine processes of cell preparation until final formulation within a single device that minimizes the risk of contamination and ensures consistently high quality of the product by a standardized and fully automated procedure. Hospitals equipped with CliniMACS Prodigy® devices would enable CAR T cell manufacturing and patient treatment to be performed at a single location without the need for cell shipments (Kaiser et al., 2015). Current standard, however, are central manufacturing sites that allow upscaling and provide infrastructure to make this therapy available to larger patient populations. However, this process is underpinned by complex logistics (Levine et al., 2017; Roberts et al., 2017) (Figure 3).
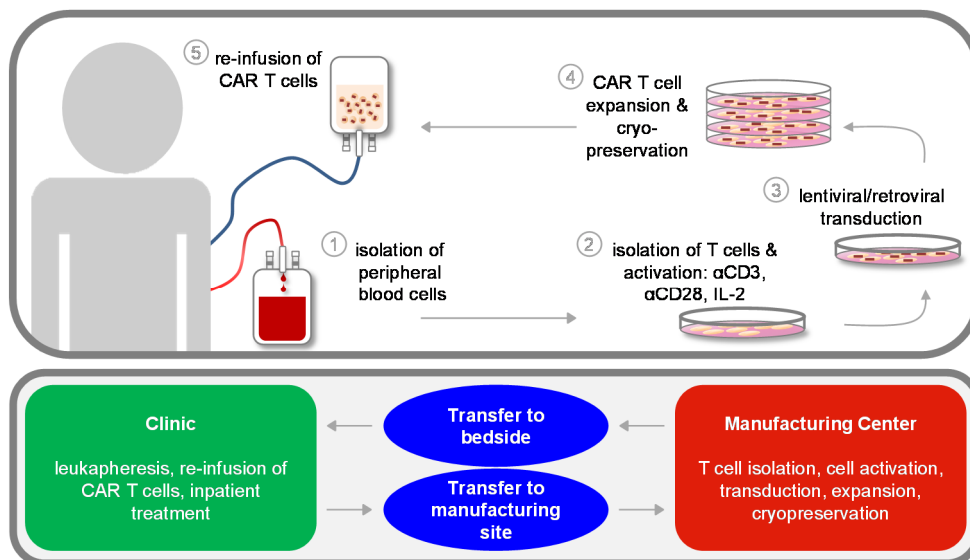
Figure 3: Centralized manufacturing process of CAR T cells
Generation of CAR T cells at central manufacturing sites requires cell shipment between the clinic and the manufacturing site. Top panel: Process of CAR T cell generation. (1) Blood cells are isolated from the patient (leukapheresis). (2) T cells are isolated and activated via αCD3 and αCD28 antibodies with the addition of cytokines (e.g. IL-2). (3) CAR gene transfer into the T cells is performed by retro- or lentiviral vector transduction (4) followed by CAR T cell expansion and cryopreservation. (5) The final CAR T cell product is re-infused into the patient. Lower panel: Facilities involved during CAR T cell therapy. Patient's treatment involving leukapheresis and re-infusion of the CAR T cells are performed at the clinic (green). CAR T cell manufacturing is carried out at the manufacturing site (red). Cell shipments between both locations are required: from the clinic to the manufacturing center and backwards (blue). Modified from (Levine et al., 2017).

Shipment of the isolated cells to the manufacturing site, preparation of cells and transfer of the cell product back to the clinic requires supply chain management with the need for precise cell product tracking from the beginning of T cell isolation until re-infusion of the product into the patient (Levine et al., 2017; Roberts et al., 2017). Furthermore, upon final formulation of the product, individualized medicinal products require single-lot-release testing to ensure high product quality and potency. This includes flow cytometry analysis

of CAR expression and phenotype analysis. Cytokine production, killing and viability assessments evaluate functional potency of the product. Sterility testing, including bacterial, fungal and endotoxin tests and absence of replication-competent viral particles ensure safety of the product (Gee, 2015; Wang and Rivière, 2015). With the approval of Kymriah™ and Yescarta™, however, this therapy will be made available for patients in need, which faces high financial efforts and technical challenges. It is desirable to translate the manufacturing process into a more automated and standardized production line-like system.

1.4   Cell type-specific gene delivery

Ex vivo modification of cells is the current gold standard in gene therapeutic approaches. However, *in vivo* modification would circumvent the highly personalized and complex procedure. To enable local or systemic vector administration, highly selective gene transfer is inevitable to prevent unwanted off-target effects. To ensure efficient and safe gene therapy, receptor-targeted lentiviral vectors have been developed to restrict gene transfer to a target cell population that is characterized by the expression of a distinct receptor.

1.4.1   Lentiviral vectors

Lentivirus-derived lentiviral vectors (LVs) ensure efficient gene delivery and integrate their genomic information stably into the host's genome, which ensures therapeutic gene expression not only in the gene-modified cells but also in all daughter cells. Several years of clinical application resulted in improved and safety-optimized LVs, which are meanwhile considered as an attractive tool for the treatment of various diseases (Kaufmann et al., 2013; Naldini et al., 2016). Derived from human immunodeficiency virus-1 (HIV-1) lentivirus of the retroviridae family, LVs carry a positive single-stranded diploid RNA genome (Knipe and Howley, 2007). However, to ensure safe gene delivery using LVs, these vector particles contain defective genomes, which allow for a single transduction but avoid replication and the release of further viral particles afterwards. To generate replication-incompetent LVs, viral vector production is performed using a trans-packaging system, splitting the viral genes onto several distinct plasmids (Zufferey et al., 1997; Pluta and Kacprzak, 2009). Using the second generation lentiviral vector system, three plasmids are co-transfected to a packaging cell line, typically human embryonic kidney 293T (HEK-293T) cells (Figure 4).
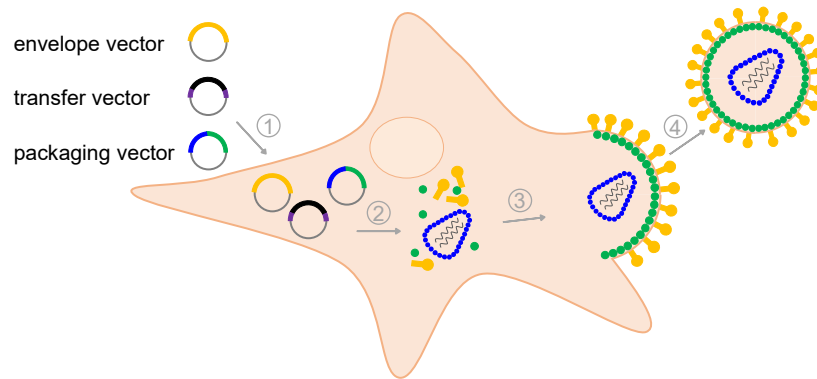
Figure 4: Production of lentiviral vectors by triple transfection
(1) Co-transfection of packaging-, envelope-, and transfer vector into a packaging cell, typically HEK-293T results in (2) transient viral gene expression. (3) Vector particles bud from the cell membrane and (4) are released into cell culture supernatant.

The packaging plasmid encodes for the structural genes *gag* and *pol*, while the envelope coding sequence is located on a separate plasmid. The transfer vector plasmid encodes the therapeutic gene driven by an internal promotor such as spleen focus forming virus (SFFV) or elongation factor 1 alpha (EF1α). Flanked by long terminal repeats (LTRs), the expression cassette of the transfer vector is the only sequence that is integrated into the host's genome. The third-generation lentiviral vector system was designed to further enhance the biosafety of LVs. The *rev* and *tat* genes had been removed from the packaging plasmids and are encoded separately (Dull et al., 1998). To further minimize the risk of insertional oncogenesis enhancer elements from the U3 region were deleted, resulting in the inactivation of internal promoter activity. These are the so-called self-inactivating LVs (SIN-LVs) (Miyoshi et al., 1998).

1.4.2 Pseudotyping of lentiviral vectors

Binding of the viral glycoprotein to the cell surface receptor represents the first contact between the viral particle and the cell, and triggers cell entry upon conformational changes. Given the specific binding of the viral glycoprotein to its target receptor, viruses show a restricted tropism to a certain cell type. Incorporating heterologous glycoproteins derived from other enveloped viruses is called pseudotyping and is used to expand or restrict the tropism of lentiviral vectors (Cronin et al., 2005; Frecha et al., 2008). Since LVs bud from the cell surface and incorporate proteins presented at the cell surface, overexpression of the desired glycoprotein is sufficient for incorporation into the vector particle. Further modifications such as cytoplasmic tail truncations might be necessary to ensure efficient glycoprotein incorporation (Merten et al., 2005; Frecha et al., 2008; Funke et al., 2008; Bender et al., 2016).

To enable transduction of various cell types such as lymphocytes, hematopoietic stem cells (HSCs), muscle cells, cancer cells and others, *ex vivo* gene therapeutic applications rely on LVs with expanded tropism. Pseudotyping LVs with the glycoprotein G of vesicular stomatitis virus (VSV) has become the gold standard for targeting human cells, since the low density lipoprotein (LDL) target receptor is present on almost every human cell entity (Naldini et al., 1996; Blömer et al., 1997; Kafri et al., 1997; Miyoshi et al., 1997; Finkelshtein et al., 2013). However, to increase the efficiency and restrict gene transfer to a certain cell type, envelope proteins, which preferentially bind to certain cell entities, are used. With this approach, lentiviral vectors have been targeted to unstimulated CD34^{+} HSCs by incorporating baboon endogenous virus (BaEV) glycoproteins (Girard-Gagnepain et al., 2014). Sendai virus and Ebola Zaire virus-derived glycoprotein demonstrated efficient transduction of airway epithelial cells (Kobinger et al., 2001; Mitomo et al., 2010).

1.4.3 Receptor-targeted lentiviral vectors

Cell-specific gene delivery is indispensable in order to prevent off-target effects, especially when on-site modification of cells is desired. Receptor-targeted LVs restrict gene delivery to a distinct cell type that is characterized by a cell surface marker.

For this purpose, natural binding sites of the incorporated glycoproteins need to be abolished and a separate binding domain is displayed, mediating selective receptor binding to a distinct cell type. Using this approach, incorporation of measles virus (MV) glycoproteins results in successful re-targeting (Anliker et al., 2010; Buchholz et al., 2015). For this purpose, the fusion protein (F) and the hemagglutinin (H) are incorporated into vector particles. Cytoplasmic tail truncations of the H (18 amino acids) and F (30 amino acids) allows efficient glycoprotein incorporation. Point mutations within the H protein abolish binding to its natural receptors CD46 and SLAM. As targeting domain, either a scFv or a DARPin can be used providing flexibility in terms of receptor usage and subsequent re-targeting to any cell type of choice. To date, several receptor-targeted LVs have been generated and proven to selectively deliver genes into their target cell population while non-target cells remained untransduced. Successful re-targeting to various cell types such as CD105^{+} endothelial and CD133^{+} hematopoietic progenitor cells as well as CD4^{+}, CD20^{+} and CD8^{+} lymphocytes has been achieved (Funke et al., 2008; Anliker et al., 2010; Zhou et al., 2012; Abel et al., 2013; Zhou et al., 2015). Recently, a new platform was established incorporating Nipah virus (NiV) glycoproteins into LVs. Truncations of 34 amino acids in the G protein and 22 amino acids in the F protein resulted in efficient incorporation of the glycoproteins. Incorporation rate of glycoproteins was three

to four times higher than for MV glycoproteins. Although less flexible in target receptor choice, several cell types were successfully targeted, including CD8 T cells (Bender et al., 2016) (Figure 5).
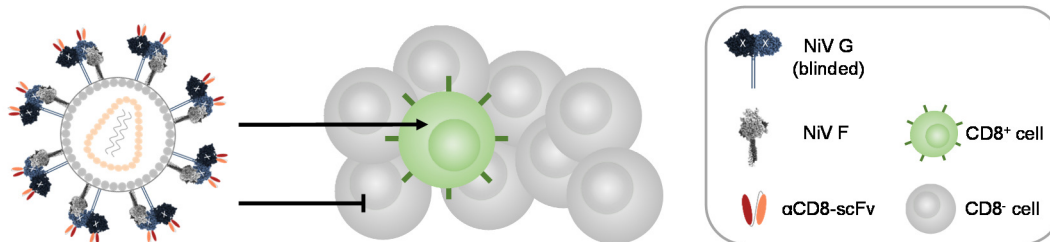
Figure 5: CD8-targeted LVs pseudotyped with NiV glycoproteins
The HIV-1-derived LV displays truncated NiV glycoproteins at the surface, namely the F protein and the G protein that is blinded for its natural receptor. A scFv, derived from a monoclonal antibody, specific for human CD8 is fused to the G protein. CD8-LV mediates selective transduction into CD8$^+$ cells (green) while CD8$^-$ cells remain untransduced (grey). F, fusion protein; G, glycoprotein; HIV-1, human immunodeficiency virus type 1; LV, lentiviral vector; NiV, Nipah virus; scFv, single chain variable fragment.

1.4.3.1 Lymphocyte-targeted LVs

Although LVs are able to transduce non-proliferating cells such as neuronal cells, transduction of quiescent lymphocytes using the VSV-G envelope is challenging due to the absence of the LDL receptor on the surface of unstimulated lymphocytes (Amirache et al., 2014). To ensure efficient gene transfer, lymphocytes need to be activated prior to transduction, which induces upregulation of the LDL receptor. However, activation of lymphocytes often results in unintentional differentiation. To overcome this hurdle, strategies involve the targeting of alternative receptors. Besides BaEV-pseudotyped LVs also receptor-targeted lentiviral vectors successful delivered genes into unstimulated lymphocytes.

First attempts in targeting B cells were made by pseudotyping LVs with Sindbis Virus glycoproteins. A monoclonal antibody, specific for CD20 and a Sindbis-derived fusion protein deficient for binding to its natural receptor were incorporated (Lei et al., 2009). Although this approach demonstrated selective B cell targeting, pH-dependent entry via endocytosis and the incorporation of a complete antibody might limit transduction efficiency. In contrast, MV-pseudotyped LVs enter cells pH-independently directly at the cell membrane by membrane fusion. Displaying a CD20-specific scFv on the MV-H resulted in exclusive transduction of B cells, while sparing CD20$^-$ cells in co-culture transduction experiments (Funke et al., 2008). Even more, the CD20-targeted MV-LV efficiently transduced resting B cells, likely, due to a proliferative stimulus triggered upon binding to CD20 receptor (Kneissl et al., 2013).

By exchanging the targeting domains, a pool of lymphocyte-targeted LVs had been generated, among them MV-pseudotyped CD4^{MV}- and CD8^{MV}-targeted LVs (Zhou et al., 2012; Zhou et al., 2015). The transfer of therapeutic transgenes *in vitro* has been shown for both vectors. The CD8^{MV}-LV-modified T cells even demonstrated higher killing activities *in vitro* upon the transfer of a TCR gene compared to VSV-G-transduced cells. Most likely, this is a result of preferential transduction of T cells with high levels of CD8 correlating with higher granzyme B and perforin expression. First *in vivo* transduction experiments had been performed with both vectors in PBMC-humanized mice. Besides successful reporter gene transfer exclusively into CD4$^+$ T cells, even stable expression of the *forkhead box P3* (*FoxP3)* gene for 2 months post CD4^{MV}-LV administration was shown (Zhou et al., 2015). Upon intraperitoneal (i.p.) injection of CD8^{MV}-LV into PBMC-humanized mice, reporter gene transfer was exclusively observed in CD8$^+$ cells, resulting in 10% transduced CD8$^+$ cells (Zhou et al., 2012). However, vector production only resulted in moderate titers, rendering the CD8^{MV}-LV inappropriate for intravenous (i.v.) vector administration. In contrast, vector productions of the CD8-targeted LV pseudotyped with NiV glycoproteins (CD8-LV) yielded much higher titers (Bender et al., 2016). Long-term transgene expression in CD8$^+$ cells within human PBMC has been demonstrated already *in vitro*. Further, in contrast to MV, the absence of neutralizing antibodies in the majority of the human population against NiV is thought to increase efficiency of *in vivo* transduction, rendering CD8-LV a promising tool for the investigation of *in vivo* gene delivery upon systemic vector administration.

1.5 Objective

Aim of this study was the *in vivo* modification of CD8 T cells to express a CD19-specific CAR and subsequent characterization of *in vivo* generated CAR T cells. CAR T cell therapy, despite its great success, is a highly personalized, complex and time-consuming therapy due to the *ex vivo* manufacturing of CAR T cells. The idea of generating CAR T cells *in vivo* by systemic administration of CAR gene-carrying vector particles represents an innovative approach, which is investigated in this thesis.

For this purpose, receptor-targeted LVs, which have been shown to deliver genes highly selective into distinct cell populations of choice, are an absolute requirement. Targeting CD8 T cells delivers the CAR transgene into cytotoxic immune cells, which are able to eliminate tumor cells once the CAR is expressed on the cell surface. NiV-pseudotyped LVs targeted to CD8$^+$ cells represent high-titer vectors, which already demonstrated stable reporter gene transfer into human PBMC and are a promising tool for the generation of CAR T cells.

First, the capability of CD8-LV to mediate *in vivo* gene transfer was evaluated in mice engrafted with human PBMC. To evaluate transduction efficiency *in vivo*, CD8-LV carrying a reporter gene was systemically injected into NOD.Cg.Prkdc^{scid}IL2rg^{tmWjl}/SzJ (NSG) mice and transgene expression was analyzed in various organs. Second, CD8-LV was investigated to generate functional CAR T cells *in vitro*. CAR encoding CD8-LVs were used to generate CAR T cells by transduction of primary cells. Functional properties of those CAR T cells were analyzed, such as the selective proliferation upon antigen exposure and killing of tumor cells. Third, *in vivo* generation of CAR T cells was evaluated upon CD8-LV(CAR) administration to PBMC-humanized NSG mice and *in vivo* generated CAR T cells were further characterized. In detail, CAR T cell proliferation was studied in the presence and absence of CD19$^+$ target cells. Elimination of target cells was analyzed as well as transgene integration on genomic level and the clonality of CAR T cells. Based on surface marker analysis, the phenotype of *in vivo* generated CAR T cells was characterized. Finally, anti-tumoral functions of *in vivo* generated CAR T cells were evaluated in a xenograft mouse model using CD19$^+$ human tumor cells.

2 Materials & Methods

2.1 Material

Chemicals and reagents were purchased from Becton Dickinson, Biochrom, Biowest, Biozym, Carl Roth, CP-Pharma, Lonza, Miltenyi Biotec, New England Biolabs, Nippon Genetics, Perkin Elmer, Roche, Sigma-Aldrich, Thermo Fisher Scientific and VWR. Consumables used for cell culture, molecular biology and animal work were purchased from 4titude, B. Braun, Becton Dickinson, Bioline, Bio-Rad, Biotix, Biozym, Cell Signaling Technology, Corning, Eppendorf, GE Healthcare, Genomed, Greiner Bio-One, Machery-Nagel, Micronic, Miltenyi Biotec, Promega, Sartorius, Thermo Fisher Scientific, Qiagen and VWR. Detailed information are given below.

2.1.1 Chemicals & Reagents

Name	Supplier
2-log DNA ladder	New England Biolabs
Agarose	Biozym
Ampicillin	Roche
BD Pharm Lyse™	Becton Dickinson
Bovine Serum Albumin (BSA)	Sigma-Aldrich
CD19$^+$ microbeads, human	Miltenyi Biotec
gentleMACS C tube	Miltenyi Biotec
D-Luciferin	Perkin Elmer
Dulbecco's Modified Eagle Medium (DMEM) High Glucose	Biowest
Ethidium bromide (1%)	Sigma-Aldrich
FcR blocking reagent, murine	Miltenyi Biotec
Fetal bovine serum (FBS, other name: FCS)	Biochrom
G418, Geneticin®	Sigma-Aldrich
Gel loading dye, purple (6X)	New England Biolabs
HEPES solution	Sigma-Aldrich
Histopaque®-1077	Sigma-Aldrich
Isoflurane CP	CP-Pharma
L-Glutamine	Sigma-Aldrich
Midori Green DNA, Direct loading dye	Nippon Genetics
PBS (w/o Mg^{2+}/Ca^{2+})	Lonza

Name	Supplier
Penicillin/Streptomycin	Paul-Ehrlich-Institut
Polyethylenimine (PEI), branched	Sigma-Aldrich
RPMI 1640 medium	Biowest
Sucrose	Sigma-Aldrich
Trypan blue	Sigma-Aldrich
UltraComp eBeads™ Compensation Beads	Thermo Fisher Scientific

2.1.2 Consumables

Name	Supplier
1.4 ml Tubes	Micronic
500 ml Rapid-Flow Bottle Top Filter, 0.45 µm SFCE	Thermo Fisher Scientific
BD Falcon Round Bottom Tube, 5 ml	Becton Dickinson
BD Microtainer® Blood Collection Tubes, Lithium Heparin (LH)	Becton Dickinson
BD Vacutainer Safety-Lok Blood Collection Set	Becton Dickinson
BD Vacutainer® CPT™ Mononuclear Cell Preparation Tube	Becton Dickinson
Cell Culture Dish, Ø 150 mm	VWR
Cell Strainer, 70 µm	Corning
Centrifuge Tube, 225 ml	VWR
Cryovial (2 ml)	Greiner Bio-One
Falcon (15 ml, 50 ml)	Greiner Bio-One
Frame Star 96 Well Plate, Roche Style	4titude
Insulin Syringes, U-100; 0.33 mm (29G) x 12.7 mm	Becton Dickinson
LD Column	Miltenyi Biotec
Pasteur Pipet, glass, 14.6 cm	VWR
PCR Tubes	Eppendorf
Petri Dish, Ø10 cm	Greiner Bio-One
Pipette Tips, filtered (10 µl, 100 µl, 300 µl, 1000 µl)	Biozym
Serological pipettes (5 ml, 10 ml, 25 ml)	Greiner Bio-One
Sterican Cannulas (G24, G30)	B. Braun
Syringe Filters, Minisart (0.45 µm, 0.2 µm)	Sartorius
Tissue Culture Flask (T25, T75, T125)	Greiner Bio-One
Tissue Culture Plates (96-, 48-, 24-, 12-, 6-well)	Thermo Fisher Scientific

2.1.3 Software

Name	Supplier
Citavi 6	Swiss Academic Software
FSC Express V4, V6	De Novo Software
GraphPad Prism 7	GraphPad Software
LightCycler® Software 4.1	Roche
Living Image	Perkin Elmer
SnapGene 4.1	SnapGene
Vector NTI®	Thermo Fisher Scientific

2.1.4 Buffers & Media

Name	Composition
Blocking solution	2% BSA in PBS w/o Mg^{2+}/Ca^{2+}
FACS fix	1% Formaldehyde in PBS w/o Mg^{2+}/Ca^{2+}
FACS washing buffer	2% FCS, 0.1% NaN_3 in PBS w/o Mg^{2+}/Ca^{2+}
Freezing medium	10% DMSO, 90% FCS
LB-medium	1% Tryptone, 0.5% Yeast extract, 1% NaCl, in H_2O, pH 7.2
PBS/EDTA	2 mM EDTA in PBS w/o Mg^{2+}/Ca^{2+}
PEI transfection reagent	18 mM 25 kDa branched PEI in H_2O
S.O.C. medium	1% Tryptone, 0.5% Yeast extract, 1% NaCl, 2.5 mM KCl, 10 mM $MgCl_2$, 10 mM $MgSO_4$, 20 mM Glucose in H_2O
Sucrose	20% Sucrose in PBS w/o Mg^{2+}/Ca^{2+}
T cell medium	RPMI 1640 supplemented with 10% FCS, 2 mM L-Glutamine, 25 mM HEPES, 0.4% Penicillin/Streptomycin
TAE buffer	40 mM Tris, 20 mM Acetic acid, 1 mM EDTA in H_2O
Trypsin working solution	2 mM EDTA, 0.25% Trypsin-Melnick in PBS w/o Mg^{2+}/Ca^{2+}

2.1.5 Antibodies

Name	clone	Dilution for flow cytometry application	Supplier
mouse anti-human CD19	LT19	1:100	Miltenyi Biotec

Name	clone	Dilution for flow cytometry application	Supplier
mouse anti-human CD28	15E8	used for T cell activation (2.3.4)	Miltenyi Biotec
mouse anti-human CD3	BW264/56	1:100	Miltenyi Biotec
mouse anti-human CD3	OKT3	used for T cell activation (2.3.4)	Miltenyi Biotec
mouse anti-human CD45	5B1	1:100	Miltenyi Biotec
mouse anti-human CD45RA	T6D11	1:100	Miltenyi Biotec
mouse anti-human CD62L	145/15	1:100	Miltenyi Biotec
mouse anti-human CD8	BW135/80	1:100	Miltenyi Biotec
mouse anti-myc	9B11	1:100	Cell Signaling Technology

2.1.6 Plasmids

Name	Description	Supplier
pCAGGS-NiV-FcΔ22	Encodes NiV-FcΔ22	(Bender et al., 2016)
pCAGGS-NiV-GcΔ34^{CD8}mut4	Encodes NiV-GcΔ34 with four mutations to abolish natural binding sites of the NiV-G, is fused to the anti-human CD8-specific scFv OKT8 humVh1	(Bender et al., 2016)
pCMVΔR8.9	HIV-1 packaging plasmid	U. Blömer (Zufferey et al., 1997)
pH-luc-IRES-Neomycin	Encodes firefly luciferase fused to neomycin resistance via an internal ribosomal entry site (IRES)	I. Schneider
pMD2.G	Encodes the glycoprotein G of VSV	D. Trono
pS-Albumin-W	HIV-1 transfer vector encoding parts of exon(13)-intron(14) junction sequence of human albumin gene	This thesis
pS-CD19CAR-W	HIV-1 transfer vector encoding CD19 CAR, generated by removing the IRES-GFP cassette from plasmid pS-63.28.z-IEW	W. Wels (Oelsner et al., 2017)
pSEW	HIV-1 transfer vector encoding GFP	M. Grez (Demaison et al., 2002)
pS-luc-gfp-W	HIV-1 transfer vector encoding firefly luciferase and GFP, linked by a T2A site	(Abel et al., 2013)

Name	Description	Supplier
pS-rfp-W	HIV-1 transfer vector encoding RFP, generated by exchanging the luc-gfp cassette in pS-luc-gfp-W with the RFP reading frame	T. Abel

2.1.7 Enzymes

Name	Supplier
Antarctic Phosphatase	New England Biolabs
KOD Hot Start DNA Polymerase	Merck Millipore
Restriction Endonucleases	New England Biolabs
Trypsin 2.5%	Paul-Ehrlich-Institut

2.1.8 Oligonucleotide

Name	Sequence (5' → 3')
albumin fwd	CAC ACT TTC TGA GAA GGA GAG AC
albumin rev	GCT TGA ATT GAC AGT TCT TGC TAT
lvLTR1	[biotin]-GAA CCC ACT GCT TAA GCC TCA
lvLTR2	AGC TTG CCT TGA GTG CTT CA
lvLTR3	AGT AGT GTG TGC CCG TCT GT
OCI	GAC CCG GGA GAT CTG AAT TCG
OCII	AGT GGC ACA GCA GTT AGG ACG
Probe-albumin	[6FAM]-ACG TGA GGA GTA TTT CAT TAC TGC ATG TGT-[BHQ1]
Probe-WPRE	[Cy5]-TGC ACT GTG TTT GCT GAC GCA AC-[BHQ3]
WPRE fwd	TCC TGG TTG CTG TCT CTT TAT G
WPRE rev	TGA CAG GTG GTG GCA ATG

2.1.9 Kits

Name	Supplier
CellTrace™ CFSE Cell Proliferation Kit	Thermo Fisher Scientific
DNeasy® Blood and Tissue Kit	Qiagen
eBioscience™ Fixable Viablity Dye eFluor™ 450	Thermo Fisher Scientific
GeneJET Gel Extraction Kit	Thermo Fisher Scientific
GeneJET Plasmid Miniprep Kit	Thermo Fisher Scientific

Name	Supplier
JETSTAR 2.0 Plasmid Midiprep Kit	Genomed
JETSTAR 2.0 Plasmid Midiprep Kit	Genomed
Liver Dissociation Kit, mouse	Miltenyi Biotec
Lung Dissociation Kit, mouse	Miltenyi Biotec
Nucleobond XtraMaxiET	Machery-Nagel
Nucleobond XtraMidi	Machery-Nagel
Luciferase Assay System	Promega
QIAamp DNA Mini Kit	Qiagen
Rapid DNA Ligation Kit	Thermo Fisher Scientific
SensiFAST™ Probe No-Rox Kit	Bioline

2.1.10 Cell lines and bacteria

Name	Description	Source
E.coli, Top 10	Highly transformable laboratory strain of *Escherichia coli*	Life technologies
HEK-293T	Human fetal kidney epithelial cells, transformed to express the adenoviral SV40 T antigen	ATCC CRL-11268
Hut-78	Human T lymphoblast cell line	ATCC TIB-161
MOLT4.8	Human T lymphoblast cell line	C. J. Buchholz, Paul-Ehrlich-Institut
Raji	Human B lymphoblast cell line	ATCC CCL-86
Raji-luc	Human B lymphoblast cell line, stable cell line, genetically engineered to express firefly luciferase, neomycin resistant	This thesis

2.2   Methods of molecular biology

2.2.1   Transformation of chemically competent bacteria

Plasmid DNA was amplified by cellular replication of transformed chemically competent *E.coli* Top 10. Bacteria were thawed on ice and 50 ng DNA or 3 µl ligation mix was added. After 30 min incubation on ice, a heat shock was performed at 42°C for 45 s and bacteria were immediately cooled on ice afterwards. S.O.C medium (100 µl) was added to the bacteria. After 30 min incubation at 37°C, shaking at 600 rpm, bacteria were plated onto

LB agar plates (4% (w/v) LB-agar containing 100 mg/l ampicillin, provided by Medienküche, Paul-Ehrlich-Institut) and incubated over night at 37°C.

2.2.2 Plasmid preparation

Plasmid DNA preparation was performed from transformed *E.coli* using silica membrane or anion exchange column-based DNA purification technique. For purification of low, medium and high amount of plasmid DNA, 5 ml, 50 ml or 250 ml LB medium were inoculated with a single bacteria clone in the presence of corresponding antibiotics and grown over night at 37°C, shaking at 180 rpm. Bacteria were harvested by centrifugation at 4600 rpm for 10 min (Multifuge 3S-R, Heraeus) or at 6000 rpm for 15 min (Sorvall® RC 26 plus, rotor: SLA-1500). DNA purification was performed using GeneJET Plasmid Miniprep Kit, JETSTAR 2.0 Plasmid Midiprep Kit or JETSTAR 2.0 Maxiprep Kit according to the manufacturer's protocol. DNA concentration was photometrically analyzed (NanoDropTM 2000c, Thermo Fisher Scientific). DNA quality was analyzed by restriction enzyme digest (2.2.3) and subsequent agarose gel electrophoresis (2.2.4).

2.2.3 Restriction of DNA

Restriction enzyme digest was performed for analytical and preparative DNA digestions. Restriction endonucleases from New England Biolab (NEB) were used according to the manufacturer's protocol. Usually, 1 µg of DNA was mixed with 10 U of the corresponding enzyme and buffer conditions. Analytical digestions were performed with 1µg DNA and preparative digestions with 1-3 µg DNA. The reaction mix was incubated at the corresponding temperature optimum for 2-4 h (analytical) or 4-6 h (preparative). DNA fragments were separated using agarose gel electrophoresis (2.2.4) and, if required, purified form the gel using the GeneJET Extraction Kit (Thermo Fisher Scientific).

2.2.4 Agarose gel electrophoresis

Agarose gels electrophoresis separates DNA fragments according to their size and was used to analyze analytical and preparative DNA digests. Usually, 1-2% (w/v) agarose gels were used for analyses. For this purpose, agarose powder was dissolved in TAE buffer by heating and the solution was poured into a gel tray for polymerization. To visualize DNA, either ethidium bromide or Midori Green were used. 50 µg/ml ethidium bromide was added to the non-polymerized agarose gel solution and DNA samples were mixed with 6x gel loading dye (NEB), prior loading them onto the polymerized gel. Midori Green was

directly added to the DNA samples using Midori Green Direct (Nippon Genetics). Gel electrophoresis was performed at 70-120 V in a Wide Mini Sub-Cell® GT chamber (Bio-Rad). DNA fragment separation was analyzed by the use of ultraviolet or green/blue LED light, gel documentation imager (Intas) and a 2-log DNA ladder (NEB).

2.2.5 Dephosphorylation and ligation of DNA

Linearized DNA with compatible ends was dephosphorylated prior to ligation. Dephosphorylation of 5'-ends of DNA using Antarctic phosphatase (NEB) was performed according to the manufacturer's protocol. In brief, 300 ng of linearized DNA were mixed with 5 U Antarctic phosphatase within appropriate buffer conditions and incubated at 37°C for 30 min. Prior to ligation, enzyme was inhibited by heat inactivation for 2 min at 80°C. For ligation, the Rapid DNA Ligation Kit (Thermo Fisher Scientific) was used according to the manufacturer's protocol. Vector DNA was mixed with insert DNA at 3:1 molar excess over vector. Usually, 50 ng of vector DNA was used and mixed with insert DNA and 5 U/µl T4 DNA Ligase under appropriate buffer conditions. After 5 min incubation at 22°C, 3 µl of reaction mixture was used for transformation (2.2.1).

2.2.6 Polymerase chain reaction

Amplification of DNA fragments using sequence-specific primers was performed with the use of KOD Hot Start DNA Polymerase (Merck Millipore) according to the manufacturer's protocol. For the introduction of restriction sites into DNA sequences, sequence-specific primers were designed with extended sequences of the desired restriction site. In general, a polymerase chain reaction (PCR) consists of several steps of different temperature cycles. Prior to the initial denaturation step, which melts double stranded DNA, an initialization step is required for activating the hot-start polymerase. After annealing of the primers at primer-specific temperature, the polymerase synthesizes a new DNA strand complementary to the template during the elongation step. Elongation time is dependent on the amplicon length and PCR reactions were prepared as shown in Table 1 with cycle conditions given in Table 2.

Table 1: PCR reaction

component	volume in µl
plasmid template DNA (10 ng)	1
10x Buffer for KOD Hot Start DNA polymerase	5
MgSO$_4$ (25 mM)	3
dNTP (2 mM each)	5
fwd primer (10 µM)	1,5
rev primer (10 µM)	1,5
KOD Pol (1 U/µl)	1
PCR grade water	32

PCR reaction was performed in a PCR thermal cycler (Bio-Rad) with following cycle reactions:

Table 2: PCR cycle conditions

	step	temperature	time
1	Polymerase activation	95°C	2 min
2	Denature	95°C	20 s
3	Annealing	50-75°C *	10 sec
4	Extension	70°C	10-25 s/kb **
	repeat step 2-4	25 cycles	
5	Final elongation	70°C	10 min
6	Cool down	4°C	hold

* lowest primer melting temperature; ** extension time is dependent on the PCR product length: <500 bp: 10 s/kb; 500-1000 bp: 15 s/kb; 1000-3000 bp: 20 s/kb; > 3000 bp: 25 s/kb

PCR product was analyzed by agarose gel electrophoresis (2.2.4) and, if required, the DNA fragment was purified using GeneJet Gel extraction Kit (Thermo Fisher Scientific) according to manufacturer's protocol.

2.2.7 DNA sequencing

Plasmid DNA sequencing was performed by GATC Biotech according to the company's guideline. Sequencing results were analyzed using ContigExpress® software (Vector NTI®, Invitrogen).

2.2.8   Isolation of genomic DNA

Genomic DNA (gDNA) was isolated from cell suspensions of organs from mice or from cell culture pellets using the DNeasy® Blood and Tissue Kit (Qiagen) or QiAamp DNA Mini Kit (Qiagen) according to the manufacturer's protocol. When isolating gDNA from blood, maximum of 100 µl blood was used as starting material. A maximum of $5x10^6$ cells was used to isolate gDNA from freshly prepared or -20°C frozen cell pellets. DNA concentration was photometrically analyzed (NanoDropTM 2000c, Thermo Fisher Scientific).

2.2.9   Quantitative polymerase chain reaction

Quantitative real-time PCR (qPCR) allows quantification of specific DNA sequences by monitoring the sequence amplification with fluorescent dyes during the PCR in real-time. Transgene integration of cells transduced by LVs was quantified by vector copy number (VCN) analysis. Vector copies were quantified by TaqMan-based qPCR in a multiplex approach using the SensiFAST Probe No Rox Kit (Bioline) and LightCycler® 480 Instrument II (Roche) (Table 3) with cycle conditions given in Table 4. Transgene was detected using woodchuck hepatitis posttranscriptional element (WPRE)-specific probe and primers. A human albumin-specific probe and primers served as an internal reference.

Table 3: qPCR reaction

component	volume in µl
2x SensiFAST Probe No ROX	10
Probe-albumin(2 µM)	2
albumin fwd (10 µM)	0.4
albumin rev (10 µM)	0.4
Probe-WPRE (2 µM)	2
WPRE fwd (10 µM)	0.4
WPRE rev (10 µM)	0.4
DNA template	up to 4.4
H_2O, nuclease free	ad 20

Table 4: qPCR cycle conditions

	step	temperature	time
1	Initial denaturation	95°C	5 min
2	Denaturation	95°C	10 s
3	Annealing + Extension	60°C	40 s
	repeat step 2-3, 40 cycles		
4	Cool down	10°C	hold

Data were analyzed using LightCycler® Software. For quantification, a plasmid standard containing sequences of WPRE and human albumin (pS-Albumin-W) was used and VCN were calculated as the ratio of (copies WPRE)/(copies albumin).

2.2.10 Ligation-mediated (LM)-PCR

Lentiviral integration sites were analyzed by amplifying the 3' LTR as described in (Schmidt et al., 2001). These analyses were performed in close collaboration with Prof. Dr. Dr. Modlichs group (group "Gene modification in Stem Cells", Paul-Ehrlich-Institut) with F. Schenk.

Isolated gDNA (2.2.8) was digested with *Tsp*5091 (Thermo Fisher Scientific) (5 U per 1 µg DNA) at 65°C for 3 h and precipitated with 100% ethanol, 20 µg glycogen and 0.1 M Na-acetate. Primer extension was performed by using the *Pfu* polymerase (Thermo Fisher Scientific) and 0.5 pmol of biotinylated lentiviral primer lvLTRI with cycle conditions given in Table 5.

Table 5: Cycle conditions for primer extension

	step	temperature	time
1	Denaturation	94°C	5 min
2	Annealing	64°C	30 min
3	Extension	72°C	15 min

The extension product was purified by QIA Quick PCR purification Kit (Qiagen), diluted in 40 µl H$_2$O and enriched using magnetic beads (Dynabeads, in 2x BW buffer (10 mM Tris [pH 7.5], 1 mM EDTA, 2 mM NaCl). The product was mixed with 40 µl magnetic beads and incubated at constant rotation for 5 h at RT. Captured DNA was washed twice using 100 µl H$_2$O, resuspended in ligation mix with 80 U of T4-Ligase and linker oligos, and incubated at 16°C overnight. For amplification, two PCR reactions followed. Hi-Fidelity PCR Master Mix (Thermo Fisher Scientific) was used and cycle conditions are given in

Table 6. For the first PCR, 1 µl of the product, lvLTR2 primer and the linker-specific primer OCI were used. The second PCR was performed with the PCR product (1:350 diluted in H_2O) under same conditions using lvLTR3 and OCII primer. PCR products were analyzed by gel electrophoresis (2.2.4).

Table 6: Cycle conditions for first and second PCR

	step	temperature	time
1	Initial denaturation	94°C	2 min
2	Denaturation	94°C	15 s
3	Annealing	60°C	30 s
4	Extension	68°C	4 min
	repeat step 2-4 for 30 cycles		
5	Final elongation	68°C	10 min

2.3 Cell culture and virological methods

2.3.1 Cultivation of eukaryotic cell lines

Cells were cultivated at 37°C, 5% CO_2 and 90% humidity in a cell culture incubator and handled under sterile conditions using a laminar flow cabinet. HEK-293T cells were cultivated in DMEM (10% FCS, 1% L-glutamine). Hut-78, MOLT4.8 and Raji cells were cultivated in RPMI (10% FCS, 1% L-glutamine). Raji-luc cells were cultivated in RPMI (10% FCS, 1% L-glutamine, 1mg/ml geneticin). Cells were passaged 2-3 times per week. For adherent cells, medium was removed. Cells were washed with phosphate buffered saline (PBS) and detached with trypsin working solution. Cells were resuspended in fresh medium and appropriate fraction of cells was transferred into a new cell culture flask with fresh medium. For passaging of suspension cells, cells were resuspended and an appropriate fraction of cells was seeded into a new cell culture flask with fresh medium. Cell lines were regularly checked for mycoplasma decontamination by PCR.

2.3.2 Freezing and thawing of cells

For freezing cells, cell suspensions were counted and centrifuged at 300xg for 3 min. Cell pellet was resuspended in appropriate volume of cold freezing medium and aliquoted. Cryovials were transferred to Mr. Frosty™ container (Thermo Fisher Scientific) and frozen

at -80°C. After 24 h, cryovials were transferred to the gas phase of liquid nitrogen for storage.

Frozen cells were thawed in a 37°C water bath and resuspended in 10 ml prewarmed medium. Cells were pelleted at 300xg for 3 min, resuspended in appropriate medium, transferred to a cell culture flask and incubated at 37°C

2.3.3 Isolation of PBMC

Human PBMC were isolated from fresh blood of healthy anonymous donors that had given informed consent, or from buffy coats purchased from the German Red Cross blood donation center (DRK-Blutspendedienst Baden-Württemberg-Hessen, Frankfurt). Cell preparation tubes or Histopaque®-1077 gradient were used to separate PBMC from other blood components by density centrifugation. PBMC isolation with CPT tubes (Becton Dickinson) was performed according to manufacturer's protocol and the mononuclear cell layer was transferred to a fresh tube. For isolation of PBMC using the Histopaque®-1077 gradient, blood was diluted 1:1 in PBS/EDTA and 35 ml of the mixture was overlaid onto 15 ml Histopaque®-1077 layer. After 30 min of centrifugation at 20°C, 1800 rpm in a swinging bucket rotor without break (Varifuge 3.0RS, Heraeus), mononuclear cell layer was aspirated and transferred to a fresh tube. PBMC were washed with 40 ml PBS/EDTA using a centrifugation step for 10 min at 300xg. To remove platelets, PBMC were resuspended in 40 ml PBS/EDTA and centrifuged for 15 min at 200xg. Erythrocytes were lysed using BD Pharm Lyse™ (Becton Dickinson) according to manufacturer's protocol. PBMC were washed twice and were either activated (2.3.4), used for cell depletion (2.3.5) or were frozen (2.3.2).

2.3.4 Activation and cultivation of T cells

Prior to activation, 24 well plates were coated with 1 µg/ml anti-human CD3 mAb (clone OKT3, Miltenyi Biotec) (dissolved in PBS) for 2 h at 37°C or overnight at 4°C. Antibody solution was removed and blocking solution was added. After 30 min of incubation at 37°C, the solution was removed and wells were washed twice with PBS.

For activation, freshly isolated or thawed PBMC were used. $2x10^6$ cells were seeded on 24 well plates in 2 ml T cell medium supplemented with 100 U/ml IL-2 (Miltenyi Biotec) and 3 µg/ml anti-human CD28 mAb (clone: 15E8, Miltenyi Biotec). PBMC were incubated for 72 h at 37°C.

For cultivation of PBMC, depending on cell density, cells were passaged every 2-3 days or supplied with fresh medium by replacing the old medium with fresh T cell medium containing 100 U/ml IL-2 every 2-3 days.

2.3.5 CD19+ cell depletion

PBMC were depleted of CD19+ cells by MACS® Separation (Miltenyi Biotec) using MicroBeads (Miltenyi Biotec) specific for CD19. According to manufacturer's protocol, cells were labelled with MicroBeads and loaded onto a LD Column (Miltenyi Biotec), which was placed in a magnetic field of the MACS Separator to retain magnetically labelled cells. Both fractions, unlabeled depleted cells as well as labelled enriched cells were analyzed for CD3 and CD19 expression by flow cytometry. Cells of the CD19-depleted fraction were either frozen (2.3.2) until further usage or activated (2.3.4).

2.3.6 Generation of vector particles

For vector particle generation, HEK-293T cells were transiently transfected using Polyethylenimine (PEI). One day prior transfection, 1×10^5 cells were seeded per T175 flask. On the day of transfection, medium was replaced with 10 ml DMEM (15% FCS, 2 mM L-glutamine) and the transfection mix was prepared. Per flask, 35 µg DNA was diluted in 2.3 ml DMEM without (w/o) additives. For CD8-LV production, 0.9 µg of plasmid pCAGGS-NiV-GcΔ34^{CD8}mut4, 4.49 µg of plasmid pCAGGS-NiV-FΔ22, 14.5 µg of the packaging plasmid pCMVΔR8.9 and 15.2 µg of the transfer vector encoding either Luc-GFP (pS-luc-gfp-W), CD19 CAR (pS-CD19CAR-W) or RFP (pS-rfp-W) were used. 140 µl PEI was diluted in 2.2 ml DMEM and both solutions were mixed and vortexed, incubated at RT for 15-20 min and added to the cells. 24 h later, medium was exchanged with DMEM (10% FCS, 2 mM L-glutamine). Two days after transfection, vector particles released into the cell supernatant were harvested and filtrated through 0.45 µm filter. Concentration and purification of vector particles was performed by ultracentrifugation through 20% (w/v) sucrose cushion at 28.000 rpm, 4°C for 3 h (Beckmann Coulter, Beckman SW28) or at 4500 rpm for 24 h at 4°C (Multifuge XR3, Heraeus). The supernatant was discarded, the pellet was dissolved in 60 µl PBS and vector particles were stored at -80°C.

2.3.7   Transduction and titration of vectors

For transduction, 2-4x10^4 MOLT 4.8 cells were seeded in 96-well plates. Vector was added to the cells (maximum total volume of 200 µl) which were incubated 96 h at 37°C prior to analysis. To determine vector titers, 2-4x10^4 MOLT 4.8 cells were seeded in 96-well plates. Vector particles were added in serial dilution and cells were incubated for 96 h at 37°C. Transgene expression was analyzed by flow cytometry. Based on dilutions showing a linear correlation between the dilution factor and the percentage of transduced cells, titer was determined as transducing units per ml (t.u./ml).

2.3.8   Transduction of PBMC

For transduction of primary human PBMC, 1x10^5 activated PBMC were seeded in T cell medium, supplied with 100 U/ml IL-2 per 48-well. Vector was added to the cells (maximum total volume of 300 µl) and spinfection was performed by centrifugation at 850xg for 90 min at 32°C. Wells were filled up to 1 ml with T cell medium, supplied with 100 U/ml IL-2. Transgene expression was determined by flow cytometry (2.3.9) five days post transduction.

2.3.9   Flow Cytometry

Adherent and suspension cells
Adherent cells were detached using trypsin working solution, resuspended in medium and transferred to micronic tubes. Suspension cells were resuspended prior to transferring them in micronic staining tubes. They were washed twice with FACS washing buffer by centrifugation at 300xg for 3 min. Cells were incubated with appropriate antibody dilution (in FACS washing buffer) for 30 min at 4°C before they were washed twice and fixed with 100-200 µl FACS fix. Flow cytometric analysis was performed at the LSRII (BD Biosciences) or MACSQuant Analyzer10 (Miltenyi Biotec) and data were analyzed using FCS Express V4 and V6 (De Novo Software).

Blood and organ-derived cell suspensions
For flow cytometry analysis, maximum of 100 µl blood or 1-5x10^6 cells were used. Cells were washed twice with FACS washing buffer and incubated with murine FcRblock (Miltenyi Biotec) according to manufacturer's protocol. After 15 min incubation at 4°C, antibody dilution (in FACS washing buffer) was added and cells were incubated for 30 min at 4°C. If required, erythrocytes were removed using BD Pharm Lyse (Becton Dickinson)

by resuspending the cells in 1 ml 1x lysis buffer. After 15 min incubation at room temperature (RT), cells were washed twice with PBS (1% FCS) and stained with LIVE/DEAD™ Fixable Dead Cell Stain (ThermoFisher Scientific) according to manufacturer's protocol for 30 min at 4°C. Cells were washed twice and fixed with FACS fix prior flow cytometry analysis.

For the analysis of cells derived from blood or organs from mice, in general, following gating strategy was applied, unless stated differently. Cells were excluded for cell debris and hierarchically gated as follows. Single cells were gated for living cells. Human cells were identified as CD45$^+$ cells and further gated for T cells by CD3 expression. CD3$^+$ cells were analyzed for CD8 expression and transgene expression was analyzed within CD3$^+$CD8$^+$ or CD3$^+$CD8$^-$ cells. CD19$^+$ cells were gated from CD45$^+$ cells, whereby CD19$^+$ Raji cells were distinguished from CD19$^+$ B cells by the MFI of CD45. Thereby, CD45^{high}CD19$^+$ cells were identified as B cells and CD45^{low}CD19$^+$ cells were identified as Raji cells. Flow cytometric analysis was performed at the LSRII (BD Biosciences) and data were analyzed using FCS Express V4 and V6 (De Novo Software).

2.3.10 Killing assay

The cytotoxicity of CAR T cells was determined by a flow cytometry-based assay. In general, CAR T cells (effector cells) were co-cultured with tumor cells (target cells) and killing efficacy was determined by analyzing dead cells after 4h of co-culture. Thereby, tumor cells were labelled with a fluorescent dye to distinguish between dead CAR T cells and killed tumor cells. Killing efficacy was evaluated in various effector to target ratios ranging from 5:1 to 0.15:1.

One day prior to killing assay, CAR expression was analyzed by flow cytometry (2.3.9). Only CAR$^+$ T cells were counted as effectors. Prior to target cell labelling, cells were washed twice with PBS by centrifugation at 300xg for 3 min. Cells were labelled with carboxyfluorescein succinimidyl ester (CFSE) according to the manufacturer's protocol. In detail, 2.5 µM CFSE working solution (in PBS) was pre-warmed at 37°C in a water bath. 1×10^6-4×10^7 target cells were resuspended in 1 ml CFSE working solution for 10 min at 37°C. 1 ml FCS was added and cells were incubated on ice for additional 10 min before they were washed twice in PBS and resuspended in RPMI (10% FCS, 1% L-glutamine). Cells were stored temporarily at 37°C. CAR T cells were washed once and resuspended in RPMI (10% FCS, 1% L-glutamine). For the different effector to target ratios, CAR T cell dilutions were prepared. For co-incubation, 5×10^4 target cells in 100 µl were transferred to round-bottom 96-well plates. 100 µl of each CAR T cell dilution was added to the designated well and cells were co-cultivated for 4 h at 37°C. Cells were washed twice

prior to dead cell staining with the Fixable Viability Dye eFluor450™ according to manufacturer's protocol. Cells were fixed using FACS fix and analyzed by flow cytometry. The percent killing of target cells was calculated by multiplying the ratio of the number of dead CFSE$^+$ cells and the total cell number of CFSE$^+$ cells with 100.

2.3.11 Irradiation of cells

Prior to irradiation, cells were expanded as needed. On the day of irradiation, cells were washed once, counted and resuspended in prewarmed RPMI medium (10% FCS, 1% L-glutamine). $2x10^8$ cells were resuspended in 50 ml medium and mitotically inactivated by γ-irradiation. Raji cells were irradiated with 15 Gy, Hut-78 cells with 25 Gy. Cells were centrifuged at 300xg for 10 min, resuspended in freezing medium, aliquoted and stored in the gas phase of liquid nitrogen until usage.

2.3.12 Proliferation assay

The proliferation assay allows evaluation of the proliferative capability of CAR T cells. In the presence of antigen-positive cells, selective expansion of CAR T cells was evaluated by flow cytometry analyzing the percentage of CAR expressing cells within co-culture.
Human PBMC were activated and transduced (2.3.4, 2.3.8). CAR expression was analyzed by flow cytometry five days post transduction. Dependent on the percentage of CAR$^+$ cells, the amount of cells was calculated to have $1x10^4$ CAR T cells present at start of the co-culture, or $1x10^4$ green fluorescent protein (GFP)-positive cells as control. To compensate for varying transgene expression and thereby varying total cell number of plated cells, wells were filled up with untransduced cells to normalize total cell numbers between co-cultures of CAR- or GFP-positive cells. Same amount as transgene-positive cells or 10-fold excess of irradiated cells (2.3.11) were added to transgene-positive cells. Co-culture was performed in 48-well plate using T cell medium, supplemented with 50 U/ml IL-2. Every 2-3 days, medium was exchanged and irradiated cells were added, or cells were passaged if required. At given time points, cells were analyzed for CD8 and CAR expression by flow cytometry.
For the proliferation assay, starting with less than 1% CAR T cells (Figure 17), $2x10^5$ cells, of which 0.5% were transgene-positive were used to start the co-culture. Due to the low amount of total CAR-positive T cells, the same amount ($2x10^5$) of irradiated target cells was added at the start of co-culture to enable cell-cell contact of CAR T cells with target cells.

2.3.13 Generation of stably transgenic cell lines

Cells, stably expressing an introduced transgene were generated by transduction with a LV encoding for the transgene. Raji-luc cells were generated by transduction with VSV-G-pseudotyped LV, transferring the luciferase transgene and neomycin resistance gene. LVs were generated by transient transfection of HEK-293T cells (2.3.6). In particular, VSV-G-pseudotyped LV were generated in 6-well format by triple transfection of HEK-293T with 3.4 µg pMD2.G, 6.3 µg pCMVΔ8.9 and 0.96 µg transfer vector (pH-Luc-IRES-Neomycin). Two days after transfection, supernatant was harvested and filtrated through 0.45 µm filter. Unconcentrated supernatant was used for transduction of Raji cells. For this, $1x10^5$ cells were seeded in 48-well and transduced with different volumes of vector stock (0.1 µl-100 µl) with a maximum total volume of 300 µl. On the next day, wells were filled up with RPMI (10% FCS, 1% L-glutamine) to 1 ml. Three days after transduction, transgene expressing cells were selected by RPMI (10% FCS, 1% L-glutamine) supplemented with geneticin (1 mg/ml). Raji-luc cells were selected for two weeks and were verified for luciferase expression using the luciferase assay system (Promega) according to the manufacturer's protocol. Raji-luc cells were expanded and frozen (2.3.2).

2.4 Experimental mouse work

Animal experiments were performed in accordance to the German animal protection law and the respective European Union guidelines. NSG mice were purchased from Jackson Laboratory and from in-house breeding facility (Paul-Ehrlich-Institut). Mice were housed in the animal facility within individually ventilated cages (IVCs) and handled under a laminar flow hood.

2.4.1 Administration of PBMC

Freshly isolated or thawed PBMC were activated for three days (2.3.4) before administration into mice. On the day of administration, PBMC were washed twice with PBS by centrifugation at 300xg for 10 min, counted using MACSQuant Analyzer10 and resuspended in appropriate volume of PBS. For intravenous administration, mice were prewarmed using red light, in particular the tail to dilate blood vessels. Mice were restrained using a mouse restrainer and $1.5x10^7$ cells resuspended in 200 µl PBS were injected into the tail vein using a 29 gauge needle. For intraperitoneal injection, mice were

restrained and $1x10^7$ cells resuspended in 200 μl PBS were administered using a 29 gauge needle.

2.4.2   Administration of tumor cells

Two weeks prior to administration, a fresh batch of Raji-luc cells was thawed and expanded as needed. On the day of administration, cells were washed twice with PBS by centrifugation at 300xg for 10 min. Cells were counted using MACSQuant Analyzer10 and resuspended in an appropriate volume of PBS. For intravenous and intraperitoneal administration, $5x10^5$ cells resuspended in 200 μl PBS were injected using a 29 gauge needle.

2.4.3   Administration of vector particles

Prior to administration, vector aliquots were thawed on ice and pooled. For intravenous administration of CD8-LV(Luc-GFP), 200 μl of vector stock was administered. Titers of three independent vector productions were determined on MOLT4.8 cells with an average titer of $9.5x10^7$ t.u./ml ± $7.1x10^6$ t.u./ml. Hence, on average $1.9x10^7$ t.u. were administered per mouse. For administration of CD8-LV(CAR), an average titer of $1.1x10^7$ t.u./ml ± $9.7x10^5$ t.u./ml was determined on MOLT4.8 cells for five independent vector productions. 200 μl of vector stock was intraperitoneally administered to mice resulting in $2.2x10^6$ t.u. per mouse. When comparing transgene delivery between CD8 LV(CAR) and CD8-LV(RFP) in mice, same amount of transducing units was administered. For this purpose, vectors were titrated on activated PBMC, which in general resulted in lower titers compared to titer determination on MOLT4.8 cell line. For example the same vector stock of CD8-LV(CAR) resulted in lower titers on PBMC than on MOLT4.8. When administering CD8-LV(CAR) and CD8-LV(RFP), on average $1.6x10^4$ t.u. were injected per mouse.

2.4.4   *In vivo* Imaging

In vivo imaging allows visualization of luciferase expressing cells in living mice. With the use of the IVIS® Imaging System (Caliper Life Science) luciferase signals can be analyzed and quantified using the Living Image software (Caliper Life Science). For this purpose, 150 mg D-luciferin (in PBS) per kg body weight was i.p. injected into mice. Mice were anesthetized with 2-3% isoflurane using a XGI-8 Gas Anesthesia system (Caliper Life Science) and imaged 10 min post luciferin administration.

2.4.5   Blood sampling

Blood was taken retroorbital from mice. For this purpose, mice were anesthetized with 2-3% isoflurane. Blood was taken using a thin sterilized glass capillaries and blood was transferred into BD microtainer® LH tubes (Becton Dickinson).

2.4.6   Preparation of single cell suspensions from organs

Mice were anesthetized with 2-3% isoflurane and sacrificed by cervical dislocation. Blood was taken, peritoneal cells were isolated by peritoneal lavage, specified organs (spleen, liver, lung, bone marrow) were removed and single cell suspensions prepared (2.4.6.1, 2.4.6.2, 2.4.6.3). Cells were used for flow cytometry analysis (2.3.9) and $1-5 \times 10^6$ cells were pelleted and frozen for gDNA isolation (2.2.8).

2.4.6.1   Isolation of peritoneal cells by peritoneal lavage

Mice were sprayed with 70% ethanol, mounted on styrofoam on its back and the outer skin was pulled back. 5-10 ml PBS were slowly injected using a 24 gauge needle into the peritoneal cavity and gently massaged prior to collecting the fluid. Cell suspension was transferred in a tube, washed once and resuspended in PBS (2% FCS).

2.4.6.2   Preparation of spleen, lung and liver cells

Spleen, lung and liver were removed, transferred to PBS and stored on ice until further processing. Single cell suspensions from spleen were obtained by meshing the tissue through a 45 µm cell strainer. For lung and liver tissue dissociation, dissociation kits for murine lung or liver tissue (Miltenyi Biotec) were used together with the gentleMACS dissociator (Miltenyi Biotec) according to manufacturer's protocol. In brief, enzyme mix was added to dissected lung or liver tissue within a gentleMACS C tube (Miltenyi Biotec). GentleMACS C tubes were placed into the gentleMACS and lung or liver program was started. Single cell suspensions were applied to a 70 µm cell strainer. Cells were washed once and resuspended in PBS (2% FCS).

2.4.6.3   Preparation of bone marrow cells

For bone marrow cell isolation, femur and tibia were removed. Residential tissue was removed and the bone was cut at both ends. Using a 30 gauge needle, cells from the

bone were flushed out with PBS until the flow through turned white. Cells were washed once and resuspended in PBS (2% FCS)

2.5 Statistical analysis

Statistical significance was determined as indicated in figure legends. In general, statistical significance between two groups was determined using unpaired student´s *t* and Mann-Whitney tests. P values are given in the figure legends. GraphPad Prism 7 software was used for statistical analysis.

3 Results

This thesis describes the usage of a CD8-targeted lentiviral vector to deliver transgenes selectively to CD8$^+$ cytotoxic T cells *in vivo*. Successful *in vivo* gene transfer into CD8 T cells was first shown via reporter gene transfer into PBMC-humanized NSG mice upon CD8-LV administration. The transfer of a gene encoding a chimeric antigen receptor resulted in the *in vitro* generation of CAR T cells. Remarkably, upon administration of CD8-LV(CAR) into mice CAR T cells were generated *in vivo*. Furthermore, *in vivo* generated CAR T cells have proven to be functional, being able to proliferate upon antigen exposure and to eliminate CD19$^+$ cells *in vivo*.

3.1 *In vivo* reporter gene transfer into CD8$^+$ lymphocytes

For the purpose of targeting CD8 T cells, NiV-pseudotyped lentiviral vectors were previously generated and well characterized (Bender et al., 2016). Concentrated vector stocks reached titers of 1x10^8 t.u./ml for particles carrying the *gfp* transgene, CD8-LV(GFP). *In vitro* analysis demonstrated selective and stable reporter gene transfer into human CD8$^+$ cytotoxic T cells. However, *in vivo* transgene delivery had not been evaluated with CD8-LV and is addressed in the following chapter.

3.1.1 *In vivo* luminescence imaging reveals organ-wide distributed reporter gene expressing cells

The ability of CD8-LV to deliver reporter genes *in vivo* into human CD8 T cells was evaluated in mice. Since the human CD8 receptor was targeted, the PBMC-humanized NSG mouse model was used. The administration of human PBMC into immunocompromised NSG mice results in engraftment of human immune cells mainly consisting of CD8$^+$ and CD4$^+$ T cells. Systemic administration of CD8-LV transferring both the *gfp* as well as the *luciferase* (*luc*) reporter genes (Luc-GFP) enabled the analysis of *in vivo* transduced cells.

In detail, 1.5x10^7 activated human PBMC were injected i.v. into immunocompromised NSG mice, followed by i.v. injection of CD8-LV(Luc-GFP) seven days later. *In vivo* transduced cells were monitored by *in vivo* bioluminescence imaging 14 days after vector administration (Figure 6).
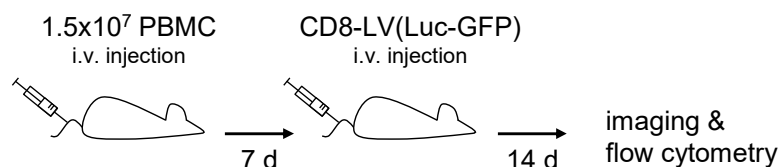
Figure 6: Experimental setting for the *in vivo* reporter gene transfer with CD8-LV into PBMC-humanized NSG mice
Human PBMC were activated for three days using IL-2, αCD3- and αCD28-antibodies. 1.5×10^7 activated PBMC were i.v. injected into NSG mice. Seven days later, CD8-LV(Luc-GFP) was i.v. administered. 14 days later, transduced cells were monitored via *in vivo* luminescence imaging. Mice were sacrificed and cell suspensions were analyzed by flow cytometry.

For PBS-treated control mice, no luciferase signals were detected (Figure 7, bottom row). In contrast, CD8-LV(Luc-GFP)-treated mice showed luciferase signals distributed all over the body. Dorsal and ventral imaging revealed stronger signals in the lung (Figure 7, upper row, left) and in the spleen (Figure 7, upper row, middle). Mice were sacrificed and spleen, liver, heart, lymph node-like structures, lung and kidney were removed and imaged immediately. Imaging of the removed organs revealed luciferase signals in the lung and in the spleen (Figure 7, upper row, right).
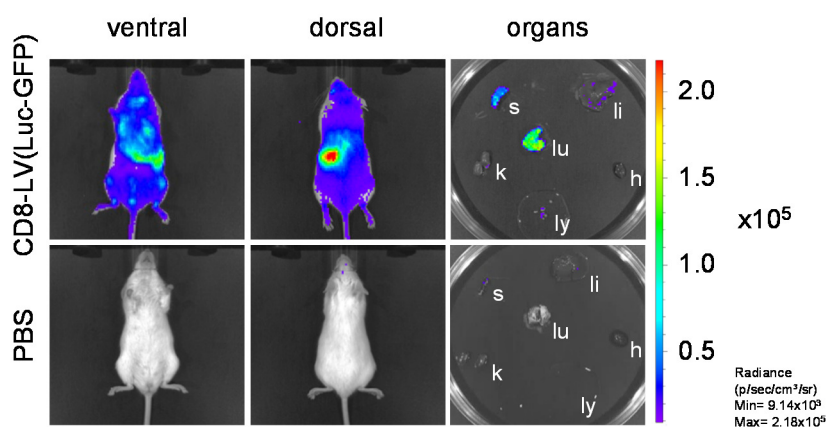
Figure 7: *In vivo* imaging of CD8-LV(Luc-GFP)-treated PBMC-humanized NSG mice
PBMC-humanized NSG mice treated with CD8-LV(Luc-GFP) were monitored for transduced cells by *in vivo* bioluminescence imaging 14 days after vector administration. PBS-treated mice served as control. Ventral and dorsal sites of the mice were imaged. Mice were sacrificed and organs were explanted and analyzed. One representative mouse from three independent experiments is shown. s, spleen; li, liver; lu, lung; k, kidney; h, heart; ly, lymph node-like structures.

The detection of luciferase signals indicated successful *in vivo* transduction of cells with CD8-LV(Luc-GFP). *luc* transgene-modified cells were distributed throughout the body with higher presence in the lung and in spleen.

3.1.2 Exclusive transduction of CD8$^+$ cells

To further assess the selectivity of CD8-LV *in vivo*, the transduced cells were characterized. Blood cells as well as cell suspensions from spleen and lung were analyzed by flow cytometry. Cell debris was excluded and single cells were gated from the main population. Dead cells were excluded and human cells were identified as CD45$^+$ cells. T cells were identified as CD3$^+$ cells further separated in CD8$^+$ and CD8$^-$ cells. Both populations were analyzed for GFP expression and fluorescence background levels were determined on CD8$^+$ and CD8$^-$ cells of identically treated cells of PBS-injected mice. Humanization level of mice ranged between 20-80% for the different organs. More than 98% of the CD45$^+$ cells were CD3$^+$ (data not shown). PBS-treated mice showed minor background levels in CD8$^+$ and CD8$^-$ cells ranging between 0-0.02% GFP$^+$ cells for all organs (Figure 8A-C, bottom panels) with highest levels in the lung (0.02% ± 0.01%). However, these events were characterized by a low mean fluorescence intensity (MFI) being close to the left gate border.
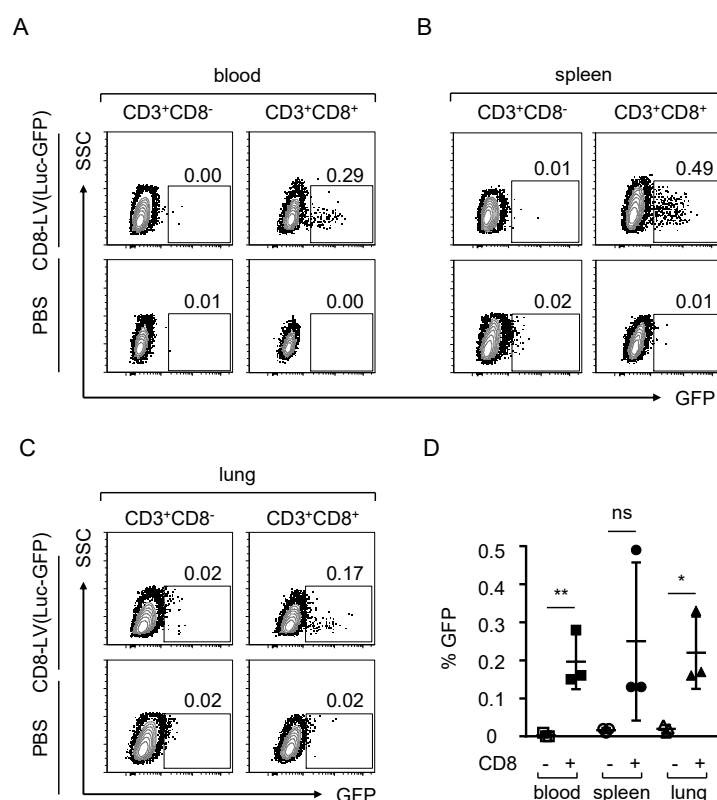
Figure 8: Flow cytometry analysis of blood, spleen and lung cells of CD8-LV(Luc-GFP)-treated PBMC-humanized NSG mice
Single cell suspensions from spleen, blood and lung of CD8-LV(Luc-GFP)- and PBS-treated mice were analyzed by flow cytometry. Dead cells were excluded and human cells were identified as CD45$^+$ cells. From all human cells, T cells were identified as CD3$^+$ cells, further distinguished for CD3$^+$CD8$^+$ and CD3$^+$CD8$^-$ cells and analyzed for GFP expression. GFP expression was determined on CD3$^+$CD8$^+$ and CD3$^+$CD8$^-$ cells in (A) blood, (B) spleen and (C) lung cells. One representative of three individual mice is shown. (D) Percentage of GFP$^+$ cells in CD8$^+$ (+) and CD8$^-$ (-) cells. N=3, mean ± standard deviation (SD) are shown. Statistical significance was determined by two-tailed unpaired t-test; *, p<0.05; **, p<0.01, ns, not significant.

Remarkably, in the blood of CD8-LV(Luc-GFP)-treated mice GFP$^+$ cells were detected exclusively within the CD8$^+$ population (Figure 8A, top panel). No GFP expression was observed in CD8$^-$ cells. Similarly, GFP$^+$ cells were detected in spleen (Figure 8B, top panel) and lung (Figure 8C, top panel) with varying frequencies of CD8$^+$GFP$^+$ cells. These events were characterized by higher MFI, compared to above mentioned events in PBS-treated mice. On average 0.2% (± 0.07%) CD8$^+$GFP$^+$ cells were detected in blood, 0.25% (± 0.21%) in spleen and 0.22% (± 0.10%) in the lung (Figure 8D).

Previous analysis was performed on CD8$^+$ and CD8$^-$ cells, pre-gated for human markers CD45 and CD3. To evaluate off-target transduction, GFP expression was analyzed on all cells, independently of murine or human origin. Hence, GFP expression was analyzed within CD8$^+$ and CD8$^-$ cells of side- and forward scatter-gated cells. This analysis, using the different gating strategy, is exemplarily shown for lung cells. As expected, the highest frequency of GFP$^+$ cells was observed in CD8$^+$ cells of CD8-LV(Luc-GFP) treated mice. Few GFP events were detected in CD8$^-$ cells, but their numbers were similar to events observed in PBS-treated control mice (Figure 9).
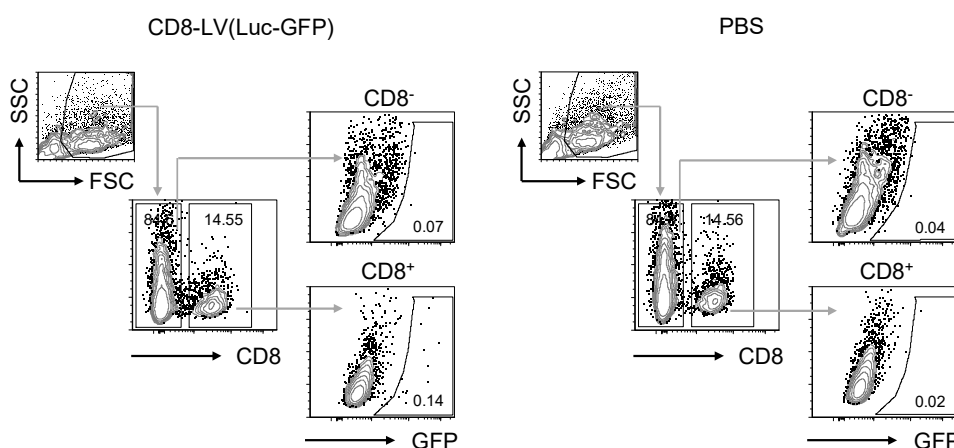
Figure 9: Analysis of off-target GFP expression in lung cells of CD8-LV(Luc-GFP)-treated PBMC-humanized NSG mice
Single cell suspensions of the lung from CD8-LV(Luc-GFP)-treated and PBS-treated mice were analyzed by flow cytometry. Side- and forward scatter gated cells including murine and human cells were analyzed for CD8 expression. GFP expression was analyzed in CD8$^+$ and CD8$^-$ cells. One representative of three individual mice is shown.

Luciferase signals and GFP$^+$ cells demonstrated successful *in vivo* reporter gene delivery upon systemic administration of CD8-LV(Luc-GFP) into PBMC-humanized NSG mice. Remarkably, CD8-LV(Luc-GFP) mediated selective gene transfer into human CD8$^+$ lymphocytes. Although some minor GFP events within CD8$^-$ cells were detected, GFP events with similar frequency were detected in PBS-treated control mice, rather indicating false-positive events than real off-target transduction. GFP expression was largely present in CD8$^+$ cells demonstrating the highly selective targeting capability of CD8-LV *in vivo*.

3.2 CD8-LV-mediated generation of CAR T cells and functional characterization *in vitro*

Having shown that CD8-LV selectively mediated reporter gene delivery in PBMC-humanized NSG mice *in vivo*, the next step was to deliver a CAR gene. To set up the system, CAR gene transfer was first evaluated *in vitro*. For this purpose, CD8-LVs encoding a CD19-specific CAR were generated and characterized on cell lines as well as on primary cells to generate functional CAR T cells *in vitro*.

3.2.1 Vector particle generation and titration

A CD19-specific CAR was used throughout this work. The scFv was derived from the CD19-specific clone FMC63 (Nicholson et al., 1997). The CAR construct was encoded on the transfer plasmid pS-CD19CAR-W (Figure 10). As second generation CAR, the SFFV promotor-driven construct consists of the intracellular signalling domain CD3ζ and the co-stimulatory domain of CD28, which are fused to the CD28 transmembrane domain. A CD8 hinge as well as a myc-tag, which can be used for detection of CAR expression, link the TM domain to the αCD19-scFv.

pS-CD19CAR-W

Figure 10: Scheme of the CAR construct
Schematic drawing of the CD19-specific CAR within the lentiviral transfer vector pS-CD19CAR-W. The CAR construct is driven by an internal SFFV promoter. The αCD19-scFv (FMC63-derived) is linked to a CD8 hinge via a myc-tag, followed by the CD28 transmembrane domain and the intracellular signaling domains of CD28 and CD3ζ. scFv, single chain variable fragment; SFFV, spleen focus forming virus; TM, transmembrane domain.

To generate functional CAR T cells, it is critical that the CAR is efficiently expressed on the cell surface. Hence, CAR expression and detection via the myc-tag was evaluated on HEK-293T cells transfected with pS-CD19CAR-W. CAR surface expression was determined 48 h post transfection by flow cytometry using a phycoerythrin (PE)-labelled anti-myc-tag antibody. Untransfected cells incubated with the anti-myc-tag antibody served as control.

99.2% of transfected cells showed CAR surface expression. The population was characterized by a high MFI (Figure 11). In conclusion, pS-CD19CAR-W mediated efficient CAR surface expression in transfected HEK-293T cells.
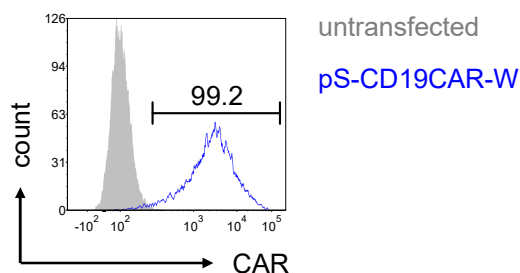
Figure 11: CAR surface expression of transfected HEK-293T cells
HEK-293T cells were transfected with pS-CD19CAR-W (blue). CAR expression was determined 48 h later by flow cytometry using PE-labelled myc-tag antibody. Untransfected cells (grey) stained with the same antibody served as control.

Next, CD8-LV(CAR) vector particles were generated via transient transfection of producer cells. HEK-293T cells were co-transfected with pCMVΔR8.9, pCAGGS-NiV-FcΔ22, pCAGGS-NiV-GcΔ34^{CD8}mut4 and pS-CD19CAR-W. Vector particles were harvested 48 h later and purified via centrifugation through sucrose cushion. CAR gene transfer with CD8-LV(CAR) into CD8$^+$ cells was evaluated on the T cell line MOLT4.8. Cells were incubated with 5 µl of vector stock at 37°C and CAR surface expression was determined four days later. Untransduced cells incubated with PE-labelled anti-myc-tag antibody served as negative control.

Low background signals were detected for untransduced cells whereas 52.81% of the CD8-LV(CAR)-treated cells showed CAR expression (Figure 12), demonstrating successful *in vitro* generation of CAR T cells using CD8-LV(CAR).
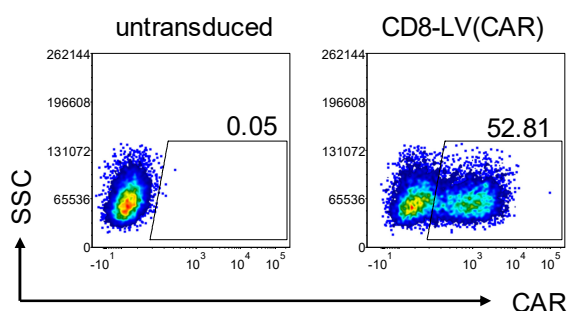
Figure 12: CAR surface expression of CD8-LV(CAR)-transduced MOLT4.8 cells
Cells were transduced with 5 µl vector stock of CD8-LV(CAR) and analyzed by flow cytometry four days later. CAR surface expression was determined by staining using PE-labelled myc-tag antibody. Untransduced cells stained with the same antibody served as a control.

For further analysis, the amount of functional vector particles was determined for each vector production by titration on MOLT4.8 cells. Cells were incubated with serial dilutions of vector particles. Four days later, the percentage of CAR expressing cells was analyzed by flow cytometry and the titer was calculated within linear correlation of the dilution factor

and the percentage of CAR$^+$ cells. Five independent productions of CD8-LV(CAR) vector stocks showed an average titer of 1.1×10^7 t.u./ml ($\pm 9.7 \times 10^5$ t.u./ml).

These data demonstrated successful production of CD8-LV(CAR) particles which mediated CAR gene transfer into CD8$^+$ T cell lines. An average titer of above 10^7 t.u./ml of concentrated vector stocks proofs that CD8-LV(CAR) allows high titer vector productions, suitable for *in vivo* gene delivery applications.

3.2.2 CD8-LV(CAR) transduction of primary human T cells results in the generation of CAR T cells *in vitro*

Successful transfer of CAR transgene into an immortalized CD8$^+$ T cell line was shown. In a next step, the capability of CD8-LV(CAR) to transduce human primary cells was evaluated. The selectivity of CD8-LV was demonstrated on primary cell cultures with mixed cell populations. Human PBMC were used, which include CD8$^+$ and CD4$^+$ T cells. The CD8-LV was evaluated to mediate CAR gene transfer into primary cells and to discriminate between CD8$^+$ and CD8$^-$ cells.

PBMC were isolated from blood and activated with αCD3- and αCD28-antibody in combination with IL-2 for three days. PBMC were transduced using a multiplicity of infection (MOI) of 2 and transgene expression was determined by flow cytometry five days later using a PE labelled anti-myc antibody.

For untransduced cells, low background signals were detected. Upon CD8-LV(CAR) transduction, PBMC showed a distinct cell population of CAR$^+$ cells. Remarkably, CAR expression was restricted to CD8$^+$ cells only (Figure 13A).
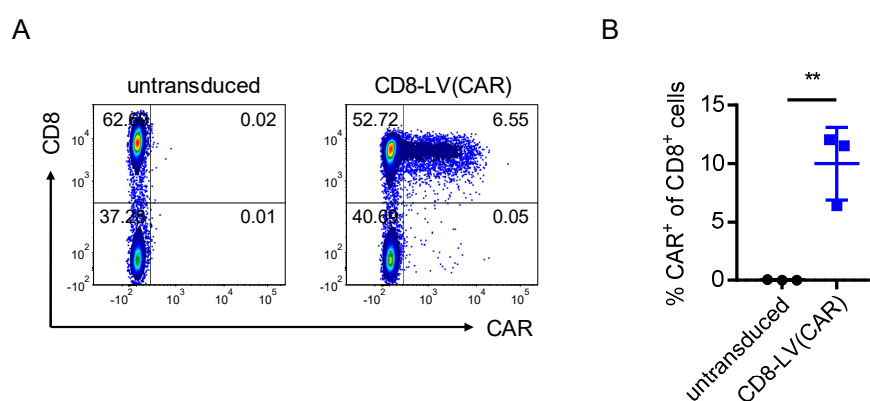
Figure 13: CD8-LV(CAR) selectively transduces CD8$^+$ primary human PBMC
PBMC were activated for three days using IL-2, αCD3- and αCD28-antibody and subsequently transduced with CD8-LV(CAR) with a MOI of 2. (A) On day five, PBMC were analyzed for CD8 and CAR expression by flow cytometry. (B) Percentage of CAR expression of CD8$^+$ cells. Data are shown from three independent experiments. N=3 with mean ± SD are shown. Statistical significance was determined by two-tailed unpaired t-test; **, p<0.01.

CD8$^-$ cells mainly remained untransduced, although some few events were detected in the CD8$^-$CAR$^+$ gate. PBMC from three different donors were transduced, resulting in 9.9% (± 3.1%) CAR expression within the CD8$^+$ population (Figure 13B).

The transduction of primary human PBMC with CD8-LV(CAR) resulted in the generation of CD8$^+$CAR$^+$ T cells demonstrating the selective CAR expression in CD8$^+$ cells mediated by CD8-LV(CAR).

3.2.3 CAR T cells efficiently kill CD19$^+$ B cells

In PBMC, other lymphocytes besides T cells are present but become overgrown in *in vitro* culture by the proliferating T cells by time. However, it was observed that remaining B cells are present for at least eight days post PBMC activation. Since B cells express the CD19 antigen on the surface, they can be regarded as target cells of CD19 CAR T cells. Thus, the ability of the generated CAR T cells to selectively target and subsequently kill CD19$^+$ B cells was evaluated.

For this purpose, CD8-LV(CAR) transduced PBMC were analyzed for CAR expression (as shown in 3.2.2) and additionally for the presence of CD19$^+$ cells five days post transduction. PBMC from three different donors were transduced and analyzed.

In untransduced PBMC, 0.65% B cells were detected (Figure 14A). Remarkably, in CD8-LV(CAR) transduced PBMC almost no B cells could be detected. Upon the generation of CAR T cells, the percentage of CD19$^+$ cells was significantly reduced (0.04%) compared to untransduced cells (0.7%)(Figure 14B) for all three donors.
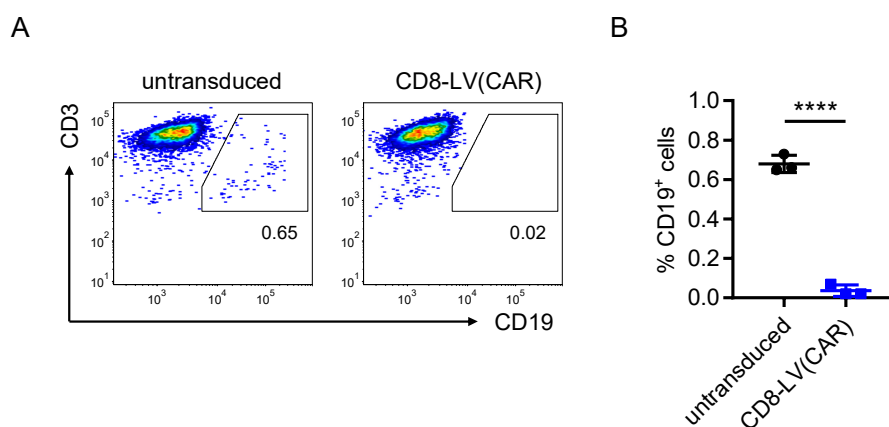
Figure 14: CD8-LV(CAR)-generated CAR T cells eliminate CD19$^+$ B cells
PBMC were activated for three days and transduced with CD8-LV(CAR) at a MOI of 2. (A) Five days post transduction, CD3 and CD19 expression were analyzed by flow cytometry. Representative density plots of one of three different donors are shown. (B) Percentage of CD19$^+$ cells. N=3 with mean ± SD are shown. Statistical significance was determined by two-tailed unpaired t-test; ****, p<0.0001.

This observation strongly indicated that the generated CAR T cells were functional in recognizing and killing CD19$^+$ B cells *in vitro*. Remaining B cells were efficiently eliminated by the CAR T cells only five days post transduction with CD8-LV(CAR).

3.2.4 CAR T cells efficiently kill CD19$^+$ tumor cells

Having shown that CAR T cells can be generated *in vitro* in primary human PBMC using CD8-LV(CAR) and that these cells were able to eliminate CD19$^+$ B cells, the functional activity of CAR T cells to eliminate CD19$^+$ tumor cells had to be further assessed.

Killing was evaluated in a flow cytometry-based assay. CAR T cells were co-cultured with CD19$^+$ tumor cells in different effector to target ratios. To distinguish tumor cells from CAR T cells, tumor cells were labelled with CFSE prior to co-culturing. After 4 h of co-culture, all cells were stained with Fixable Viability Dye eFluor™ and double positive cells were identified as dead tumor cells. Additionally, unspecific killing of tumor cells, which were co-cultured with untransduced PBMC, was assessed for each tumor cell line. Unspecific killing increased with higher effector to target ratios and was in the range of 1-18% (Figure 15, dark and light grey). When CAR T cells were co-cultured in a 5:1 ratio with CD19$^+$ tumor cells (Raji), CAR T cells selectively killed these target cells, showing up to 60% killed cells in the highest effector to target ratio (Figure 15, blue). Reduction of effector cells resulted in a decreased killing demonstrating a concentration-dependent killing effect of the CAR T cells. No specific killing was observed in the co-culture of non-target CD19$^-$ Hut-78 cells and CAR T cells (black).
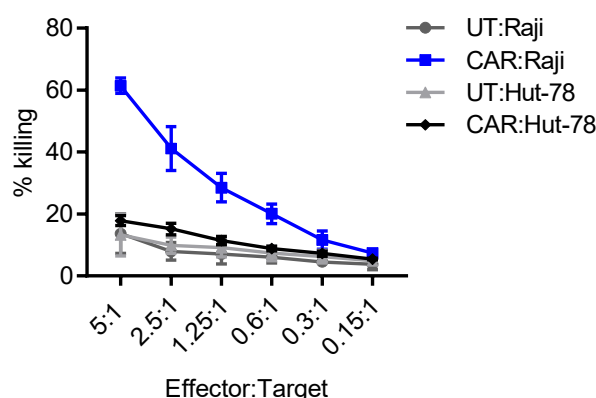
Figure 15: CD8-LV(CAR)-generated CAR T cells selectively kill CD19$^+$ target tumor cells
In a flow cytometry-based killing assay CAR T cells (effector cells) were co-cultured with CFSE-stained tumor cells (target cells) in different ratios for 4 h at 37°C. To assess selective killing of target cells, all cells were stained with a Fixable Viablity Dye eFluor™ and double positive cells were referred as killed target cells. Percentage of killed target cells is shown. CAR T cells were co-cultured together with CD19$^+$ tumor cells (Raji) (blue). To assess non-selective killing, CAR T cells were co-cultured together with CD19$^-$ non-target cells (Hut-78) (black). For determination of background killing, untransduced PBMC (UT) were co-cultured with CD19$^+$ Raji (dark grey) and CD19$^-$ Hut-78 cells (light grey). N=3 with mean ± SD are shown from three independent experiments.

These data demonstrated that CD8-LV(CAR)-generated CAR T cells selectively target and kill CD19$^+$ tumor cells *in vitro* but do not harm CD19$^-$ cells.

3.2.5 Selective proliferation of CAR T cells upon antigen stimulation

Besides killing activity towards target cells, the ability to proliferate upon antigen stimulus is an important feature of CAR T cells. After demonstrating their killing activity, the proliferation capacity of CD8-LV(CAR)-generated CAR T cells upon antigen stimulation was analyzed. For *in vivo* generation of CAR T cells using CD8-LV(CAR) it was expected that only few CAR T cells would be generated. However, CAR T cells are expected to expand upon antigen stimulation. Hence, the capability of the generated CAR T cells to expand *in vitro* upon antigen stimulation was assessed.

For this purpose, a proliferation assay was established in which CAR T cells were cultivated over long periods. Irradiated CD19$^+$ Raji cells were added to the CAR T cells every two to three days to provide a repeated antigen stimulus. The enrichment of CAR T cells was monitored over 32 days by flow cytometry analyzing CD8$^+$CAR$^+$ cells. The co-culture was started with a CAR T cell to tumor cell ratio of either 1:1 or 1:10. Co-cultures of irradiated cells and CD8$^+$GFP$^+$ cells, which were generated by transduction with CD8-LV(GFP), served as control.

CD8$^+$GFP$^+$ cells did not show enrichment within the observed time period but rather decreased from 2% to 0.5% (Figure 16, light and dark grey). In contrast, a strong increase in percentage of CD8$^+$CAR$^+$ cells was observed for both ratios (Figure 16, blue). Starting with 4% of CAR T cells in the beginning, on day 32 as much as 14% (1:1 ratio, blue circle) and 16% (for 1:10 ratio, blue square) CD8$^+$CAR$^+$ T cells were observed.
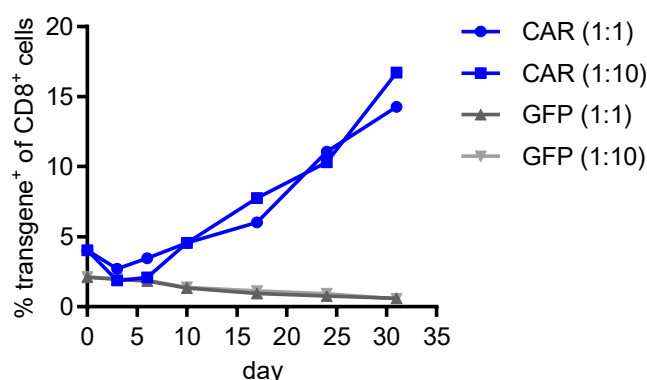
Figure 16: CD8-LV(CAR)-generated CAR T cells selectively proliferate upon antigen stimulation
CD8-LV(CAR)- or CD8-LV(GFP)-transduced cells were co-cultured with irradiated CD19$^+$ Raji cells in either 1:1 or 1:10 effector to target ratio. Every two to three days irradiated Raji cells were added to the co-culture. Cells were analyzed for CD8, CAR and GFP expression by flow cytometry. Percentage of transgene$^+$ cells of CD8$^+$ cells is shown. Selective proliferation of CAR T cells (blue) and GFP cells (grey) was followed over time.

The proliferative capability of CAR T cells generated by CD8-LV(CAR) was further confirmed when only very few CAR T cells were present in the initial co-culture. This proliferation assay had been started with as few as 0.5% CAR T cells (Figure 17A). After 14 days of co-culture, CAR T cells were enriched 3-fold (Figure 17B).

Altogether, these data demonstrated that CD8-LV(CAR)-generated CAR T cells reacted to their cognate antigen and were able to selectively proliferate upon antigen stimulation. For *in vivo* gene delivery, raising the detection level through expansion of CAR T cells by antigen stimulation seems possible.
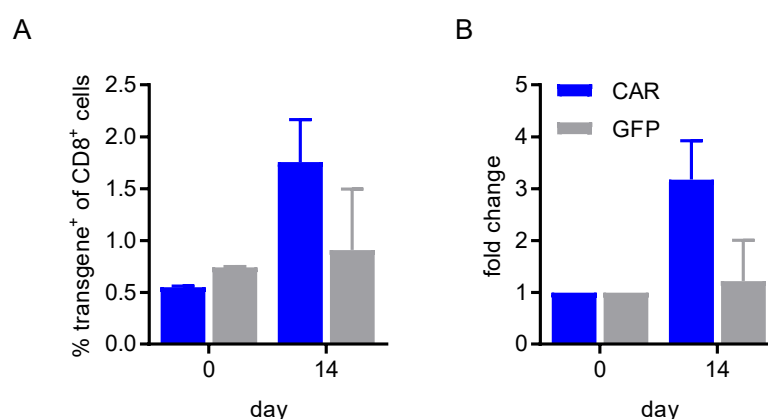
Figure 17: Enrichment of low amounts of CAR T cells upon antigen stimulation
CD8-LV(CAR)- or CD8-LV(GFP)-transduced cells were co-cultured together with irradiated CD19$^+$ Raji cells in an 1:1 effector to target ratio. Every two to three days irradiated Raji cells were added to the co-culture. Cells were analyzed for CD8, CAR and GFP expression by flow cytometry. Selective proliferation of CAR T cells (blue) and GFP$^+$ cells (grey) was analyzed on day 14. (A) Percentage of transgene$^+$ cells of CD8$^+$ cells at day 0 and day 14. (B) Enrichment of transgene expressing cells after 14 days of co-culture. The percentage of transgene expressing CD8$^+$ cells was normalized to one for day 0. Fold change enrichment of transgene expressing CD8$^+$ cells is shown for day 14. N=3 with mean ± SD are shown from three technical replicates.

3.3 *In vivo* CAR delivery and characterization of *in vivo* generated CAR T cells

The previous data demonstrated successful *in vitro* CAR T cell generation upon transduction of PBMC with CD8-LV(CAR). It was also shown that CAR T cells efficiently and selectively killed target tumor cells and specifically proliferated upon antigen exposure.

The following chapter addresses the feasibility of generating CAR T cells *in vivo* upon administration of CD8-LV(CAR) into PBMC-humanized NSG mice. *In vivo* generated CAR T cells are then further characterized in detail for their proliferative potential, killing efficacy and phenotype.

3.3.1 Detection of *in vivo* generated CAR T cells

Upon CD8-LV(CAR) administration to PBMC-humanized NSG mice, it was evaluated whether CAR T cells were generated *in vivo*. Having shown that the *in vivo* transduction rate was below 1% when transferring the reporter gene *luc-gfp* (see chapter 3.1.2), the expectation regarding the transduction rate using CD8-LV(CAR) was at most the same, rather below. This might lead to detection hurdles due to reaching the detection limit of the flow cytometry-based detection method. However, the advantage of transferring a CAR transgene is the generation of potentially functional CAR T cells that should be able to proliferate upon antigen exposure. In order to proof this hypothesis, the *in vivo* generation and detection of CAR T cells was evaluated.

In a first attempt, CD8-LV(CAR) was injected to PBMC-humanized NSG mice engrafted with CD19$^+$ Raji-luc tumor cells. In this setting, Raji-luc cells provided an antigen stimulus to potentially generated CAR T cells. In detail, $5x10^5$ Raji-luc cells were i.p. administered into NSG mice. Six days later, $1x10^7$ activated PBMC were administered via the same route, followed by i.p. injection of CD8-LV(CAR) one day later (Figure 18).
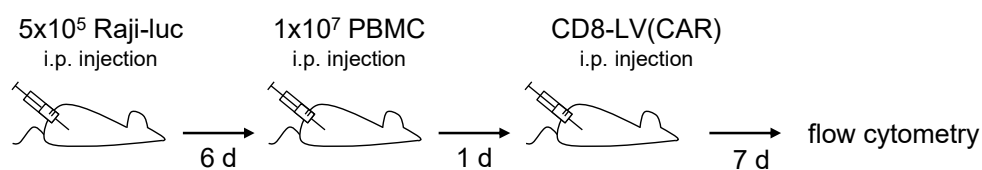
Figure 18: Experimental setting for the *in vivo* CAR gene delivery with CD8-LV(CAR) in PBMC-humanized NSG mice engrafted with tumor cells
Tumor cells (Raji-luc) were i.p. injected into NSG mice followed by an i.p. injection of activated PBMC six days later. One day later, CD8-LV(CAR) was i.p. injected. Mice were sacrificed seven days post vector injection and cells from peritoneum, spleen and blood were analyzed for CD45, CD3, CD8, CD19 and CAR expression by flow cytometry.

To evaluate the *in vivo* generation of CAR T cells, mice were sacrificed seven days after CD8-LV(CAR) administration and cells from various organs were analyzed for CAR expression by flow cytometry analysis. Blood and spleen cells as well as isolated cells from the peritoneal cavity were included in the analysis. Background signals for CAR events were determined on cell suspensions of organs of PBS-treated mice.

Humanization levels (determined by the percentage of CD45$^+$ cells) of mice ranged between 20-70% for the different organs. Thereby, more than 98% of the CD45$^+$ cells were CD3$^+$ (data not shown). CAR background signals were below 0.5% for all analyzed organs. Strikingly, in CD8-LV(CAR)-treated mice, a distinct CAR expression was observed in peritoneal cells. Hereby, CAR expression was exclusively present within the CD8$^+$ population (Figure 19A). Remarkably, on average 47% of the CD8$^+$ cells were CAR-positive (Figure 19B). CAR expression was also observed in other organs. In spleen,

9.74% of the CD8$^+$ cells were CAR-positive, whereas in blood 9.16% CD8$^+$CAR$^+$ cells were detected (Figure 19B).

Figure 19: CAR expression of CD8$^+$ cells of CD8-LV(CAR)-treated PBMC-humanized NSG mice
NSG mice were engrafted with Raji-luc cells and PBMC, and treated with CD8-LV(CAR). Seven days post vector administration, mice were sacrificed and cell suspensions from indicated organs were analyzed by flow cytometry. CD45$^+$CD3$^+$ cells were analyzed for CAR and CD8 expression. (A) Density plots are shown exemplarily for peritoneal cells. (B) Percentage of CAR$^+$ cells of CD8$^+$ cells is shown for peritoneal, spleen and blood cells. N=3, mean ± SD are shown. Statistical significance was determined by two-tailed unpaired t-test; **, p<0.01; ****, p<0,0001; ns, not significant.

These data show *in vivo* CAR transfer upon i.p. administration of CD8-LV(CAR) into PBMC-humanized NSG mice. High frequency of CAR T cells were detected in the peritoneum, but also in spleen and blood. Compared to *in vivo* reporter gene delivery (3.1.2), which resulted in less than 1% transgene expressing CD8$^+$ cells, transferring the CAR transgene resulted in up to 56% of the CD8$^+$ cells expressing the CAR.

3.3.2   Selective CAR transfer into CD8$^+$ lymphocytes

Cell type-specific CAR transfer is critical to restrict CAR expression to target cells and minimize off-target effects. Thus, the selectivity of CD8-LV(CAR) was evaluated *in vivo*.
To analyze off-target transfer, CAR expression was analyzed in CD8$^-$ cells by flow cytometry. Cells from peritoneum, spleen and blood were included in the analysis. PBS-treated mice served as a control to determine background signals.
Background levels, hence percentages of CAR$^+$ cells in PBS-treated mice, were below 0.2% for all organs (Figure 20, black). Highest background signals were detected in spleen (0.13%), some signals in peritoneal cells (0.03%) and no background signals were detected in blood cells (0%). CAR signals within the CD8$^-$ cell population in CD8-LV(CAR)-treated PBMC-humanized mice were below 0.3% for all analyzed organs (Figure 20, blue). Looking at the individual organs, higher levels of CAR$^+$ cells within the CD8$^-$ population of CD8-LV(CAR)-treated mice were only observed in the peritoneum.

0.12% CD8$^-$CAR$^+$ events in CD8-LV(CAR)-treated mice compared to 0.03% events in PBS-treated mice. A minor difference was observed in the blood and no difference in the spleen.

Figure 20: CAR expression in CD8$^-$ cells of CD8-LV(CAR)-treated PBMC-humanized NSG mice
NSG mice were engrafted with Raji-luc cells and PBMC, and treated with CD8-LV(CAR). Seven days post vector administration, mice were sacrificed and cell suspensions from indicated organs were analyzed by flow cytometry. CAR expression was analyzed in CD3$^+$CD8$^-$ cells. Percentage of CAR$^+$ cells of CD3$^+$CD8$^-$ cells is shown for peritoneal, spleen and blood cells. N=3, mean ± SD are shown.

Taken together, no major off-target events were observed upon CD8-LV(CAR) injection to PBMC-humanized NSG mice. Some signals were observed, but were below 0.3% and close to background. Altogether, these data indicate selective CAR transfer *in vivo* upon systemic administration of CD8-LV(CAR) into PBMC-humanized NSG mice.

3.3.3   Elimination of CD19$^+$ cells

CAR T cells were generated *in vivo* and were present in high frequencies already seven days post vector administration. Next, it was evaluated whether *in vivo* generated CAR T cells were able to recognize and kill CD19$^+$ target cells.

The presence of CD19$^+$ cells was analyzed in flow cytometry in various organs. For this purpose, single living cells were pre-gated and CD19$^+$ cells were gated from CD45$^+$ cells. Cell suspensions from the peritoneal cavity, spleen and blood were included in the analysis.

In PBS-treated mice, on average 0.8% CD19$^+$ cells were detected in the peritoneum (Figure 21A and B). Further CD19$^+$ cells were detected in spleen (0.3%) and blood (0.09%) (Figure 21B, black). Remarkably, all CD19$^+$ cells were eliminated from the peritoneal cavity of CD8-LV(CAR)-treated mice (Figure 21B, blue). Even in cell suspensions from spleen and blood, no CD19$^+$ cells were detected.
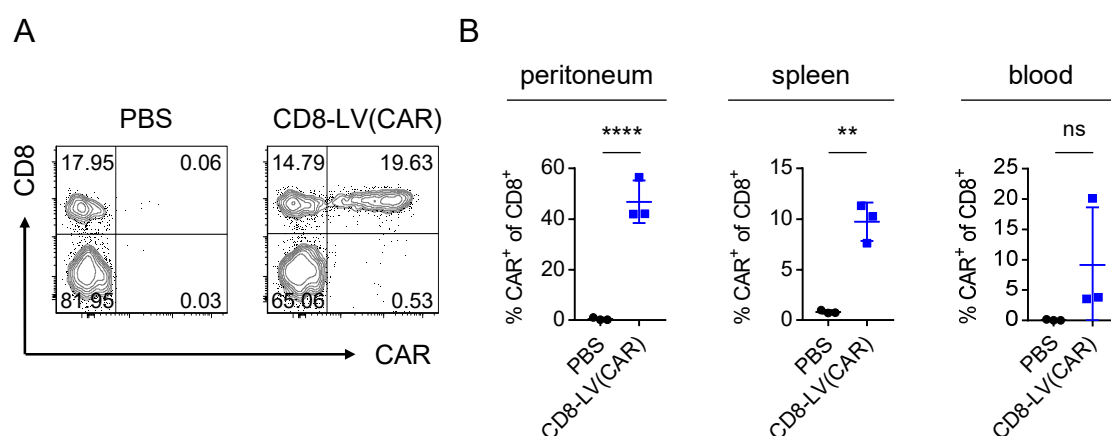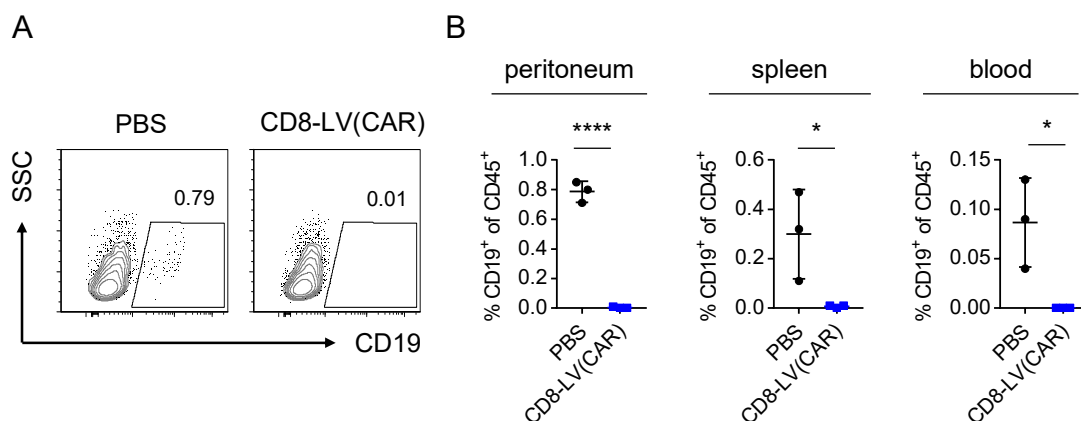
Figure 21: CD19 expression of CD45+ cells of CD8-LV(CAR)-treated PBMC-humanized NSG mice
NSG mice were engrafted with Raji-luc cells and PBMC, and treated with CD8-LV(CAR). Seven days post vector administration, mice were sacrificed and cell suspensions from indicated organs were analyzed by flow cytometry. CD45+ cells were analyzed for CD19 expression. (A) Exemplary density plots are shown for peritoneal cells. (B) Percentage of CD19+ cells of CD45+ cells is shown for peritoneal, spleen and blood cells. N=3, mean ± SD are shown. Statistical significance was determined by two-tailed unpaired t-test; *, p<0.05; ****, p<0,0001.

The complete elimination of CD19+ cells in all analyzed organs of CD8-LV(CAR)-treated mice indicated that *in vivo* generated CAR T cells were functional in recognizing and killing CD19+ target cells.

3.3.4 Proliferative advantage of CAR T cells

The interaction between CD19+ cells and CAR T cells *in vivo* resulted in complete elimination of CD19+ cells. A second process that is induced upon antigen recognition is the proliferation of CAR T cells. In chapter 3.3.1, high frequencies of *in vivo* generated CAR T cells were detected. Frequency of transgene expressing cells was about 100-fold higher compared to those observed for *luc-gfp* reporter gene delivery shown in chapter 3.1.2. The high frequency of detected CAR T cells might already indicate CAR T cell proliferation upon target cell stimulation. Since CAR transfer was, as shown above, almost exclusively restricted to CD8+ cells, it was assumed that antigen-stimulated CAR T cell proliferation only affected CD8+ cells. Hence it was expected, that CAR transfer resulted in an enriched CD8 population.

Thus, the frequency of CD8+ cells in CD8-LV(CAR)-treated mice was analyzed by flow cytometry and compared to the frequency of CD8+ cells in PBS-treated mice.

The CD8+ cells in CD8-LV(CAR)-treated mice were significantly enriched in the peritoneum (33.48%) compared to PBS-treated mice (17.13%) (Figure 22A, B). Only a slight increase of CD8+ cells was observed in the spleen and no difference was observed in the blood (Figure 22B).
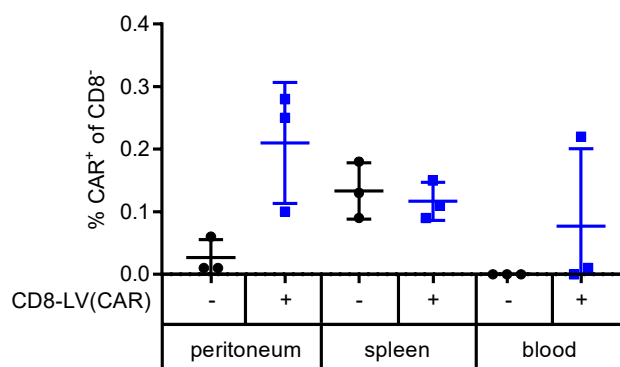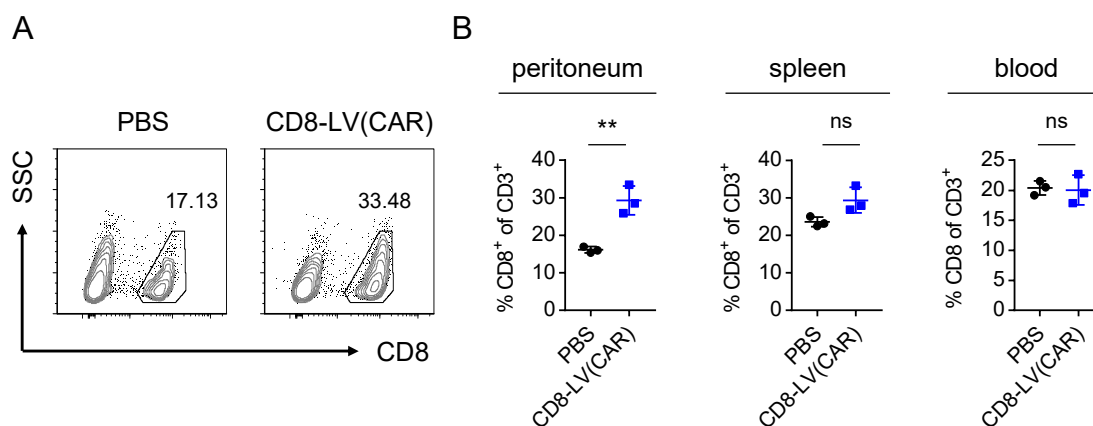
Figure 22: CD8 expression of CD3⁺ cells of CD8-LV(CAR)-treated PBMC-humanized NSG mice
NSG mice were engrafted with Raji-luc cells and PBMC, and treated with CD8-LV(CAR). Seven days post vector administration, mice were sacrificed and cell suspensions from indicated organs were analyzed by flow cytometry. CD45⁺CD3⁺ cells were analyzed for CD8 expression. (A) Density plots are shown exemplarily for peritoneal cells. (B) Percentage of CD8⁺ cells of CD3⁺ cells is shown for peritoneal, spleen and blood cells. N=3, mean ± SD are shown. Statistical significance was determined by two-tailed unpaired t-test; **, $p<0.01$; ns, not significant.

These data demonstrated that the treatment with CD8-LV(CAR) resulted in an elevated level of CD8⁺ cells in the peritoneum. Together with the high frequency of CAR T cells, these data indicated CAR T cell proliferation due to antigen stimulus already after a short period of only seven days. However, this assumption of antigen-driven proliferation of *in vivo* generated CAR T cells needed to be evaluated further.

3.3.4.1 Proliferative advantage of CAR T cells in the presence and absence of CD19⁺ tumor cells

Antigen-induced proliferation can lead to significant enrichment of CAR T cells. However, upon removal of the antigen, CAR T cells lack specific proliferation stimulus. To evaluate whether the high frequency of CAR⁺ cells as seen in chapter 3.3.1 was a result of antigen-driven proliferation, the next experiment was designed to abolish the interaction between CAR T cell and antigen.

To disturb antigen-specific CAR T cell proliferation, removing the antigen or exchanging the CAR for a reporter gene are possible options. The following experiment consisted of four groups either missing the antigen or the CAR transgene. Mice were engrafted with or without tumor cells and PBMC and were treated with CD8-LV(CAR). Two further groups, either engrafted with tumor cells or without were treated with CD8-LV carrying the reporter gene *rfp* (CD8-LV(RFP)). For all groups, CAR expression as well as CD8 and CD19 expression were analyzed by flow cytometry of cell suspensions from peritoneum, spleen and blood.

First, CAR expression was analyzed in CD8-LV(CAR)-treated mice, injected with or without CD19⁺ tumor cells. Surprisingly, no difference in CAR expression was observed between tumor cell-injected (Figure 23, blue, filled square) and tumor- negative mice (blue, empty square). In both groups, 15-55% CD8⁺CAR⁺ cells were detected in the peritoneum. CAR T cells were detected in spleen and blood cells. As seen for the peritoneum, independently from having tumor cells or not, the same range of CAR expression was observed for both groups in the different organs. On average 27% CD8⁺CAR⁺ cells were detected in the spleen and 22% CD8⁺CAR⁺ cells in the blood. Strikingly, when transferring the *rfp* transgene much less cells were transgene-positive (Figure 23, red). In the peritoneum, the frequency of CD8⁺RFP⁺ cells ranged from 0.5-5%. In spleen and in blood, on average 2% CD8⁺RFP⁺ cells were detected.

Figure 23: Transgene expression of CD8⁺ cells of CD8-LV(CAR)- and CD8-LV(RFP)-treated PBMC-humanized NSG mice
NSG mice were injected with Raji-luc tumor cells (+) or with PBS (-) and engrafted with PBMC. Mice were treated with CD8-LV(CAR) or CD8-LV(RFP). Seven days post vector administration, mice were sacrificed and cells from indicated organs were analyzed for transgene and CD8 expression. Percentages of transgene-positive cells within the CD8⁺ population are shown for CD8-LV(CAR)- (blue) and CD8-LV(RFP)- (red) treated PBMC-humanized NSG mice. N=3-4, mean ± SD are shown. Statistical significance was determined by two-tailed unpaired t-test; **, p<0.01; ***, p< 0,001; ****, p<0,0001.

These data revealed similar CAR transfer efficiency as seen in chapter 3.3.1 with 20-60% CD8⁺CAR⁺ cells in the peritoneum. However, no difference in the frequency of CAR T cells was observed regardless of the presence or absence of tumor cells. Obviously, the presence of CD19⁺ tumor cells did not influence the frequency of CAR T cells. However, *rfp* gene transfer in general resulted in much less transgene positive cells. Higher transgene expression in CAR mice indicated specific CAR T cell proliferation for CD8⁺CAR⁺ cells but no specific proliferation of CD8⁺RFP⁺ cells.

In chapter 3.3.4, enrichment of CD8⁺ cells was shown for CD8-LV(CAR)-treated mice when compared to a control group. To assess whether CAR T cell proliferation was reflected in an increased level of CD8⁺ cells, CD8 frequencies were analyzed. Comparing

the CD8 levels of both CD8-LV(CAR)-treated groups, the influence of CD19⁺ tumor cells on CAR T cell proliferation, hence, the enrichment of the CD8⁺ cells was evaluated. Additionally, ratios of CD8⁺ cells were compared between CD8-LV(CAR)-treated and CD8-LV(RFP)-treated mice in order to evaluate the influence of the transgene on the CD8 frequency.

By comparing both CD8-LV(CAR)-treated groups, no difference in CD8 frequency was observed. On average 43% CD8⁺ cells were detected in the peritoneum (Figure 24, blue). In spleen and blood, comparison of both groups also revealed no difference within the same organ. Similar CD8⁺ frequencies of 41% (spleen) and 35% (blood) were observed. However, when transferring the *rfp* transgene, CD8 levels were significantly lower in the peritoneum (Figure 24, red). In spleen, CD8 frequencies were reduced in CD8-LV(RFP)-treated mice (41%) compared to CD8-LV(CAR)-treated mice (46%). The same was true for CD8 frequencies in blood, which were also slightly reduced in CD8-LV(RFP)-treated mice (35%) compared to CD8-LV(CAR)-treated mice (40%).
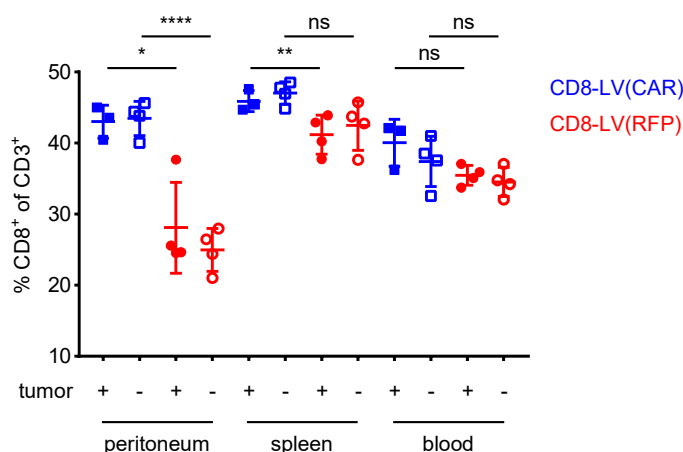
Figure 24: CD8 expression of CD3⁺ cells of CD8-LV(CAR)- and CD8-LV(RFP)-treated PBMC-humanized NSG mice
NSG mice were injected with Raji-luc tumor cells (+) or with PBS (-) and engrafted with PBMC. Mice were treated with CD8-LV(CAR) or CD8-LV(RFP). Seven days post vector administration, mice were sacrificed and cells from indicated organs were analyzed for CD3 and CD8 expression. Percentage of CD8⁺ cells of CD3⁺ cells are shown for CD8-LV(CAR)- (blue) and CD8-LV(RFP)- (red) treated PBMC-humanized NSG mice. N=3-4, mean ± SD are shown. Statistical significance was determined by two-tailed unpaired t-test; *, p<0.05; **, p<0.01; ****, p<0,0001; ns, not significant.

Taken together, the frequency of CAR⁺ and CD8⁺ cells was not influenced by the presence of CD19⁺ tumor cells in CD8-LV(CAR)-treated mice. However, when transferring the reporter gene *rfp*, transgene levels and CD8 levels were lower. These data indicated proliferation of CAR T cells for both CD8-LV(CAR)-treated groups but no selective proliferation of RFP⁺ cells in the CD8-LV(RFP)-treated groups.

As already shown in chapter 3.2.3 and 3.2.4 in *in vitro* experiments, CAR T cells were able to selectively kill CD19$^+$ cells. Elimination of CD19$^+$ cells was assessed for each group. As expected, CD19$^+$ cells were eliminated from all organs of CD8-LV(CAR)-treated mice (Figure 25, blue). In CD8-LV(RFP)-treated mice, which were pretreated with tumor cells, CD19$^+$ cells were mainly detectable in peritoneum and spleen with frequencies ranging between 0.025-2.5% (Figure 25, red). Surprisingly, CD19$^+$ cells were also detected in CD8-LV(RFP)-treated mice not pretreated with tumor cells. On average, similar frequencies as in tumor-pretreated mice were observed in spleen (0.27%) and blood (0.08%). Up to 0.92% CD19$^+$ cells were observed in the peritoneal cavity.
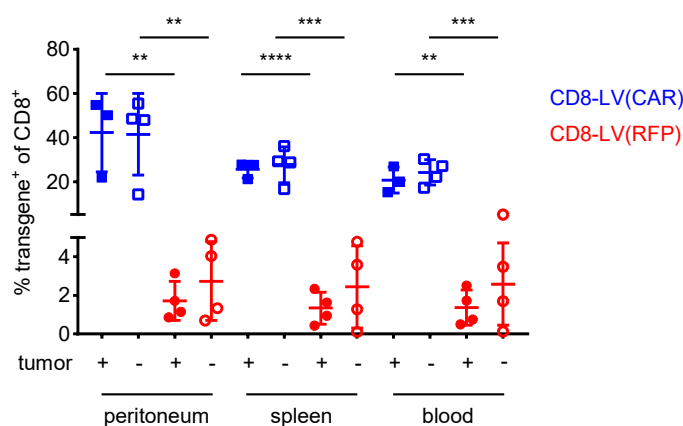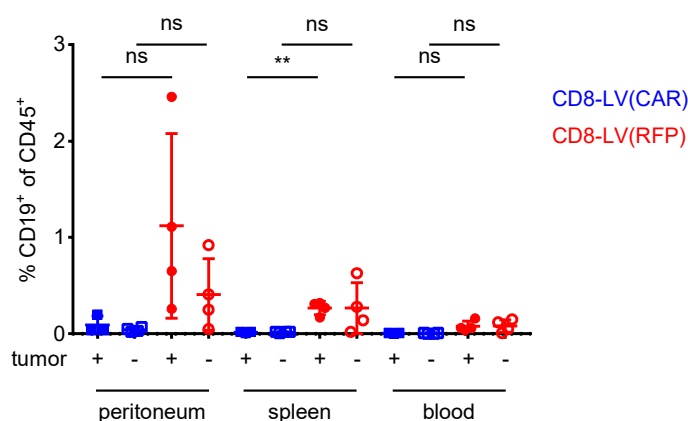

Figure 25: CD19$^+$ cells of CD45$^+$ cells in CD8-LV(CAR)- and CD8-LV(RFP)-treated PBMC-humanized NSG mice
NSG mice were injected with Raji-luc tumor cells (+) or with PBS (-) and engrafted with PBMC. Mice were treated with CD8-LV(CAR) or CD8-LV(RFP). Seven days post vector administration, mice were sacrificed and cells from indicated organs were analyzed for CD45 and CD19 expression. Percentage of CD19$^+$ cells of CD45$^+$ cells are shown for CD8-LV(CAR)- (blue) and CD8-LV(RFP)- (red) treated PBMC-humanized NSG mice. N=3-4, mean ± SD are shown. Statistical significance was determined by two-tailed unpaired t-test; **, p<0.01; ns, not significant.

To conclude, in CD8-LV(CAR)-treated mice all CD19$^+$ cells were completely eliminated. In CD8-LV(RFP)-treated mice, as expected, CD19$^+$ cells were still present. However, even when tumor cells were not administered, CD19$^+$ cells were detectable.

3.3.4.2 Proliferative advantage of CAR T cells in the absence of CD19$^+$ B cells

Initially, it was assumed that CD19$^+$ tumor cells induce CAR T cell proliferation. However, the absence of CD19$^+$ tumor cells unexpectedly did not affect the frequency of CAR T cells. Having seen that CD19$^+$ cells were detected in mice although they were not injected with tumor cells was unexpected (chapter 3.3.4.1). It was assumed that these CD19$^+$ cells were B cells that were transferred together with the PBMC transplant into mice. Thus, as antigen-CAR T cell interaction was assumed to trigger CAR T cell proliferation, remaining B cells might have triggered proliferation. Therefore, B cells were

further investigated for their potential to act as proliferation stimulus for *in vivo* generated CAR T cells.

To investigate B cells as the proliferation stimulus for CAR T cells, B cells were depleted from PBMC prior to injection into NSG mice. PBMC were isolated from three healthy donors and B cells were depleted by magnetic cell isolation using microbeads against CD19$^+$ cells. To determine successful depletion of CD19$^+$ cells, cells were analyzed for CD3 and CD19 expression by flow cytometry prior and post CD19$^+$ depletion.

Prior to CD19$^+$ depletion, the main population consisted of CD3$^+$ T cells (55%) and CD3$^-$CD19$^-$ cells (37%) (Figure 26). Less than 10% of the cells were CD19$^+$. B cell frequencies from three different donors ranged from 2-8%. After CD19 depletion, 99.99% of the cells were CD19$^-$, demonstrating the successful depletion of CD19$^+$ cells.
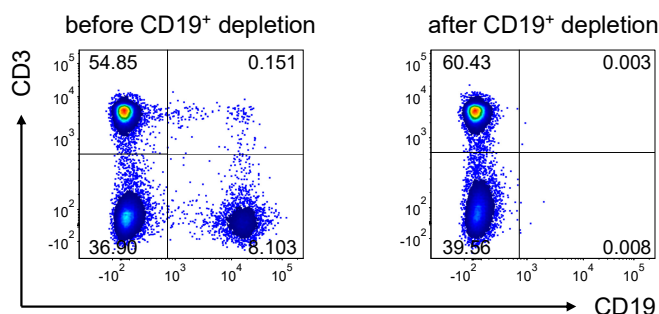
Figure 26: *In vitro* CD19$^+$ B cell depletion of PBMC
PBMC were isolated from blood and CD19$^+$ cells were depleted from PBMC via MACS® technology using microbeads against CD19$^+$ cells. Cells were separated using magnetic separation. PBMC were analyzed by flow cytometry for CD3 and CD19 expression before and after CD19$^+$ cell depletion. Representative density plots from three individual experiments are shown.

To evaluate if B cells are the proliferation stimulus for *in vivo* generated CAR T cells, CD8-LV(CAR) was administered into PBMC-humanized NSG mice, either engrafted with PBMC or PBMC that were depleted for CD19$^+$ B cells.

In detail, NSG mice were i.p. injected with 1x10^7 activated PBMC or PBMC$^{CD19-depleted}$. One day later, CD8-LV(CAR) or PBS, as control, was injected. Seven days later, mice were sacrificed and CAR expression as well as CD8 and CD19 expression were analyzed in peritoneal, spleen and blood cells. Control groups (PBMC- or PBMC$^{CD19-depleted}$-humanized mice treated with PBS) served as control for background signals in all organs.

CAR background levels for blood and peritoneal cells were below 0.5% (Figure 27, black and grey). Cells from spleen showed a slightly higher background of up to 2%. In CD8-LV(CAR)-treated PBMC-humanized mice, CAR expression within CD8$^+$ peritoneal cells was in the range of 20-37% (Figure 27, blue). Remarkably, CD8-LV(CAR)-treated PBMC$^{CD19-depleted}$-humanized mice showed much less CAR T cells ranging between 2-8% CD8$^+$CAR$^+$ cells (Figure 27, orange). In CD8-LV(CAR)-treated PBMC-humanized mice,

CAR T cells were detected in spleen (5%) and in blood (7%) (Figure 27, blue). Contrarily, in CD8-LV(CAR)-treated PBMC$^{CD19-depleted}$-humanized mice, CAR T cells detected in the spleen were not above background (Figure 27, orange). In blood, CAR T cells were slightly above background detection (1%), being in the range of 2% (Figure 27, orange).
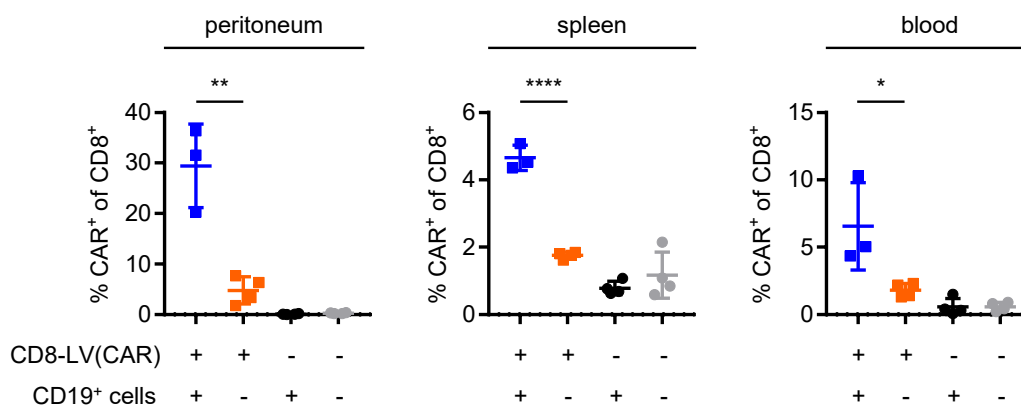
Figure 27: CAR expression of CD8$^+$ cells of CD8-LV(CAR)-treated PBMC- or PBMC$^{CD19-depleted}$-humanized NSG mice
NSG mice were injected with PBMC or CD19-depleted PBMC. Seven days post vector administration, mice were sacrificed and cells from indicated organs were analyzed for CD8 and CAR expression by flow cytometry. Percentage of CAR$^+$ cells of CD8$^+$ cells are shown for CD8-LV(CAR) (blue) or PBS (black) treated PBMC-humanized NSG mice and for PBMC$^{CD19-depleted}$-humanized NSG mice treated with CD8-LV(CAR) (orange) or PBS (grey). N=3-4, mean ± SD are shown. Statistical significance was determined by two-tailed unpaired t-test; *, p<0.05; **, p<0.01; ****, p< 0,0001.

In conclusion, significantly less CAR T cells had been detected in CD8-LV(CAR)-treated PBMC$^{CD19-depleted}$ mice compared to CD8-LV(CAR)-treated PBMC mice. Being much less, but still detectable in the peritoneal cavity and in blood, CAR T cells in the spleen were in the range of background detection. This strongly indicated antigen-specific CAR T cell proliferation in the presence of CD19$^+$ B cells.

As shown in the previous chapters 3.3.4 and 3.3.4.1, an enrichment of CD8$^+$ cells in CD8-LV(CAR)-treated mice indicated a selective proliferation advantage of CAR-modified CD8$^+$ cells Thus, CD8 levels were evaluated in peritoneal, spleen and blood cells from CD8-LV(CAR)-treated PBMC- or PBMC$^{CD19-depleted}$-humanized mice.

However, no significant differences were observed between CD8-LV(CAR)-treated PBMC- or PBMC$^{CD19-depleted}$-humanized mice (Figure 28, blue and orange). In the peritoneum and spleen, CD8$^+$ cells were in the range of 30-40% and less frequent in the blood ranging between 20-30%. However, in PBS-treated mice differences were observed for peritoneal cells. The frequency of CD8$^+$ cells was enriched in PBMC$^{CD19-depleted}$-humanized mice (38%), compared to PBMC-humanized mice (25%). Also in spleen and blood, a tendency towards enrichment of CD8$^+$ cells in PBMC$^{CD19-depleted}$-humanized mice was observed compared to PBMC-humanized mice.
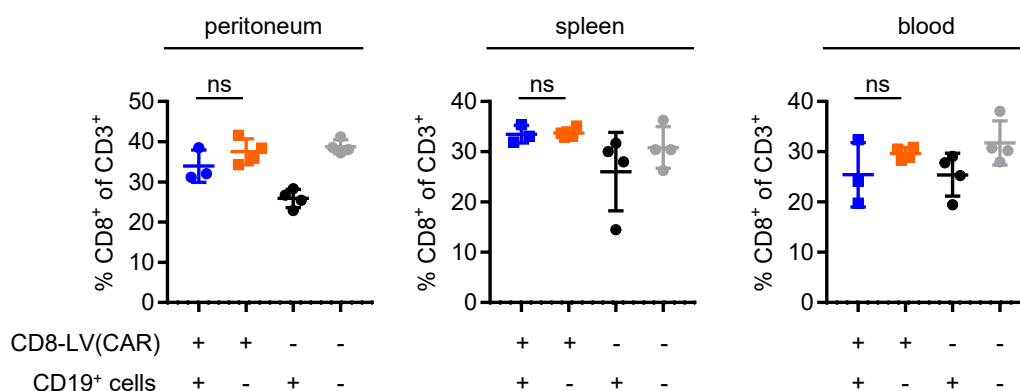
Figure 28: CD8 expression of CD3+ cells of CD8-LV(CAR)-treated PBMC- or PBMC^CD19-depleted-humanized NSG mice
NSG mice were injected with PBMC or CD19-depleted PBMC. Seven days post vector administration, mice were sacrificed and cells from indicated organs were analyzed for CD3 and CD8 expression by flow cytometry. Percentage of CD8+ cells of CD3+ cells is shown for CD8-LV(CAR) (blue) or PBS (black) treated PBMC-humanized NSG mice and for PBMC^CD19-depleted-humanized NSG mice treated with CD8-LV(CAR) (orange) or PBS (grey). N=3-4, mean ± SD are shown. Statistical significance was determined by two-tailed unpaired t-test; ns, not significant.

The *in vivo* generation of CAR T cells was shown to be accompanied by the elimination of CD19+ cells (3.3.3). Hence, the presence of CD19+ cells in PBMC- or PBMC^CD19-depleted-humanized mice was evaluated by flow cytometry of peritoneal, spleen and blood cells.

As expected, in all organs, no CD19+ cells were detected in CD8-LV(CAR)-treated PBMC- or PBMC^CD19-depleted-humanized mice (Figure 29, blue and orange). Also in PBS-treated PBMC^CD19-depleted mice (grey) CD19+ cells were absent in all organs. Only in PBS-treated PBMC-humanized mice (black) up to 2% of CD19+ cells were detected in all organs.
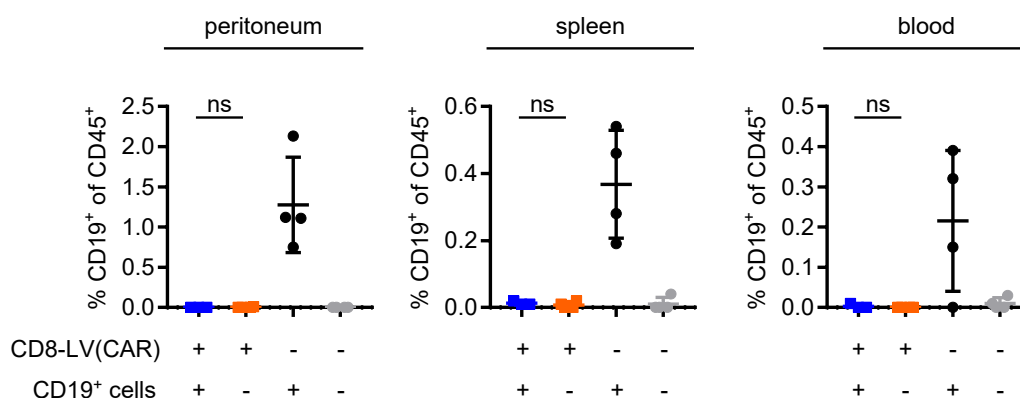
Figure 29: CD19 expression of CD45+ cells CD8-LV(CAR)-treated PBMC- or PBMC^CD19-depleted-humanized NSG mice
NSG mice were injected with PBMC or CD19-depleted PBMC. Seven days post vector administration, mice were sacrificed and cells from indicated organs were analyzed for CD45 and CD19 expression by flow cytometry. Percentage of CD19+ cells of CD45+ cells is shown for CD8-LV(CAR) (blue) or PBS (black) treated PBMC-humanized NSG mice and for PBMC^CD19-depleted-humanized NSG mice treated with CD8-LV(CAR) (orange) or PBS (grey). N=3-4, mean ± SD are shown. Statistical significance was determined by two-tailed unpaired t-test; ns, not significant.

The absence of CD19$^+$ cells in PBS-treated PBMC$^{CD19\text{-depleted}}$-humanized mice confirmed the successful B cell depletion. Taken together, the comparison of CD8-LV(CAR)-treated PBMC and PBMC$^{CD19\text{-depleted}}$-humanized mice showed a significant enrichment of CAR T cells in mice engrafted with CD19$^+$ B cells. Although CD8 levels were not enriched in CD8-LV(CAR)-treated PBMC-humanized mice, the significantly higher frequency of CAR T cells strongly argues for the CD19$^+$ B cells to be the antigen stimulus that induced the proliferation of *in vivo* generated CAR T cells.

3.3.5   Phenotypic characterization of CAR T cells

CAR T cells behave differently in presence or absence of antigen. In the presence of CD19$^+$ B cells they proliferate and expand. Furthermore, the interaction with antigen can induce the differentiation into a different T cell subtype. To evaluate potential differences in their differentiation status, antigen-experienced and antigen-unexperienced CAR T cells were characterized for their phenotype.

In vivo generated CAR T cells from the peritoneal cavity (chapter 3.3.4.2) were phenotypically analyzed based on the surface expression of CD62L and CD45RA by flow cytometry. Subsequently, they were classified into stem cell memory/naïve T cells ($T_{SCM/Naïve}$: CD62L$^+$/CD45RA$^+$), central memory T cells (T_{CM}: CD62L$^+$/CD45RA$^-$), effector memory T cells (T_{EM}: CD62L$^-$/CD45RA$^-$) and effector T cells (T_{Eff}: CD62L$^-$/CD45RA$^-$) (Figure 30). CAR$^-$ cells (CD8$^+$CAR$^-$ cells and CD8$^-$ cells) were analyzed as controls, representing cells being unaffected by the CD19 antigen.
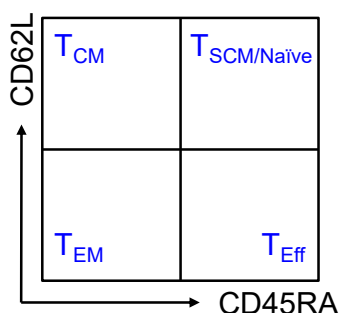
Figure 30: Scheme of subset-phenotyping of T cells by flow cytometry analysis
T cells were analyzed for CD45RA and CD62L surface expression. According to their combinatorial expression, T cells were classified into stem cell memory/naïve T cells ($T_{SCM/Naïve}$: CD45RA$^+$CD62L$^+$), effector memory T cells (T_{EM}: CD45RA$^-$CD62L$^-$), central memory T cells (T_{CM}: CD45RA$^-$CD62L$^+$) and effector T cells (T_{Eff}: CD45RA$^+$/CD62L$^-$).

For PBMC-humanized mice and PBMC$^{CD19\text{-depleted}}$-humanized mice, the average subset distribution in CD8$^-$ cells was very similar independently of CD8-LV(CAR)- or PBS-treatment (Figure 31A and B, right panel). The majority were T_{EM} (54.84% ± 3.23%)

followed by T_{CM} (30.36% ± 2.64%) a small fraction of $T_{SCM/Naïve}$ (6.45% ± 0.82%) and few T_{Eff} (0.77% ± 0.11%). When comparing CD8$^+$CAR$^-$ cells, again, a similar distribution pattern was observed (Figure 31A and B, middle panel). They were characterized by a majority of T_{EM} (41.0% ± 4.47%) followed by two equally large populations, T_{CM} (16.25% ± 2.17%) and $T_{SCM/Naïve}$ (17.23% ± 3.2%). The smallest fraction was T_{Eff} (5.52% ± 1.28%).
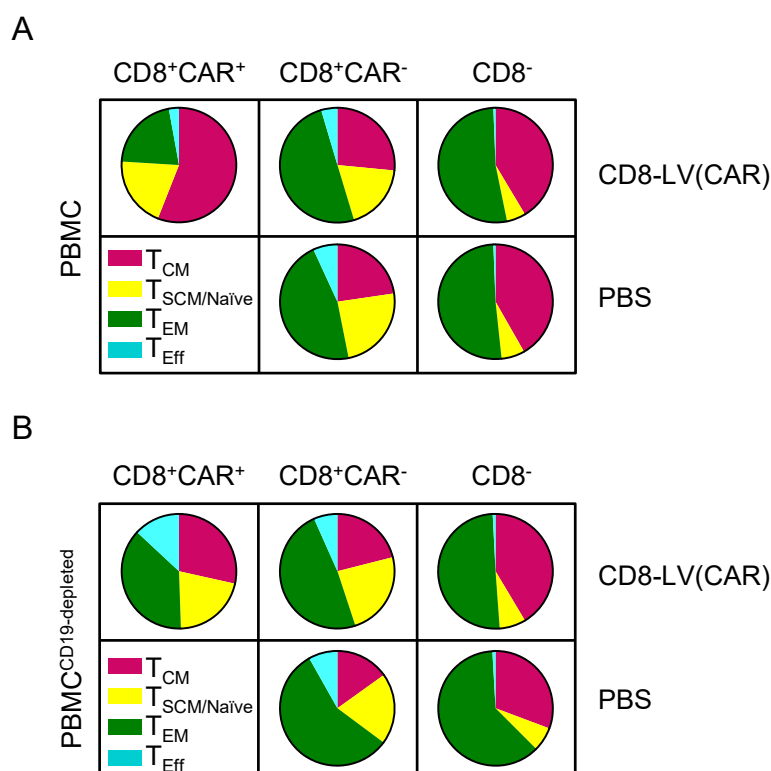
Figure 31: Subset-phenotype analysis of *in vivo* generated CAR T cells
NSG mice were injected with PBMC or CD19-depleted PBMC. Seven days post vector administration, mice were sacrificed and cells from indicated organs were analyzed for CD45, CD3, CD8, CAR, CD62L and CD45RA expression by flow cytometry. Human T cells were identified by CD45 and CD3 expression. CD8$^+$CAR$^+$, CD8$^+$CAR$^-$ and CD8$^-$ cells were analyzed for CD62L and CD45RA expression and classified into subset-phenotypes. Subsets are defined as pink: central memory T cells (T_{CM}: CD45RA$^-$CD62L$^+$); yellow: stem cell memory/naïve T cells ($T_{SCM/Naïve}$: CD45RA$^+$CD62L$^+$); green: effector memory T cells (T_{EM}: CD45RA$^-$CD62L$^-$); and turquoise: effector T cells (T_{Eff}: CD45RA$^+$CD62L$^-$). Pie chart representations of mean subset-phenotype percentages for CD8$^+$CAR$^+$, CD8$^+$CAR$^-$ and CD8$^-$ cells are shown for CD8-LV(CAR)- or PBS-treated PBMC-humanized NSG mice and for PBMC$^{CD19-depleted}$-humanized NSG mice, treated with CD8-LV(CAR) or PBS. N=3-4.

To evaluate differences in the phenotype of CD8$^+$CAR$^+$ cells, CD8-LV(CAR)-treated PBMC-humanized and PBMC$^{CD19-depleted}$-humanized mice were analyzed. CD8$^+$CAR$^+$ cells from PBMC$^{CD19-depleted}$-humanized mice showed a similar average distribution as observed for CD8$^+$CAR$^-$ cells (Figure 31B, left panel). The largest fraction was T_{EM} (37.48% ± 4.99%) followed by two equally large T_{CM} (28.54% ± 1.32%) and $T_{SCM/Naïve}$ (20.92% ± 2.65%) fractions and the smallest fraction, T_{Eff} (13.06% ± 4.43%). Remarkably, CD8$^+$CAR$^+$ cells from PBMC-humanized mice showed a different subset

distribution (Figure 31A, left panel). They were characterized by a majority of T_{CM} (53.64% ± 5.31) followed by two equally large $T_{SCM/Naïve}$ (21.41% ± 2.61%) and T_{EM} (20.96% ± 3.58%) populations. The smallest fraction was the T_{Eff} population (4.0% ± 1.91%).

Taken together, the average subset-phenotype distributions for CD8⁻ and CD8⁺CAR⁻ populations were similar for all four groups. Remarkably, differences were observed when comparing antigen-experienced CAR T cells (CD8⁺CAR⁺ cells of PBMC-humanized mice) and antigen-unexperienced CAR T cells (CD8⁺CAR⁺ cells of PBMC$^{CD19-depleted}$-humanized mice). Antigen-experienced CAR T cells showed an increased T_{CM} fraction and lower frequencies of T_{EM} and T_{Eff}.

These data demonstrated that the interaction of CAR T cells and CD19⁺ cells influenced the phenotype of CAR T cells. Cells unaffected by this interaction (CD8⁺CAR⁻ and CD8⁻ cells) did not show a changed phenotype in absence of CD19⁺ cells.

3.3.6 Characterization of transgene integration of *in vivo* generated CAR T cells

In vivo gene transfer using CD8-LV was shown for CAR and *rfp* transgenes. Additionally, CAR transfer was performed in the presence or absence of CD19⁺ B cells. In the following chapter, transgene integration and clonality of the *in vivo* transduced cells were analyzed.

3.3.6.1 Determination of vector copy number

So far, successful *in vivo* gene transfer was determined as transgene expressing cells analyzed by flow cytometry. To calculate VCN, transgene integration was analyzed on genomic DNA by qPCR.

Cells from peritoneum, spleen and blood were analyzed for lentiviral transgene integration in a probe-based qPCR assay. Genomic DNA was isolated and transgene integration was evaluated using woodchuck hepatitis virus posttranscriptional regulatory element (WPRE)-specific primers. The qPCR assay was a multicolour assay detecting the transgene and the human reference gene albumin. To determine the vector copy number, the ratio of transgene and albumin amounts was calculated. Cells from two individuals of PBS-, CD8-LV(CAR)-, CD8-LV(RFP)-treated PBMC-humanized NSG mice and cells from CD8-LV(CAR)-treated PBMC$^{CD19-depleted}$-humanized mice were analyzed.

In PBS-treated mice, VCN of 0 were determined for cells isolated from peritoneum, spleen and blood (Figure 32A, ctrl, black). For peritoneal cells from CD8-LV(CAR)-treated PBMC-humanized mice, a VCN of 0.41 was determined (CAR, blue). Cells from

CD8-LV(CAR)-treated PBMC$^{CD19\text{-}depleted}$-humanized mice showed a lower VCN of 0.1 (CARu, grey). Even lower was the VCN in CD8-LV(RFP)-treated mice with 0.05 (RFP, red). Overall, reduced VCN were observed in spleen and blood for CD8-LV(CAR)-treated PBMC-humanized mice (0.27) and for CD8-LV(CAR)-treated PBMC$^{CD19\text{-}depleted}$-humanized mice (0.07). An average VCN of 0.15 was detected for CD8-LV(RFP)-treated mice.

To correlate transgene integration with transgene expression, vector copy numbers were compared to transgene expression analyzed by flow cytometry. CAR expression was analyzed on all human cells. For this purpose, human CD45$^+$ cells were identified and the percentage of CAR expression was determined.

CD8-LV(CAR)-treated PBMC-humanized mice showed the highest VCN in all organs (Figure 32A, blue) and the highest transgene expression (Figure 32B, blue). In spleen and blood, the second highest VCN were observed for CD8-LV(RFP)-treated PBMC mice, which also showed second highest transgene expression by flow cytometry. Lowest VCN were observed in CD8-LV(CAR)-treated PBMC$^{CD19\text{-}depleted}$-humanized mice, which was in accordance to lowest transgene expression levels. In the peritoneum, unexperienced CAR T cells showed a higher VCN and higher transgene expression level compared to RFP cells.
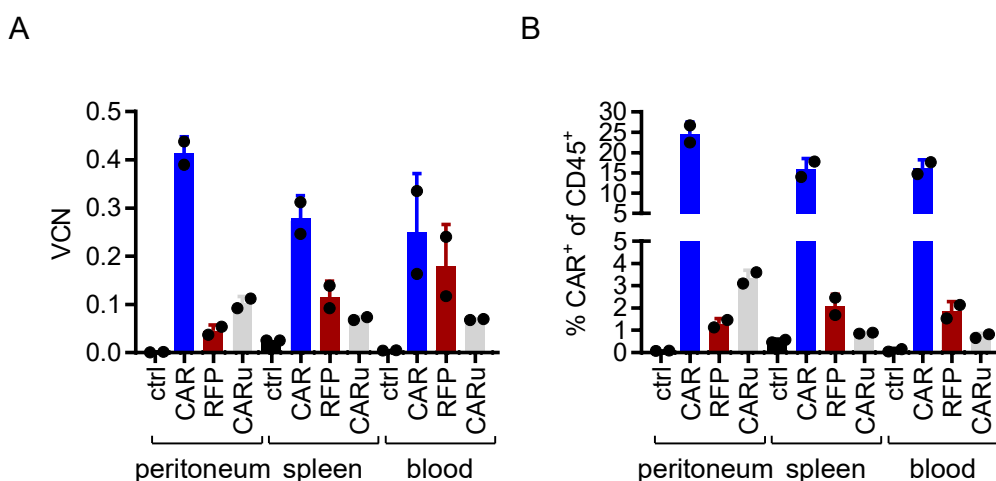
Figure 32: Transgene integration analysis by VCN determination and flow cytometry
Transgene integration and expression of peritoneal, spleen and blood cells from PBS-treated PBMC-humanized NSG mice (ctrl), CD8-LV(CAR)-treated PBMC-humanized NSG mice (CAR), CD8-LV(RFP)-treated PBMC-humanized NSG mice (RFP) and CD8-LV(CAR)-treated PBMC$^{CD19\text{-}depleted}$-humanized NSG mice (CARu). Single cell suspensions were analyzed by flow cytometry and transgene integration was analyzed on genomic DNA. Two representative mice of each group were analyzed and individual values are shown for each mouse as black dots. (A) Transgene integration analysis. Transgene integration was determined by qPCR with WPRE-specific primers on genomic DNA. Albumin-specific primers were used for reference gene detection and vector copy numbers were calcuated as the ratio of WPRE-copies/ albumin-copies. (B) Flow cytometry analysis. CAR and CD45 expression were analyzed on single cell suspensions. Percentage of CAR$^+$ cells of CD45$^+$ cells are shown. N=2 with mean ± SD are shown.

Successful *in vivo* gene delivery of CD8-LV in PBMC-humanized mice was confirmed by transgene integration and transgene expression analysis. Furthermore, VCN ratios were well in accordance with the percentage of CAR^{+} cells. The highest VCN was observed for CD8-LV(CAR)-treated PBMC-humanized mice, correlating to the highest CAR[+] levels. CD8-LV(RFP) and CD8-LV(CAR)-treated PBMC[CD19-depleted]-humanized mice showed three- to fourfold lower VCNs and less CAR^{+} cells.

3.3.6.2 Clonality analysis

As transgene integration was confirmed by qPCR, lentiviral integration sites were analyzed to evaluate clonality of *in vivo* transduced cells, revealing information about a potential *in vivo* selection of affected clones.

Transgene integration sites were analyzed in LM-PCR assay using HIV-1 specific primers on genomic DNA that was isolated from peritoneal and spleen cells (LM-PCR analysis was performed in close collaboration with Prof. Dr. Dr. Modlich and F. Schenk (group "Gene modification in Stem Cells", Paul-Ehrlich-Institut)).

As expected, the internal band was absent in the water control and in genomic DNA from control mice due to the absence of the transgene (Figure 33). For CD8-LV(CAR)-treated PBMC (CAR) and PBMC[CD19-depleted]humanzed mice (CARu) as well as for CD8-LV(RFP)-treated PBMC mice (RFP), internal bands were detected. A strong internal band surrounded by a faint smear characterized the amplified LV integration site pattern from transduced cells isolated from the peritoneal cavity. This indicated a rather polyclonal integration site pattern. In spleen cells, amplified LV integration sites were characterized by a strong internal band and several faint bands of various sizes, which indicated a more oligoclonal transgene integration site pattern.
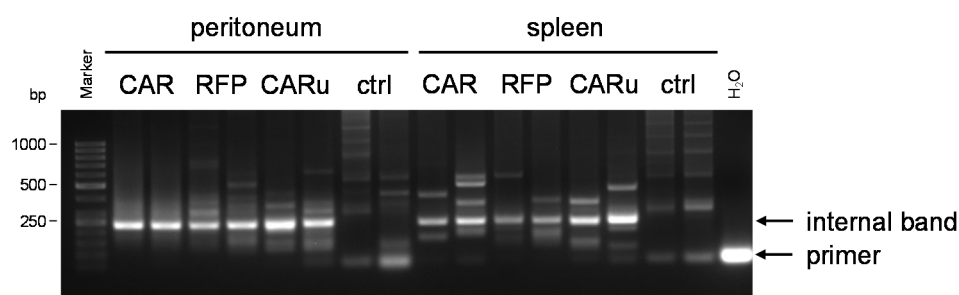
Figure 33: Detection of LV integration sites
LV integration sites were analyzed on genomic DNA by LM-PCR. Isolated gDNA of peritoneal and spleen cells from PBS-treated PBMC-humanized NSG mice (ctrl), CD8-LV(CAR)-treated PBMC-humanized NSG mice (CAR), CD8-LV(RFP)-treated PBMC-humanized NSG mice (RFP) and CD8-LV(CAR)-treated PBMC[CD19-depletd]-humanized NSG mice (CARu) were analyzed. Two representative mice of each group are shown. Internal control band (at 245 bp), primer band and the water control (H_2O) are shown.

In conclusion, specific transgene integration was observed for all mice treated with CD8-LV independently from the type of transgene. While a polyclonal integration pattern was observed for isolated cells from the peritoneal cavity, cells from the spleen showed a rather oligoclonal transgene integration site pattern. These data suggest polyclonal proliferation of *in vivo* transduced cells without any signs of monoclonal outgrowth.

3.4 Evaluating anti-tumoral functions of *in vivo* generated CAR T cells

Anti-tumoral functions of *ex vivo* generated CD19-specific CAR T cells had been demonstrated by others. NSG mice were i.v. injected with Raji-luc cells and successfully treated with CAR T cells (Xu et al., 2014; Hudecek et al., 2015; Sommermeyer et al., 2015). *In vivo* generated CAR T cells, however, remain to be evaluated for their anti-tumoral functions.

It was shown that systemic administration of CD8-LV(CAR) to PBMC-humanized NSG mice mediated *in vivo* generation of CAR T cells (chapter 3.3.1). In short-time experiments, *in vivo* generated CAR T cells completely eliminated $CD19^+$ cells and proliferated upon antigen stimulation. However, it remains to be seen whether the *in vivo* generated CAR T cells have anti-tumoral functions and are able to prevent tumor outgrowth.

For this purpose, 5×10^5 Raji-luc cells were i.v. injected into NSG mice. Five days later, 1×10^7 PBMC were injected followed by i.p. administration of CD8-LV(CAR) or PBS one day later (Figure 34).
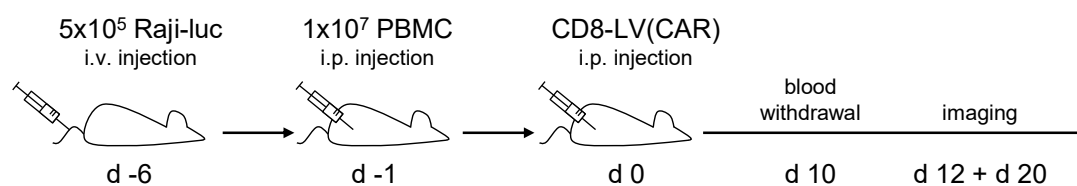
Figure 34: Experimental setting to evaluate anti-tumoral functions of *in vivo* generated CAR T cells in Raji-luc xenograft PBMC-humanized NSG mice
NSG mice were i.v. injected with 5×10^5 Raji-luc cells. Five days later 1×10^7 activated PBMC were i.p. injected, followed by i.p. administration of CD8-LV(CAR). On day ten, blood was taken to evaluate *in vivo* generation of CAR T cells. Tumor growth was monitored by *in vivo* bioluminescence imaging at indicated time points.

Tumor growth was monitored by *in vivo* bioluminescence imaging. Mice were regularly checked for their health status and sacrificed when termination criteria were reached. As seen in chapter 3.3.1, upon administration of CD8-LV(CAR) into PBMC-humanized mice, *in vivo* generated CAR T cells had been detected seven days after CD8-LV(CAR) administration. To evaluate *in vivo* generation of CAR T cells for CD8-LV(CAR)-treated

mice during the ongoing experiment, blood was taken on day ten and analyzed by flow cytometry for CD45, CD8 and CAR expression. PBS-treated mice served as control.

For PBS- and CD8-LV(CAR)-treated mice, on average 30% CD45$^+$ cells were detected in the blood (data not shown). On average 50% of the cells were CD8$^+$ cells. Seven out of eight CD8-LV(CAR)-treated mice showed CAR expression. On average 16.5% of the CD8$^+$ cells were CAR-positive (Figure 35A). To calculate the frequency of CAR T cells in the blood, the percentage of CD45$^+$CAR$^+$ cells was determined ranging between 5.8-12.7% (Figure 35B).
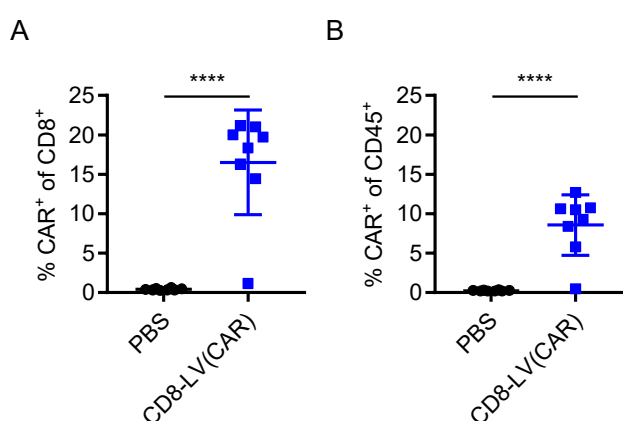
Figure 35: CAR expression of CD8$^+$ and CD45$^+$ cells in the blood of CD8-LV(CAR)-treated Raji-luc xenograft PBMC-humanized NSG mice
NSG mice were engrafted with Raji-luc cells and PBMC, and treated with CD8-LV(CAR). Ten days after vector administration, blood was taken from mice and analyzed by flow cytometry for CD45, CD8 and CAR expression. Percentage of (A) CAR$^+$ cells of CD8$^+$ cells and (B) CAR$^+$ cells of CD45$^+$ cells is shown for PBS-treated (black) and CD8-LV(CAR)-treated (blue) mice. N=8, mean ± SD are shown. Statistical significance was determined by two-tailed unpaired t-test; ****, p<0,0001.

These data demonstrated successful *in vivo* generation of CAR T cells in seven out of eight mice. Whether these CAR T cells mediated anti-tumoral effects was evaluated by tumor growth monitoring via *in vivo* bioluminescence imaging.

3.4.1 Monitoring tumor growth via *in vivo* imaging

Mice were imaged five days post Raji-luc administration (referred as day -1) and 12 and 20 days post CD8-LV(CAR) administration.

On day -1, luciferase signals were comparable between both groups. Until day 12, the luciferase signals further increased (Figure 36), indicating tumor growth for both, PBS and CD8-LV(CAR)-treated mice. For all mice, luciferase signals were distributed over the whole body. The highest signals were observed in the lower region of the body co-localizing with the knees of the mice, suggesting that these signals indicated tumor growth within the bone marrow. For some mice in both groups, signals coming from the

abdominal region were observed. In control mice, three out of eight mice had higher signals coming from the head region. However, on day 20, luciferase signals strongly decreased in PBS-treated mice. Luciferase signals were not covering the whole body, but were only present in distinct regions. Two out of four mice showed only two to three remaining regions of luciferase signals. All CD8-LV(CAR)-treated mice showed stronger luciferase signals compared to PBS-treated mice. However, compared to day 12, two of four CD8-LV(CAR)-treated mice also showed decreased luciferase signals. But the decrease of luciferase signals was not as pronounced as for PBS-treated mice.
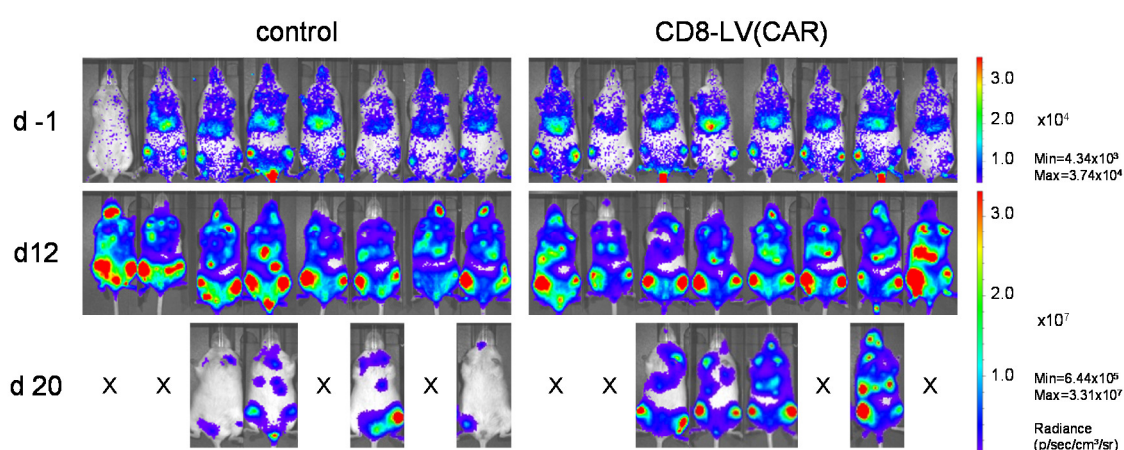
Figure 36: Tumor cell growth monitoring by *in vivo* bioluminescence imaging of CD8-LV(CAR)-treated Raji-luc xenograft PBMC-humanized NSG mice
NSG mice were engrafted with Raji-luc cells and PBMC, and treated with CD8-LV(CAR). Control mice were treated with PBS. Tumor cell growth was monitored by *in vivo* bioluminescence imaging one day prior vector administration (day -1) and on day 12 and 20 post CD8-LV(CAR) administration. Sacrificed mice are marked with X.

In vivo bioluminescence imaging data revealed a completely unexpected outcome concerning anti-tumoral effects. Luciferase signals on day 20 post PBMC administration indicated that PBS-treated mice had a lower tumor burden than CD8-LV(CAR)-treated mice.

3.4.2 Presence of *in vivo* generated CAR T cells in various organs

The *in vivo* bioluminescence imaging data from day 20 were completely unexpected. Having seen that PBS-treated mice had a lower tumor burden than CD8-LV(CAR)-treated mice was against all expectations. Until day 17, four mice of each group had to be sacrificed at earlier time points reaching termination criteria. Symptoms were characterized by partial or complete hind-limb-paralysis, hunching, weight loss and reduced mobility. From day 18 on, however, none of the mice had to be sacrificed because of hind-limb-paralysis. Stagnating or even decreasing luciferase signals on day 20 was in

line with missing tumor burden symptoms. For endpoint analysis, mice were sacrificed and analyzed in detail.

For all mice, independently of being sacrificed at early time points or later for endpoint analysis, single cell suspensions from spleen, peritoneum, blood and bone marrow were prepared and analyzed by flow cytometry for the presence of CAR T cells. To evaluate CAR T cell distribution among different organs, CAR expression of CD45$^+$ cells was analyzed. To distinguish between mice sacrificed at early time points and mice sacrificed for endpoint analysis, mice were marked differently in the scatter plots shown below. Mice sacrificed until day 17 were marked by empty circles/squares. Mice sacrificed later were marked with filled circles/squares.

PBS-treated mice served as control (Figure 37, black). Seven out of eight mice CD8-LV(CAR)-treated mice showed CAR expression. One mouse did not show CAR expression in the blood at day ten and had to be sacrificed at an early time point (Figure 35) (Figure 36, mouse at the far right). Flow cytometry of cells from various organs confirmed the absence of CAR T cells. Therefore, this mouse was excluded in further analyses. In peritoneal cells from CD8-LV(CAR)-treated mice, on average 18% CD45$^+$CAR$^+$ cells were detected. In spleen, CAR expression was on average 8% and further CAR T cells had also been detected in blood and bone marrow. On average, 6% CD45$^+$CAR$^+$ T cells were detected in the blood and 10% in the bone marrow (Figure 37, blue). Surprisingly, mice, which had been sacrificed at early time points, showed the higher frequencies of CAR T cells (Figure 37, blue, empty square).
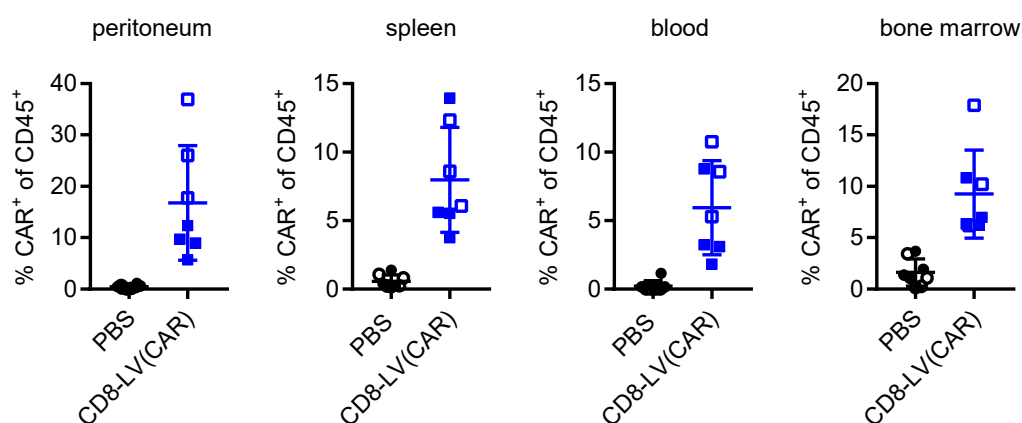
Figure 37: CAR expression of CD45$^+$ cells in various organs of CD8-LV(CAR)-treated Raji-luc xenograft PBMC-humanized NSG mice
NSG mice were engrafted with Raji-luc cells and PBMC, and treated with CD8-LV(CAR). Mice were sacrificed at early time points due to termination criteria (empty circles/squares) or for endpoint analysis (filled circles/squares). Single cell suspensions of indicated organs were prepared and analyzed for CD45 and CAR expression by flow cytometry. Percentage of CAR$^+$ cells of CD45$^+$ cells of peritoneal, spleen, blood and bone marrow is shown for PBS-treated (black) and CD8-LV(CAR)-treated mice (blue). N=7-8, mean ± SD are shown.

These data demonstrated that CAR T cells were generated in mice treated with CD8-LV(CAR). CAR T cells were distributed throughout the whole body being present in the peritoneal cavity, in the spleen, blood and in the bone marrow. Highest frequencies of CAR T cells were present in the peritoneal cavity followed by bone marrow. Strikingly, mice, which had to be sacrificed at early time points showed higher frequencies of CAR T cells within all organs compared to mice, which had been sacrificed for of endpoint analysis.

3.4.3 Analysis of the presence of CD19$^+$ B cells and CD19$^+$ tumor cells in various organs

CAR expression for CD8-LV(CAR)-treated mice was observed in various organs. However, luciferase signals indicated continuous tumor growth suggesting that the *in vivo* generated CAR T cells were not able to prevent outgrowth of CD19$^+$ Raji-luc tumor cells. Therefore, CD19$^+$ tumor cells were analyzed in detail in single cell suspensions of peritoneum, spleen, blood and bone marrow by flow cytometry. With the engraftment of Raji-luc cells and PBMC into NSG mice, the assumption was that CD19$^+$ tumor cells and CD19$^+$ B cells were present in the mice. Both populations had to be analyzed separately to evaluate effects of the *in vivo* generated CAR T cells on tumor cells and B cells, respectively. The different CD19$^+$ populations were distinguished by their CD45 expression, in particular by their different MFI for CD45. While CD19$^+$ B cells were characterized by a higher MFI for CD45, CD19$^+$ tumor cells showed a lower MFI for CD45. Thereby CD45^{high}CD19$^+$ cells were identified as B cells and CD45^{low}CD19$^+$ cells as tumor cells. To evaluate the effect of *in vivo* generated CAR T cells on B cells and tumor cells, single cell suspensions of peritoneal, spleen, blood and bone marrow were assessed for the percentages of CD45^{high}CD19$^+$ B cells and CD45^{low}CD19$^+$ tumor cells by flow cytometry.

In PBS-treated mice, CD45^{high}CD19$^+$ B cells were detected in the peritoneal cavity and in the spleen (Figure 38, top panel). The highest frequency (0.14%) was detected in the peritoneal cavity of mice sacrificed at early time points (black). In spleen, a minor frequency of B cells close to background was detected. For CD8-LV(CAR)-treated mice sacrificed at early time points (dark blue) almost no B cells were detected. Some remaining B cells in CD8-LV(CAR)-treated mice sacrificed for endpoint analysis were detected and were comparable to PBS-treated mice. However, these events were in a very low range between 0-0.5%. For both groups, CD45^{low}CD19$^+$ tumor cells were mainly detected in the bone marrow (Figure 38, lower panel). In all other organs, tumor cell frequencies were below 0.1% for all groups. Strikingly, a difference between

CD8 LV(CAR)- and PBS-treated mice was observed in the subgroup of mice sacrificed at early time points. CD8-LV(CAR)-treated mice showed less tumor cells (4.6%) than PBS-treated mice (10.2%). However, comparing endpoint analyzed mice more tumor cells had been found in CD8-LV(CAR)-treated mice compared to PBS-treated mice.
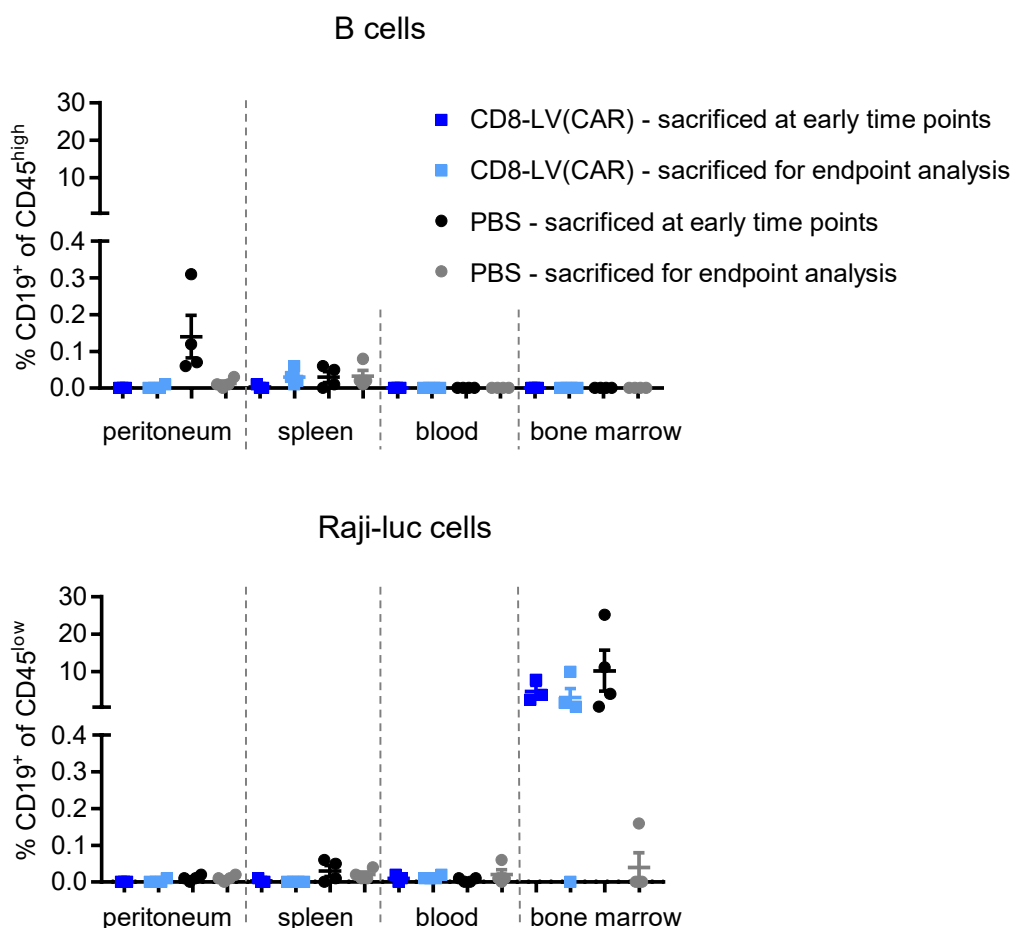
Figure 38: Analysis of CD19$^+$ Raji-luc or B cells in various organs from CD8-LV(CAR)-treated Raji-luc xenograft PBMC-humanized NSG mice
NSG mice were engrafted with Raji-luc cells and PBMC, and treated with CD8-LV(CAR). Mice were sacrificed at early time points due to termination criteria (dark blue and black) or for endpoint analysis (light blue and grey). Single cell suspensions were prepared from indicated organs and analyzed for CD45 and CD19 expression by flow cytometry. Percentage of B cells (CD19$^+$ of CD45^{high}) is shown in the upper panel and percentage of Raji-luc cells (CD19$^+$ of CD45^{low}) in the lower panel. N=7-8, mean ± SEM are shown.

These data suggest that B cells were mainly present in peritoneum and spleen and absent in blood and bone marrow in PBS-treated mice. For CD8-LV(CAR)-treated mice, B cells had been almost completely eliminated. Tumor cells were primarily detected in the bone marrow. Strikingly, mice, which had to be sacrificed at early time points showed higher frequencies of tumor cells in PBS-treated mice compared to CD8-LV(CAR)-treated mice. This indicated anti-tumoral CAR T cell activity until day 17. However, at endpoint analysis, CD8-LV(CAR)-treated mice showed a higher tumor cell frequency in the bone marrow than PBS-treated mice.

The luciferase signals and the presence of CD19$^+$ tumor cells in CD8-LV(CAR)-treated mice indicated that *in vivo* generated CAR T cells were not able to prevent tumor outgrowth. Besides others, one reason might be CD19 antigen loss of tumor cells. Upon CAR T cell activation against CD19$^+$ tumor cells, loss of the CD19 antigen can occur (Grupp et al., 2013). CAR T cells would not be able to recognize tumor cells anymore and therefore would not exert anti-tumoral functions. However, downregulation of the targeted antigen does not affect the surface expression of other antigens. Raji cells express, besides other surface markers, the CD20 antigen.

To evaluate antigen loss of tumor cells single cell suspensions from bone marrow were analyzed for the co-expression of CD19 and CD20 by flow cytometry analysis. As control, *in vitro* cultivated Raji-luc cells were analyzed.

Co-staining of CD20 and CD19 of *in vitro* cultured Raji-luc cells demonstrated 86.4% of the Raji-luc cells to be double positive for both markers (Figure 39). Co-staining of single cell suspensions from bone marrow cells of CD8-LV(CAR)-treated mice sacrificed for endpoint analysis revealed 85.8% of all CD20$^+$ cells to express CD19. Some few CD19$^+$ cells showed a lower MFI, indicating lower expression of CD19. Furthermore, some cells were detected to be CD19$^-$. However, these were only very few cells (3%).

These data demonstrated that the majority of tumor cells explanted from CD8-LV(CAR)-treated mice expressed the CD19 antigen on the cell surface although some few cells downregulated or did not express the CD19 antigen.
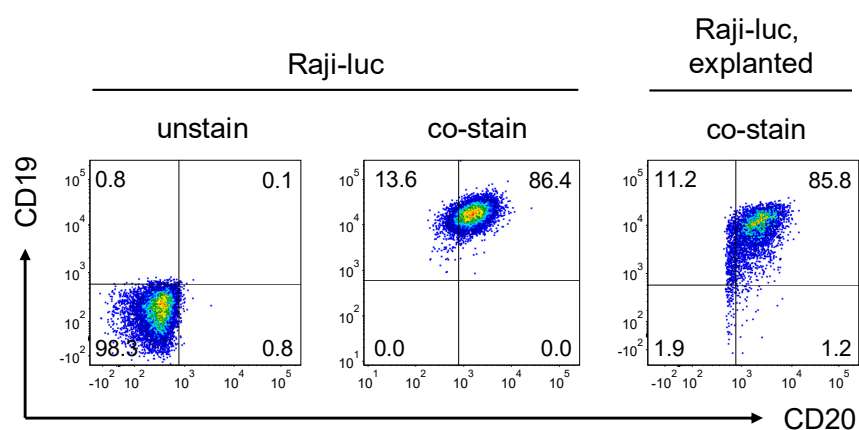
Figure 39: CD19 and CD20 co-expression analysis of Raji-luc cells explanted from bone marrow from CD8-LV(CAR)-treated Raji-luc xenograft PBMC-humanized NSG mice
NSG mice, engrafted with PBMC and Raji-luc cells were treated with CD8-LV(CAR). Mice were sacrificed for endpoint analysis and single cell suspensions from bone marrow were analyzed for CD19 and CD20 expression by flow cytometry. One representative density plot is shown (far right, N=2). *In vitro* cultivated Raji-luc cells were analyzed for CD19 and CD20 co-expression as control (Raji-luc).

3.4.4 Phenotypic characterization of CAR T cells in various organs

In vivo generated CAR T cells were distributed to various organs including peritoneum, spleen, blood and bone marrow. They were able to eliminate CD19$^+$ B cells, but the outgrowth of tumor cells was not prevented. CAR T cells were further characterized for their subset phenotype to investigate functionality of the CAR T cells in detail. CAR T cells were analyzed by flow cytometry for CD62L and CD45RA surface expression, classifying them into $T_{SCM/Naïve}$, T_{CM}, T_{EM} and T_{Eff}. CAR$^-$ cells (CD8$^+$CAR$^-$ cells and CD8$^-$ cells) were analyzed as controls representing cells being unaffected by the interaction of CAR T cells and antigen. The following analysis included four mice of each group, which had been sacrificed for endpoint analysis. Subset distribution was separately evaluated for the different organs: peritoneum, spleen, blood and bone marrow.

For peritoneal cells, the average distribution in CD8$^-$ cells was similar in CD8-LV(CAR)- and PBS-treated mice. The majority were T_{CM} (51.91% ± 3.99%) followed by T_{EM} (47.94% ± 3.98%). Almost no $T_{SCM/Naïve}$ (0.07% ± 0.08%) or T_{Eff} (0.09% ± 0.05%) were present (Figure 40A, right panel). Comparing CD8$^+$CAR$^-$ cells, a similar distribution pattern was observed for both treatments with a majority of T_{CM} (53.51% ± 5.96%) followed by T_{EM} (45.44% ± 5.99%). Only very few $T_{SCM/Naïve}$ (0.59% ± 0.22%) and T_{Eff} (0.09% ± 0.05%) were detected (Figure 40A, middle panel). The subset-phenotype distribution of CD8$^+$CAR$^+$ cells showed the same overall distribution pattern as in CD8$^+$CAR$^-$ and as in CD8$^-$ cells having almost no $T_{SCM/Naïve}$ (0.21% ± 0.25%) and T_{Eff} (0.42% ± 0.35%) present. However, the fraction of T_{CM} was enriched (64.95% ± 9.52%) and less T_{EM} (34.41% ± 9.87%) were detected (Figure 40A, left panel). In the spleen, cells were characterized by the same overall subset distribution with two major populations of T_{EM} and T_{CM} and two smaller population represented by $T_{SCM/Naïve}$ and T_{Eff}. In detail, CD8$^-$ cells showed the same distribution in CD8-LV(CAR)- as in PBS-treated mice. T_{EM} were of highest frequency (57.35% ± 9.94%) followed by 37.61% ± 7.75% T_{CM}. Remaining cells were $T_{SCM/Naïve}$ (2.94% ± 1.76%) and T_{Eff} (2.11% ± 1.08%) (Figure 40B, right panel). A similar distribution was observed in CD8$^+$CAR$^-$ cells independently of being treated with PBS or CD8-LV(CAR). Most cells were T_{EM} (52.51% ± 7.32%) followed by T_{CM} (37.45% ± 8.22%). $T_{SCM/Naïve}$ (6.15% ± 2.76%) and T_{Eff} (3.89% ± 2.58%) being the smallest fractions (Figure 40B, middle panel). CD8$^+$CAR$^+$ cells showed higher frequencies of T_{CM} (49.32% ± 7.01%) and lower frequencies of T_{EM} (44.62% ± 1.0%). $T_{SCM/Naïve}$ (3.34% ± 3.72%) and T_{Eff} (2.72% ± 3.59%) cell fractions were comparable to CD8$^+$CAR$^-$ and CD8$^-$ cells (Figure 40B, left panel).

Blood cells were also characterized by two major populations of T_{EM} and T_{CM}. CD8$^-$ cells from PBS and CD8-LV(CAR)-treated mice showed a similar distribution pattern of subset

phenotypes. Almost equally large T_{CM} (47.6% ± 7.25%) and T_{EM} (45.11% ± 10.71%) fractions and few $T_{SCM/Naïve}$ (5.58% ± 3.16%) and T_{Eff} (1.70% ± 0.63%) (Figure 40C, right panel) were observed. $CD8^+CAR^-$ cells showed a slightly different pattern, having more T_{CM} (59.35% ± 5.69%), T_{EM} (26.07% ± 6.86%) and a larger portion of $T_{SCM/Naïve}$ (11.56% ± 5.69%). Few T_{Eff} were present (3.03% ± 1.35%) (Figure 40C, middle panel). Against all previous data, for blood cells, the distribution of $CD8^+CAR^+$ cells was similar to the pattern of $CD8^+CAR^-$ cells. The largest fraction was T_{CM} (66.89% ± 1.20%), followed by T_{EM} (22.21% ± 7.03%), $T_{SCM/Naïve}$ (9.56% ± 6.22%) and a small fraction of T_{Eff} (1.34% ± 0.33%) (Figure 40C, left panel).

In contrast to all previous organs, subset distribution in the bone marrow within $CD8^-$ and $CD8^+CAR^-$ cells were different between CD8-LV(CAR)- and PBS-treated groups. $CD8^-$ cells of CD8-LV(CAR)-treated mice were characterized by higher frequencies of T_{EM} (54.1% ± 17.34%) and T_{Eff} (15.78% ± 17.48%) (Figure 40D, right panel). In contrast, PBS-treated mice had less T_{Eff} (3.34% ± 1.13%) and more T_{EM} (70.7% ± 13.85%). Frequencies of $T_{SCM/Naïve}$ and T_{CM} were similar with on average 3.23% ± 3.01% $T_{SCM/Naïve}$ and 24.06% ± 10.4% T_{CM}. A similar distribution was observed for $CD8^+CAR^-$ cells with similar average frequencies of $T_{SCM/Naïve}$ (1.35% ± 0.81%) and T_{CM} (6.6% ± 3.87%) (Figure 40D, middle panel). Similarly, as observed for $CD8^-$ cells, CD8-LV(CAR)-treated mice showed higher T_{Eff} (19.15% ± 19.84%) with 73.11% ± 18.48% T_{EM}. PBS-treated mice showed lower frequencies of T_{Eff} (3.75% ± 1.43%) with 88.11% ± 6.81% T_{EM}. Remarkably, the subset distribution of $CD8^+CAR^+$ cells was strikingly different. The fraction was characterized by a high frequency of T_{Eff} (43.02% ± 28.62%). T_{EM} still made up the biggest portion (46.25% ± 25.62%) followed by a smaller T_{CM} fraction (7.5% ± 5.08%) and a minor $T_{SCM/Naïve}$ fraction (3.23% ± 3.93) (Figure 40D, left panel).
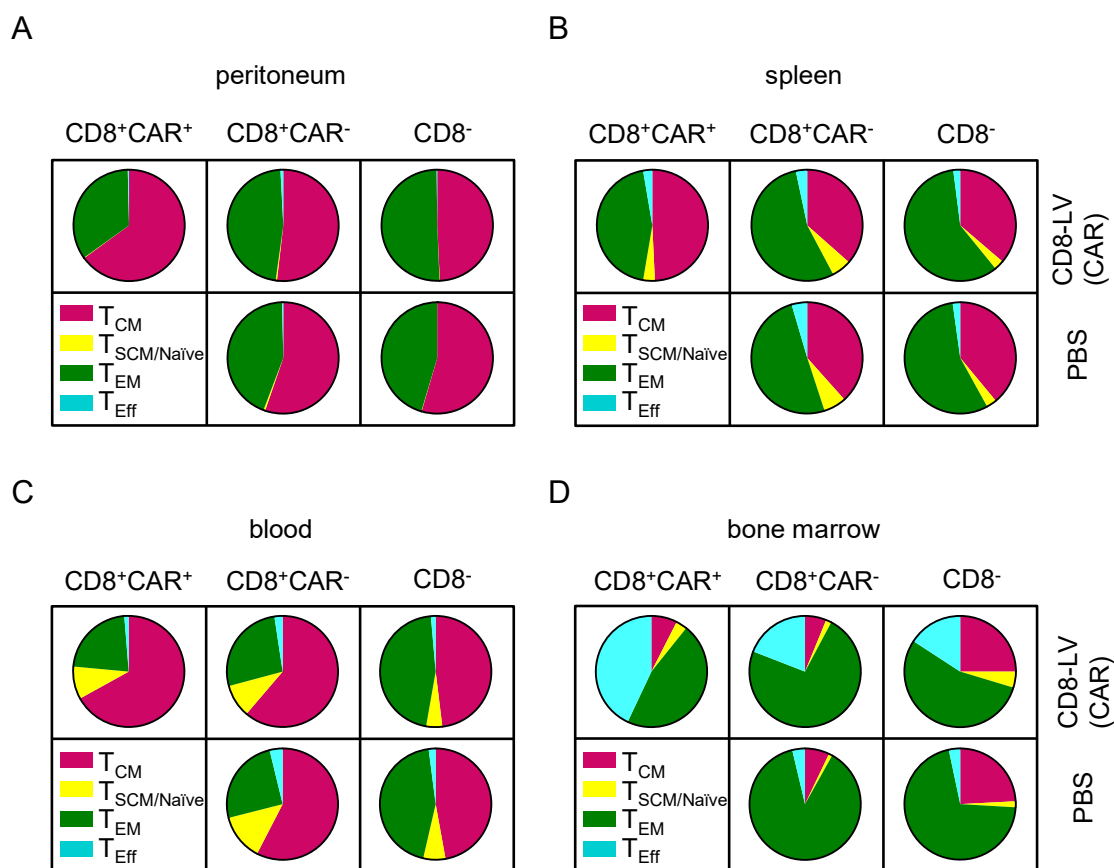
Figure 40: Subset-phenotype analysis of *in vivo* generated CAR T cells in various organs from CD8-LV(CAR)-treated Raji-luc xenograft PBMC-humanized NSG mice
NSG mice were engrafted with Raji-luc cells and PBMC, and treated with CD8-LV(CAR). Mice were sacrificed for endpoint analysis. Single cell suspensions from peritoneum, spleen, blood and bone marrow were analyzed for CD45, CD3, CD8, CAR, CD62L and CD45RA expression by flow cytometry. Human T cells were identified as $CD45^+CD3^+$ cells. $CD8^+CAR^+$, $CD8^+CAR^-$ and $CD8^-$ cells were analyzed for CD62L and CD45RA expression and classified into subset-phenotypes. Subsets are defined as pink: central memory T cells (T_{CM}: $CD45RA^-CD62L^+$); yellow: stem cell memory/naïve T cells ($T_{SCM/Naïve}$: $CD45RA^+CD62L^+$); green: effector memory T cells (T_{EM}: $CD45RA^-CD62L^-$); and turquoise: effector T cells (T_{Eff}: $CD45RA^+CD62L^-$). Pie chart representations of mean subset-phenotype percentages for $CD8^+CAR^+$, $CD8^+CAR^-$ and $CD8^-$ cells are shown for CD8-LV(CAR)- or PBS-treated PBMC-humanized NSG mice. N=4.

Taken together, these data demonstrate, that $CD8^+CAR^-$ and $CD8^-$ cells often show the same subset distribution pattern within individual organs, independently of the treatment, either treated with PBS or CD8-LV(CAR). Peritoneal, spleen and blood cells, were mostly characterized by two main populations of T_{EM} and T_{CM}. $T_{SCM/Naïve}$ and T_{Eff} were underrepresented in the three organs. Being absent in the peritoneum, some $T_{SCM/Naïve}$ and T_{Eff} were detected in spleen and blood. In these three organs, CAR T cells showed a different pattern compared to $CD8^+CAR^-$ and $CD8^-$ cells with larger frequencies of T_{CM}, but had the tendency for a similar overall subset distribution, and were characterized by high frequencies of T_{EM}. Strikingly, in the bone marrow the overall subset distribution was changed, showing more T_{Eff}. Remarkably, highest frequency of T_{Eff} were observed in CAR T cells in CD8-LV(CAR)-treated mice.

4   Discussion

Successful CAR T cell therapy currently relies on *ex vivo* modification of cells and thereby faces financial hurdles and logistic expenses due to its highly personalized and complex manufacturing process. *In vivo* generation of CAR T cells by vector administration would de-personalize the current process and facilitate CAR T cell therapy as an off-the-shelf product for cancer immunotherapy.

This thesis demonstrates the first proof-of-principle study for the *in vivo* generation of human CAR T cells in a preclinical mouse model using CD8-receptor-targeted LVs. First conclusions can be made on transduction efficiency, functionality of the CAR T cells, such as proliferation, killing of CD19$^+$ cells, and phenotypic characteristics. These data suggest CD8-LV as a highly promising candidate for further investigations to be a powerful tool for the *in vivo* generation of CAR T cells.

4.1   CD8-targeted LV for *in vivo* gene delivery into T cells

Current genetic modifications of lymphocytes require the isolation of blood cells from the patient to engineer them *ex vivo* using VSV-G-pseudotyped LVs. Two main reasons hinder direct *in vivo* modification of cells: (i) selective gene delivery without off-target transduction and (ii) a non-permissive status of resting cells for VSV-G LV transduction. Due to the lack of the LDL receptor, gene delivery by VSV-G LV to unstimulated lymphocytes, such as HSCs, monocytes and resting B and T lymphocytes is inefficient (Amirache et al., 2014). Receptor-targeted LVs address both issues. They have been shown to reliably and selectively deliver genes into the target cell population while non-target cells remain untransduced. So far, *in vitro* and *in vivo* studies demonstrated successful targeting to diverse cell entities, among them CD133$^+$ hematopoietic cells, CD20$^+$ B lymphocytes as well as CD4$^+$ and CD8$^+$ T lymphocytes (Funke et al., 2008; Anliker et al., 2010; Zhou et al., 2012; Zhou et al., 2015). Furthermore, for some of these vectors, the targeting domain induced mild activation of the target cells allowing gene transfer into resting cells. Gene delivery into resting B cells was achieved by the CD20- and CD19-targeted LVs inducing the transfer of cells into the G1b cell cycle phase (Kneissl et al., 2013). Also for CD4-LV, transduction of unstimulated T cells was demonstrated (Zhou et al., 2015). These studies had been performed using MV-pseudotyped LVs requiring further investigations for NiV-pseudotyped LVs. However, since the activating stimulus is mediated by the incorporated scFv displayed on the vector particle it is assumed to be independent from the type of incorporated glycoproteins. The scFv used either for NiV- or MV-pseudotyped CD8-targeted LV is derived from OKT8,

which has been shown to mediate activating functions and to trigger effector functions upon binding, whereas six other CD8-specific antibodies did not (Clement et al., 2011). Therefore, the type of incorporated scFv can be chosen in a way to equip the vector with activating modulation properties and thereby enhancing transduction efficiency into resting lymphocytes. Studies incorporating additional molecules such as IL-7 into the LVs demonstrated activation of lymphocytes and might provide a further tool for transduction of unstimulated T cells without the usage of broad activating modulating agents (Verhoeyen et al., 2003).

To evaluate the capability of CD8-LV to deliver transgenes *in vivo*, studies shown in this thesis were performed in preclinical mouse models. Thereby, the PBMC-humanized NSG mouse model with a stable T cell engraftment was chosen, which enables a comprehensive analysis on transduction efficiency. While selective gene delivery into CD8 T cells had been shown *in vitro* for NiV- and MV-pseudotyped CD8-LV, *in vivo* gene delivery requires vector stocks to be producible in reasonable titers. Only with the establishment of NiV-pseudotyped LVs, sufficient titers of CD8-LV being 100-fold higher compared to CD8^{MV}-LV allowed systemic administration of vector particles (Bender et al., 2016). In the present study, successful *in vivo* gene delivery was demonstrated by luciferase and GFP expressing cells upon intravenous administration of CD8-LV(Luc-GFP) into mice (Figure 7, Figure 8). Although luciferase signals were distributed over the whole body and CD8$^+$GFP$^+$ cells were detected in lung, spleen and blood, on average only 0.2% of the CD8 T cells were GFP-positive. Compared to CD4^{MV}-LV, showing on average 6% of CD4 transduced cells upon systemic administration (Zhou et al., 2015), transduction efficiency was unexpectedly low. While the reasons are not yet clear, individual properties of the vectors might have contributed to the different transduction efficiency. Whereas CD8-LV is pseudotyped with NiV glycoproteins displaying a scFv, CD4^{MV}-LV is pseudotyped with MV glycoproteins displaying a DARPin as targeting domain (Zhou et al., 2015; Bender et al., 2016). DARPins usually show higher binding affinities than scFV, which might have contributed to the increased transduction efficiency (Plückthun, 2015). However, direct comparison was not performed so far and it remains to be evaluated whether CD8-specific DARPins mediate higher transduction efficiency *in vivo*.

When vectors were intraperitoneally administered, transduction efficiency became more similar for both vectors with slightly higher levels of transduced cells (12%) for CD4^{MV}-LV transferring *blue fluorescent protein* (*bfp*) gene compared to 3% transduced cells by CD8-LV transferring *rfp* (Figure 23) (Zhou et al., 2015). While the type of the reporter gene is not expected to influence transduction efficiency, the administration route of PBMC and

vector affects engraftment kinetics of human cells and distribution of the vector, thereby influencing the likelihood of vector-cell contact. Intravenously administered PBMC directly enter circulation resulting in faster distribution of human cells and various localizations. Diverse distribution of human cells and vector particles probably limits their contact frequencies resulting in lower transduction efficiency. In contrast, intraperitoneally injected PBMC require 7-14 days to drain from the peritoneal cavity to the circulation (King et al., 2008). Therefore, i.p. injection of PBMC and vector brings these two components in close proximity, most likely increasing transduction efficiency. Although low transduction levels upon i.v. administration were disappointing in the first place, doubting the potential of CD8-LV, i.p. injection demonstrated that administration routes influence transduction efficiency. Furthermore, low amounts of initially transduced cells must not be disadvantageous, especially with CAR gene delivery, which was expected to confer proliferative advantage.

Off-target transduction is a major concern of *in vivo* CAR gene delivery. Given the wide distribution of luciferase signals, CD8-LV appeared to be unspecific on the first view. However, this is rather the result of circulating transduced CD8 T cells present in the blood. Another reason for these signals also might be the infiltration of CD8 T cells into the skin as a result from graft-versus-host disease (GvHD), which is known as xenogeneic reaction occurring in NSG mice transplanted with PBMC. Stronger luciferase signals were observed in the lung and in the spleen – organs that have been shown by others to be homing sites of transferred T cells (van Rijn et al., 2003; King et al., 2009). To characterize off-target transduction in detail, the specificity of the vector was evaluated by analyzing non-target cells. A closer look at CD8⁻ cells revealed some events in the GFP-positive gate (Figure 8). These events, however, had a low MFI compared to GFP events within the CD8⁺ cells, which were of higher MFI. Additionally, the percentage of GFP events within the CD8⁻ cells of vector-treated mice was similar to those observed in the PBS-treated control mice indicating that these events can be considered as background signal. When including murine cells in the analysis, also no off-target GFP expression was observed (Figure 9). For *in vitro* transduction experiments, events within the gate of target-negative cells were observed, however, they were always below 1% (Figure 13). These observations were also seen with the CD4^MV-LV, which were in this case explained by a temporary downregulation of the receptor upon vector particle binding and incorporation (Zhou et al., 2015). Whether these few events result from real off-target transduction requires detailed analysis of the potentially transduced cells. With the exception of these few events, the CD8-LV demonstrated high selectivity with transgene expression almost exclusively present in CD8-positive cells.

Taken together, CD8-LV represents a new receptor-targeted LV mediating *in vivo* gene delivery. Importantly, CD8-LV demonstrated *in vivo* gene delivery upon systemic administration, which was not achieved with CD8^{MV}-LV. Although transduction efficiency is different from that observed with CD4^{MV}-LVs it is unclear whether this is a result from targeting different cell populations or caused by individual vector properties. This requires further studies with direct comparisons. Transduction efficiency, however, was increased when administering PBMC and vector intraperitoneally. This indicated that a rather restricted area bringing vector and target cells in close proximity is beneficial for transduction efficiency. Furthermore, GFP expressing cells within CD8$^+$ cells demonstrated selective gene delivery of CD8-LV, a critical prerequisite for a potential usage of CD8-LV for *in vivo* gene delivery.

4.2 *In vivo* generation of CAR T cells and their functionality

The capability of CAR T cells to mediate anti-tumoral activity is extensively studied in animal models, particularly in murine models before their clinical potential is studied in humans. Hereby, different mouse models can be distinguished: syngeneic and humanized, xenograft mouse models (Figure 41). Many preclinical studies are performed in xenograft models, in which human CAR T cells and human tumor cell lines are engrafted into immune-incompetent mice. This model was also used in the present study.
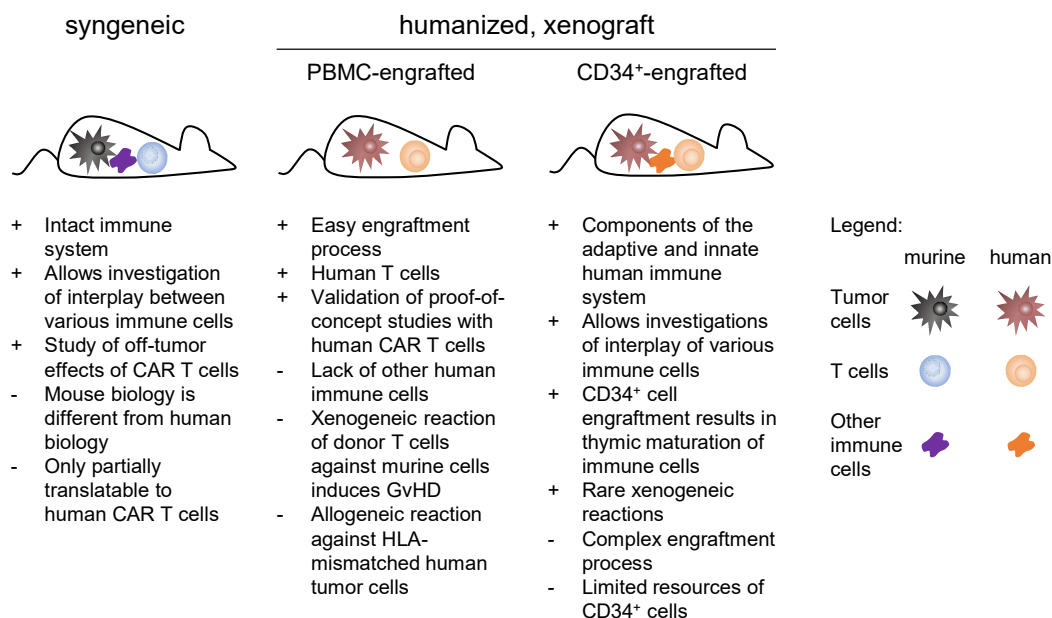
Figure 41: Schematic overview of mouse models used for CAR T cell studies
Depiction of immune components and tumor cells in syngeneic and humanized, xenograft mice. Advantages (+) and disadvantages (-) for CAR T cell studies are shown below each model. GvHD, graft-versus-host disease; HLA, human leukocyte antigen.

In this thesis, for the first time, the *in vivo* generation of human CAR T cells was demonstrated. Key for this achievement was the used CD8-LV and PBMC-humanized NSG mice allowing first insights into the functionality of *in vivo* generated CAR T cells. Remarkably, intraperitoneal administration of CD8-LV(CAR) resulted in on average 50% of the CD8$^+$ cells being CAR-positive. Using the same administration route with CD8-LV(RFP), however, resulted in at least ten-fold less transgene-positive cells (Figure 23). Additionally, higher percentages of CD8$^+$ cells were observed in CD8-LV(CAR)-treated mice, compared to PBS- or CD8-LV(RFP)-treated mice (Figure 24).

Both observations suggest a selective enrichment of CD8$^+$CAR$^+$ T cells. Once the CAR was expressed and presented on the surface of the transduced cell a selective proliferation of CAR T cells must have been triggered by antigen stimulus – most likely by CD19$^+$ cells. Although it was initially assumed that Raji cells provide this proliferation stimulus, this hypothesis turned out to be at least partially wrong. The frequency of CAR T cells was unaltered in mice engrafted with or without Raji-luc cells (Figure 23). In contrast, the engraftment of B cell-depleted PBMC resulted in lower transgene expression of CD8-LV(CAR)-treated mice demonstrating that the CD19$^+$ B cells were the proliferation stimulus that triggered selective proliferation of the *in vivo* generated CAR T cells in this experiment. However, it cannot be excluded that Raji cells also triggered CAR T cell proliferation, but this requires further investigation. Even more, CAR T cells eliminated CD19$^+$ cells not only in the peritoneum, but also in spleen and in blood, which besides circulating activities of the CAR T cells also proves their ability to recognize and to kill target cells providing strong evidence for their functionality.

Although these short-term experiments were meant to provide first proof-of-principle of *in vivo* CAR T cell generation, additional conclusions about the functionality of *in vivo* generated CAR T cells already can be drawn. In fact, both observations: elimination of B cells and proliferation of CAR T cells are very promising observations for generating functional CAR T cells and are critical determinants in clinical studies. CAR T cell proliferation highly correlates with anti-tumoral activities, having sufficient CAR T cell numbers around to enable tumor destruction (Kalos et al., 2011; Grupp et al., 2013; Lee et al., 2015). B cell elimination correlates with successful clinical outcome in B cell malignancy patients treated with CD19 CAR T cells (Maude et al., 2014). Hence, these two observations can be regarded as promising indications that *in vivo* generated CAR T cells are functional.

While the work of this thesis was ongoing, also other groups put efforts in the *in situ* modification of T cells to express a chimeric antigen receptor. Smith and colleagues used targeted nanoparticles to generate murine CAR T cells *in vivo* in immunocompetent mice

(Smith et al., 2017). Consisting of several layers of polymers, these nanoparticles incorporate DNA molecules and have an outer layer of polyglutamic acid coupled to an anti-CD3e f(ab')2 fragment to enable targeting of murine $CD3^+$ T cells. Selective targeting was demonstrated in syngeneic mouse models transferring a mouse CD19-specific CAR. Co-integration of a transposase encoding plasmid into nanoparticles ensured stable integration of the CAR transgene. They were able to show, that *in vivo* engineered CAR T cells are as effective as *ex vivo* manufactured CAR T cells regarding anti-tumoral activities. However, *in vitro* transduction efficiency of 3% upon administration of a nanoparticle to T cell ratio of 3000 indicate inefficient transduction. This was further underlined by the bolus applications of $3x10^{11}$ nanoparticles on five consecutive days to achieve *in situ* T cell modification. Off-target CAR expression was observed in 6% of non-target cells, including neutrophils, B cells, monocytes, natural killer (NK) cells and eosinophils, stating phagocytic uptake of the nanoparticles as the reason for off-target expression. Although off-target events and transduction efficiency need to be further investigated and improved, nanoparticles represent a further tool for *in vivo* engineering of T lymphocytes with anti-tumoral functions upon CAR transfer.

Despite the fact that syngeneic models allow functional studies of CAR T cells within an immunocompetent environment, results obtained in this model cannot easily be transferred to the human system. The fully murine-derived components impede transferring the obtained results into human context, since the murine immune system does not always reflects the human biology (Siegler and Wang, 2018) (Figure 41). It is unknown, whether transduction with nanoparticles works equally well on human cells and whether nanoparticle-engineered human CAR T cells are functional. Thereby, murine CAR T cells only provide limited insights into human CAR T cell mechanism. In contrast to Smith et al., modification with the CD8-LV enables analysis and characterization of human CAR T cells within PBMC-engrafted NSG mice. Functional testing and detailed characterization of human CAR T cells including transgene integration analysis and phenotype characterization provide first insights into characteristics of *in vivo* generated human CAR T cells.

Transgene integration and clonality analysis provided further insights into CD8-LV-modified human cells. The clonality analysis revealed a polyclonal integration pattern (Figure 33) demonstrating the absence of clonal dominance or monoclonal outgrowth after vector-mediated transgene insertion. Although this short-time experiment does not allow comprehensive conclusions about safety, it did not reveal any evidence for clonal expansion.

Ex vivo generated CAR T cells often have multiple integrations due to the transduction with multiple transducing particles per cell. Resultant overexpression of CAR molecules on the surface, however, has been shown to be of disadvantage. In fact, physiological CAR expression controlled by endogenous TCR promotor outperformed conventional CAR T cells in murine tumor models (Eyquem et al., 2017). Thus, as long as transgene expression is sufficient to mediate therapeutic effects single transgene integrations are preferred over multiple insertion sites in terms of safety and functional aspects. Upon CD8-LV administration, the highest VCN (0.4) was found on peritoneal cells, which was in line with the flow cytometry data showing the highest transgene expression in the peritoneum (Figure 32). Given this low VCN multiple integrations rather can be excluded for the *in vivo* approach, which might contribute to a lower risk of insertional mutagenesis and a potentially better CAR T cell product.

Observations in this xenograft mouse model also provided insights into the differentiation status of *in vivo* generated CAR T cells. Phenotype analysis suggested a pool of diversely differentiated CAR T cells generated with CD8-LV. Not only effector CAR T cells but also less differentiated phenotypes such as $T_{SCM/Naïve}$ and both memory T cell phenotypes T_{CM} and T_{EM} showed CAR expression demonstrating that CD8-LV-mediated transduction of T cells generates all types of CAR T cells. Even more, clear differences between antigen-experienced and unexperienced CAR T cells were observed. Phenotype analysis was performed on cells isolated from the peritoneal cavity seven days post vector administration. At this time point, $CD19^+$ cells were already eliminated in CD8-LV(CAR)-treated mice. In mice transplanted with CD19-depleted PBMC, however, they were absent from the beginning of this experiment. CAR T cells generated in these two settings revealed differences in the phenotypic patterns. Antigen-experienced CAR T cells showed higher frequencies of T_{CM} subtypes, whereas antigen-unexperienced CAR T cells were predominantly composed of T_{EM} and T_{Eff}. This observation might be explained by the circumstance that $CD19^+$ cells had been already eliminated by the CAR T cells. It is well known that T_{EM} as well as T_{EM} vanish after antigen clearance, which is part of the negative feedback-loop of the immune systems to shut off an immune reaction upon antigen clearance and prevent over-activation. This might be the reason for the lower frequency of these cells within the CD8-LV(CAR)-treated PBMC engrafted mice. In mice engrafted with CD19-depleted PBMC, in contrast, CAR T cells did not yet encounter their antigen. They therefore circulate to increase the likelihood of antigen encounter. However, this analysis only refers to floating cells, which had been isolated by peritoneal lavage. Dependent on the surface receptor expression of T cells and the ligand expression on the associated tissue T cells traffic and home to respective tissues. Especially effector T cells express receptors specific for homing to peripheral tissue such

as gut- or skin-associated tissue (Mora and Andrian, 2006). Therefore, for detailed analysis of the distribution of the different T cell subtypes other tissues would need to be analyzed.

However, the presence of CAR T cells of different phenotypes clearly suggests that CD8-LV(CAR) is in principle able to transduce different T cell phenotypes *in vivo*, which is highly preferred in terms of generating a pool of CAR T cells with various effector and proliferative functions. Each phenotype contributes to successful therapeutic effects as seen in clinical studies (Golubovskaya and Wu, 2016). Effector CAR T cells provide immediate anti-tumoral activity, critical to stop fast growing tumors in the first place. However, their limited proliferative capability provides only short-term activities. Less differentiated CAR T cells ensure long-term persistence of CAR T cells and memory CAR T cells, ideally, provide long-term protection against relapsing tumors.

4.3   Properties influencing anti-tumoral functions of CAR T cells

Anti-tumoral activity of CAR T cells is studied in murine models, mainly in xenograft models in order to facilitate transferring outcomes to human physiology. To evaluate anti-tumoral efficiency of *in vivo* generated human CAR T cells, pre-established tumors in NSG mice were monitored for tumor growth after PBMC and vector administration. Although successful *in vivo* generation of CAR T cells was demonstrated by the presence of CAR T cells in the blood ten days post vector administration, tumor growth was not impaired. Even more astounding, the control group showed less tumor signals than the CD8-LV(CAR) group (Figure 36). Clearly, this outcome was unexpected and anti-tumoral effects of CAR T cells were missing here. Which criteria determine the success of CAR T cell therapy, and which properties must CAR T cells meet to confer anti-tumoral functions?

Anti-tumoral efficiency is dependent on various factors. A critical determinant, among others is the status of differentiation of a CAR T cell. While effector CAR T cells rather confer immediate killing activities towards the tumor cells, less differentiated CAR T cells give rise to further daughter cells, ensuring long-term persistence of CAR T cells.

Detailed analysis of CD8-LV(CAR)-treated mice revealed the presence of CAR T cells in various organs such as peritoneum, spleen, blood and even bone marrow. Remarkably, all different phenotypes were detected, whereby a particular subset distribution was observed for each organ (Figure 42).
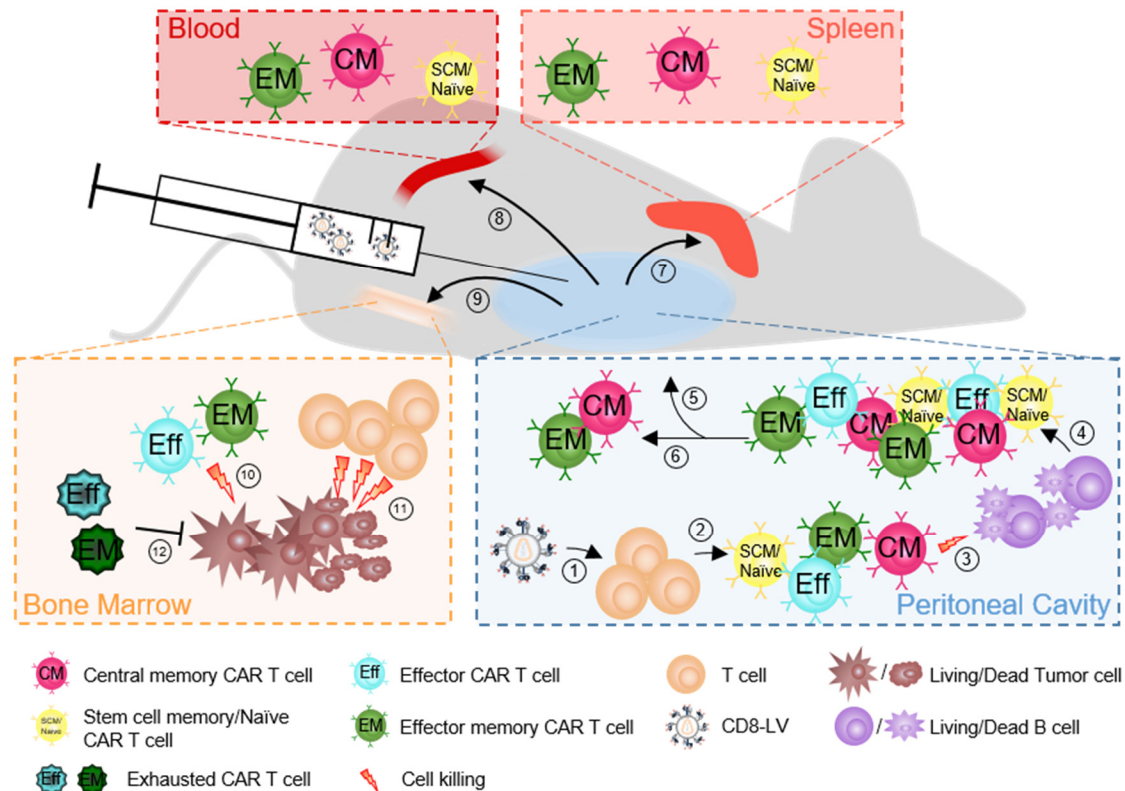
Figure 42: Schematic overview and proposed model of *in vivo* CAR T cell generation, their functions and migration into other tissues

Tumor cells were i.v. injected into NSG mice, followed by i.p. injection of PBMC and CD8-LV(CAR). (1) CD8-LV(CAR) transduces CD8$^+$ T cells delivering the CAR transgene. (2) A pool of diversely differentiated CAR T cells is generated: stem cell memory/naïve (SCM/Naïve), central memory (CM), effector memory (EM) and effector CAR T cells. (3) CAR T cells recognize and kill CD19$^+$ B cells, which are completely eliminated from the peritoneal cavity. (4) CAR T cells selectively expand due to the provided antigen stimulus by the CD19$^+$ B cells and (5) emigrate from the peritoneal cavity to other organs, which results in organ-specific distribution of diversely differentiated CAR T cells. At the time point of analysis, (6) predominantly CM and EM CAR T cells are observed in the peritoneal cavity, (7) CM, EM and SCM/Naïve CAR T cells in the spleen and (8) blood. (9) The bone marrow mainly consists of EM and Eff CAR T cells. Anti-tumoral functions are exerted by (10) EM and Eff CAR T cells and (11) HLA-mismatched T cells, which exert more efficient anti-tumoral activity than CAR T cells. (12) The development of an exhausted phenotype in CAR T cells might contribute to the absence of anti-tumoral functions of CAR T cells.

This suggests that the initial transduction event must have generated all kinds of phenotypes. Most likely, the B cells contributed to proliferation of CAR T cells, which subsequently emigrated to other organs. In particular, CAR T cells in the peritoneal cavity were mainly composed of T_{CM} and T_{EM} subtypes at the time point of analysis. These cell types were also found in blood and in spleen, additionally accompanied by few $T_{SCM/Naïve}$. The presence of less differentiated $T_{SCM/Naïve}$ and T_{CM} CAR T cells is favourable since these cells are currently investigated to be of advantage for CAR T cell therapy due to their increased expansion and long-term persistence profile (Wang et al., 2012; Xu et al., 2014). However, for immediate anti-tumoral activities T_{Eff} and T_{EM} CAR T cells are critical. Indeed, these have been detected in higher frequencies in the bone marrow, the region from which strong tumor signals were coming up (Figure 40). However, although these data demonstrated successful migration of CAR T cells to various organs and even

homing of CAR T cells to tumor bearing tissues the presence of T_{Eff} and T_{EM} somehow was not sufficient to prevent tumor outgrowth. Therapy failure can in principle be caused by downregulation of the targeted CD19 antigen, however, antigen loss was excluded (Figure 39).

Several previous studies demonstrated successful tumor cell eradication by CD19 CAR T cells in the very same xenograft model when administering *in vitro* generated CAR T cells (Hudecek et al., 2015; Liu et al., 2016). However, administration of high amounts of CAR T cells immediately conferring anti-tumoral functions is a major difference to the present study. Upon vector administration, the generation of CAR T cells requires some time from transduction event to CAR surface expression. Even though CAR T cell proliferation had been demonstrated (3.3.4), it might well be that CAR T cell numbers were not sufficient to mediate a strong anti-tumoral response. Most likely, the kinetics of CAR T cell generation, expansion and emigration to tumor sites were delayed in the present study contributing to the missing anti-tumoral effects. Several clinical studies demonstrated that the magnitude of CAR T cell expansion is becoming a key predictor for therapeutic success and that the amount of CAR T cells correlates with therapeutic response (Turtle et al., 2016; Roberts et al., 2017). Even clinical studies underlined this aspect correlating therapy failure to a low level of CAR T cells in the blood of the patients within the first two weeks (Maude et al., 2014; Lee et al., 2015). However, total CAR T cell numbers were not determined in the present study, which does not allow comparison to other pre-clinical studies with successful anti-tumoral functions. Further investigations are required to evaluate whether low numbers of CAR T cells contributed to therapy failure.

Nevertheless, complete elimination of CD19$^+$ B cells demonstrated *in vivo* generated CAR T cells to be functional. As explained above, the amount of CAR T cells might have been sufficient to eliminate B cells but not tumor cells. However, some observations suggest that CAR T cells were active at earlier time-points. Higher frequencies of CAR T cells were observed in CD8-LV(CAR)-treated mice sacrificed at early time points compared to CD8-LV(CAR)-treated mice sacrificed for endpoint analysis (Figure 37). Further, higher frequencies of tumor cells were detected in PBS-treated mice than in CD8-LV(CAR)-treated mice when comparing mice, which had been sacrificed at early time points. This might indicate CAR T cell activity at early time points.

A state of unresponsiveness called T cell exhaustion is known to render T cells non-functional over time. Although initially functional, prolonged antigen exposure can trigger T cell exhaustion characterized by poor effector functions (Wherry, 2011). This might explain initial killing activities against B cells, which were present at the initial

location of CAR T cell generation. However, CAR T cell exhaustion at later time points might have contributed to therapy failure. Further, previous studies demonstrated that additionally introduced intracellular signalling domains by CAR expression might favour T cell exhaustion. Clustering of sticky scFvs on the surface of CAR T cells contributes to a permanent signalling activity, so-called tonic signalling, which induces slight and permanent activation of the CAR T cell resulting in early exhaustion and less functional T cells. Although the FMC63-derived scFV, which was used in the present study, was shown to be less prone to exhaustion by scFv clustering (Long et al., 2015), CAR T cell exhaustion cannot be excluded but requires further investigation such as the analysis of exhaustion markers PD-1, TIM-3 and LAG-3.

4.4 Limitations of the PBMC-humanized NSG mouse model for the study of CAR T cell functions

Several factors might have contributed to the therapy failure in CD8-LV(CAR)-treated mice, however, this does not explain tumor shrinkage in control mice. Xenograft models represent models, in which the functions of CAR T cells towards human tumor cells can be studied within an organism. However, the murine-human chimerism comes along with several downsides and limitations (Figure 41). GvHD, caused by the xenogeneic reaction of the engrafted T cells towards the murine host, is one side effect. Transplanted adult T cells exert a comprehensive immune reaction against murine cells, causing the death of transplanted mice within 4-6 weeks independently from tumor growth (Ito et al., 2009; Schroeder and DiPersio, 2011). However, the reaction against foreign antigens is not only restricted to murine antigens but can also be mounted against the engrafted human tumor cells when MHC-type of engrafted PBMC and tumor cells are not matched. In fact, this phenomenon was observed in clinics when allogeneic transplantation of HSC induced a graft-versus-leukemia effect in the recipient (Kolb, 2008). In the present study, allogeneic reactivity of the T cells most likely caused the strong rejection of the tumor cells in control mice. The strong alloreactive effect in control mice impedes evaluating anti-tumoral function of CAR T cells. Why this effect is much more pronounced in control mice having no CAR T cells is unknown. As discussed above, CAR T cells might have exerted less potent anti-tumoral functions compared to allogeneic untransduced T cells due to an exhaustion status characterized by poor effector functions. Higher amounts of untransduced functional allogeneic T cells might have contributed to tumor shrinkage in the control mice. Clearly, this model is limited by xenogeneic and alloreactive reactions. Overlaying alloreactive reactions impede the evaluation of anti-tumoral functions of *in vivo* generated CAR T cells, and xenogeneic reactions limit observation periods to 4-6 weeks

due to the development of GvHD. It will be necessary to test anti-tumoral effects of *in vivo* generated CAR T cell in better suited models.

To overcome these limitations, efforts had been made to generate a murine model, which even better reflects the human immune system. The engraftment of CD34+ hematopoietic stem cells into immune-incompetent mice leads to the development of a human immune system, consisting of innate and adaptive components (Ishikawa et al., 2005) (Figure 42). Here, T cells go through thymic development, not reacting to murine environment, which makes GvHD less likely (Pearson et al., 2008). Further, T cells are in a resting status, more reflecting the clinical situation of unstimulated T cells. First studies already demonstrated successful CAR T cell generation upon intravenous administration of CD8-LV in CD34+ engrafted NSG mice (Pfeiffer et al., submitted). To enhance transduction rates, mice were pre-treated with IL-7, which was administered systemically prior to vector administration. Importantly, B cell elimination correlated with the presence of CAR T cells. The presence of other immune cells in this model allows the observation of interaction between CAR T cells and other components of the adaptive and innate immune system. Indeed, some mice showed signs of CRS with elevated cytokine levels – a side-effect, which is not occurring in PBMC-humanized NSG mice, however, a well-known adverse reaction in patients treated with CAR T cells (Pfeiffer et al., submitted). This underlines even more the potential of CAR T cell studies in CD34+-engrafted NSG mice better reflecting the patients situation than PBMC-humanized NSG mice. Detecting CAR T cells in the blood seven weeks post vector administration rather indicated delayed kinetics of CAR T cell generation. However, further investigations will reveal whether *in vivo* generated CAR T cells confer anti-tumoral functions and also allow further kinetic studies, particularly since this model allows long-term studies due to the low probability of GvHD development. Yet, the successful *in vivo* generation of CAR T cells in this model further underlines the potential of CD8-LV for *in vivo* CAR delivery.

4.5 Clinical potential of CD8-LV for *in vivo* CAR delivery

In vivo generation of CAR T cells using receptor-targeted LVs represent a promising tool to circumvent *ex vivo* manufacturing of CAR T cells. Although nanoparticles might be a further option, lentiviral vectors represent a tool already well known in the clinics. Several years of practice resulted in a documented safety profile of LVs. Risk of insertional oncogenesis and mobilization of replication competent particles have remained theoretical since recent follow-up clinical trials did not indicate such events with the latest generation of vectors (Kaufmann et al., 2013; Naldini et al., 2016).

Although intravenous administration is performed in preclinical models, direct administration of vector particle into lymph nodes appears to be a reasonable application for patients, providing close contact between vector particles and target cells. Major concerns, however, are the risk of off-target transduction and toxicity of the vector upon administration. As the CD8 receptor is expressed on other cell entities, transduction might occur in CD8$^+$CD4$^+$ double positive immature T cells, CD8$^+$ NK cells and CD8$^+$ DCs. Transduction of immature T cells can be hardly seen as a concern. Even if differentiation into a CD4 T cell occurs, transduction of CD4 T cells is current standard in *ex vivo* manufacturing of CAR T cells. Further, CD4 CAR T cells have been shown to be supportive for CAR T cell proliferation increasing anti-tumoral effects. However, if a transduced immature double positive cell differentiates into a regulatory T cell (T$_{reg}$), CAR T cell-directed immune response might be dampened. In contrast, CAR expression in NK cells might be actually beneficial since CAR NK cells also have been shown to be of therapeutic relevance (Glienke et al., 2015). Transduction of DCs, however, might be harmful due to the professional presentation of vector and transgene components, which could trigger an unintended immune response. To address this issue and to prevent antigen presentation, Brown and colleagues demonstrated successful suppression of transgene expression in DCs by incorporating an APC-specific micro RNA (miRNA) target sequence (Brown et al., 2006). Toxicity-induced adverse events triggered by innate and adaptive immune responses upon vector administration are another concern. Stimulation of toll-like receptors and subsequent cytokine secretion, complement activation, and pre-existing neutralizing antibodies might contribute to an immune reaction against the vector particles (Nayak and Herzog, 2010). Neutralizing antibodies would even impair transduction efficiency, which is a downside of MV-pseudotyped LVs, and makes these vectors rather unsuitable for *in vivo* applications due to the broad immunization against MV. This issue, however, is expected to be of a minor concern for CD8-LV. Bender et al. have demonstrated the absence of neutralizing antibodies against NiV-pseudotpyed LVs when NiV-based LVs pre-incubated with pooled human sera still mediated transduction while MV-based LVs did not (Bender et al., 2016). However, toxicity studies and safety concerns need to be addressed prior to clinical studies. Since the OKT8-derived scFV incorporated into CD8-LV is cross-reactive to macaca mulatta, non-human primate studies can be performed without the need for adjustments in the targeting domain.

The current CAR T cell therapy procedure consists of administering high amounts of CAR T cells at a time. In contrast, vector administration is assumed to mediate a slow increase in CAR T cell numbers. Upon transduction, CAR surface expression and CAR T cell proliferation probably requires some time until high numbers of CAR T cells

are expanded. This might avoid CRS, which is currently a matter of concern, induced by high amounts of highly activated CAR T cells. Although it is also possible that kinetics and CRS development occur delayed. However, when side effects become severe, current emergency protocols for CRS treatment are available. Incorporation of off-switches or suicide genes, which control or eliminate CAR T cells, is another tool currently investigated to increase safety (Jones et al., 2014; Wu et al., 2015).

Not only that complex *ex vivo* manufacturing of CAR T cells including logistic and financial hurdles could be circumvented, patients in need would not need to wait until their personalized product is manufactured, but rather get the vector immediately administered. Furthermore, *ex vivo* manipulation might impair functional properties of cells influencing the functionality of the CAR T cell product. Dependent on the culture conditions, it has been shown to drive them into differentiation. However, since preclinical trials suggested less differentiated CAR T cells to mediate superior anti-tumoral activities, efforts are being made to keep cells as undifferentiated as possible by the usage of homeostatic cytokines such as IL-7 and IL-15 (Xu et al., 2014; Sabatino et al., 2016). Although still a long way to go, it will be interesting to investigate whether *in vivo* generated CAR T cells are as good as their *ex vivo* generated counterparts or even outperform them due to the absence of *ex vivo* manipulation, which might influence their functionality.

In conclusion, CD8-LV represents a highly promising tool for the *in vivo* generation of CAR T cells. The potential of tremendously simplifying CAR T cell therapy by circumventing the *ex vivo* manufacturing process represents a highly attractive approach for future CAR T cell therapy enabling broad and flexible applicability to patients.

5   References

Abel, T., El Filali, E., Waern, J., Schneider, I.C., Yuan, Q., Münch, R.C., Hick, M., Warnecke, G., Madrahimov, N., and Kontermann, R.E., et al. (2013). Specific gene delivery to liver sinusoidal and artery endothelial cells. Blood *122*, 2030-2038.

Almeida, L., Lochner, M., Berod, L., and Sparwasser, T. (2016). Metabolic pathways in T cell activation and lineage differentiation. Seminars in immunology *28*, 514-524.

Amirache, F., Levy, C., Costa, C., Mangeot, P.-E., Torbett, B.E., Wang, C.X., Negre, D., Cosset, F.-L., and Verhoeyen, E. (2014). Mystery solved: VSV-G-LVs do not allow efficient gene transfer into unstimulated T cells, B cells, and HSCs because they lack the LDL receptor. Blood *123*, 1422-1424.

Anliker, B., Abel, T., Kneissl, S., Hlavaty, J., Caputi, A., Brynza, J., Schneider, I.C., Münch, R.C., Petznek, H., and Kontermann, R.E., et al. (2010). Specific gene transfer to neurons, endothelial cells and hematopoietic progenitors with lentiviral vectors. Nature methods *7*, 929-935.

Bender, R.R., Muth, A., Schneider, I.C., Friedel, T., Hartmann, J., Plückthun, A., Maisner, A., and Buchholz, C.J. (2016). Receptor-Targeted Nipah Virus Glycoproteins Improve Cell-Type Selective Gene Delivery and Reveal a Preference for Membrane-Proximal Cell Attachment. PLoS pathogens *12*, e1005641.

Berard, M., and Tough, D.F. (2002). Qualitative differences between naive and memory T cells. Immunology *106*, 127-138.

Blömer, U., Naldini, L., Kafri, T., Trono, D., Verma, I.M., and Gage, F.H. (1997). Highly efficient and sustained gene transfer in adult neurons with a lentivirus vector. Journal of virology *71*, 6641-6649.

Boyman, O., Létourneau, S., Krieg, C., and Sprent, J. (2009). Homeostatic proliferation and survival of naïve and memory T cells. European journal of immunology *39*, 2088-2094.

Brentjens, R.J., Rivière, I., Park, J.H., Davila, M.L., Wang, X., Stefanski, J., Taylor, C., Yeh, R., Bartido, S., and Borquez-Ojeda, O., et al. (2011). Safety and persistence of adoptively transferred autologous CD19-targeted T cells in patients with relapsed or chemotherapy refractory B-cell leukemias. Blood *118*, 4817-4828.

Brown, B.D., Venneri, M.A., Zingale, A., Sergi Sergi, L., and Naldini, L. (2006). Endogenous microRNA regulation suppresses transgene expression in hematopoietic lineages and enables stable gene transfer. Nature medicine *12*, 585-591.

Buchholz, C.J., Friedel, T., and Buning, H. (2015). Surface-Engineered Viral Vectors for Selective and Cell Type-Specific Gene Delivery. Trends in biotechnology *33*, 777-790.

Butcher, E.C., Williams, M., Youngman, K., Rott, L., and Briskin, M. (1999). Lymphocyte Trafficking and regional immunity. Adv. Immunol. *72*, 209-253.

Casati, A., Varghaei-Nahvi, A., Feldman, S.A., Assenmacher, M., Rosenberg, S.A., Dudley, M.E., and Scheffold, A. (2013). Clinical-scale selection and viral transduction of human naïve and central memory CD8+ T cells for adoptive cell therapy of cancer patients. Cancer immunology, immunotherapy : CII *62*, 1563-1573.

Chan, A.C., Iwashima, M., Turck, C.W., and Weiss, A. (1992). ZAP-70: A 70 kd Protein-Tyrosine Kinase That Associates with the TCR zeta Chain. Cell *71*, 649-662.

Chaplin, D.D. (2010). Overview of the immune response. The Journal of allergy and clinical immunology *125*, S3–23.

Cieri, N., Camisa, B., Cocchiarella, F., Forcato, M., Oliveira, G., Provasi, E., Bondanza, A., Bordignon, C., Peccatori, J., and Ciceri, F., et al. (2013). IL-7 and IL-15 instruct the generation of human memory stem T cells from naive precursors. Blood *121*, 573-584.

Clement, M., Ladell, K., Ekeruche-Makinde, J., Miles, J.J., Edwards, E.S.J., Dolton, G., Williams, T., Schauenburg, A.J.A., Cole, D.K., and Lauder, S.N., et al. (2011). Anti-CD8 antibodies can trigger CD8+ T cell effector function in the absence of TCR engagement and improve peptide-MHCI tetramer staining. Journal of immunology (Baltimore, Md. : 1950) *187*, 654-663.

Cronin, J., Zhang, X.-Y., and Reiser, J. (2005). Altering the Tropism of Lentiviral Vectors through Pseudotyping. Curr Gene Ther *5*, 387-398.

Dai, H., Wang, Y., Lu, X., and Han, W. (2016). Chimeric Antigen Receptors Modified T-Cells for Cancer Therapy. J Natl Cancer Inst *108*.

Davila, M.L., Riviere, I., Wang, X., Bartido, S., Park, J., Curran, K., Chung, S.S., Stefanski, J., Borquez-Ojeda, O., and Olszewska, M., et al. (2014). Efficacy and toxicity management of 19-28z CAR T cell therapy in B cell acute lymphoblastic leukemia. Science translational medicine *6*, 224ra25.

Davis, M.M., and Bjorkman, P.J. (1988). T-cell antigen receptor genes and T-cell recognition. Nature *334*, 395-402.

Demaison, C., Parsley, K., Brouns, G., Scherr, M., Battmer, K., Kinnon, C., Grez, M., and Thrasher, A.J. (2002). High-level transduction and gene expression in hematopoietic repopulating cells using a human immunodeficiency correction of imunodeficiency virus type 1-based lentiviral vector containing an internal spleen focus forming virus promoter. Human gene therapy *13*, 803-813.

Dudley, M.E., Gross, C.A., Langhan, M.M., Garcia, M.R., Sherry, R.M., Yang, J.C., Phan, G.Q., Kammula, U.S., Hughes, M.S., and Citrin, D.E., et al. (2010). CD8+ enriched "young" tumor infiltrating lymphocytes can mediate regression of metastatic melanoma. Clinical cancer research : an official journal of the American Association for Cancer Research *16*, 6122-6131.

Dudley, M.E., Wunderlich, J.R., Robbins, P.F., Yang, J.C., and Hwu, P. (2002). Cancer Regression and Autoimmunity in Patients After Clonal Repopulation with Antitumor Lymphocytes. Science (New York, N.Y.) *298*, 850-854.

Dudley, M.E., Wunderlich, J.R., Yang, J.C., Sherry, R.M., Topalian, S.L., Restifo, N.P., Royal, R.E., Kammula, U., White, D.E., and Mavroukakis, S.A., et al. (2005). Adoptive cell transfer therapy following non-myeloablative but lymphodepleting chemotherapy for the treatment of patients with refractory metastatic melanoma. Journal of clinical oncology : official journal of the American Society of Clinical Oncology *23*, 2346-2357.

Dull, T., Zufferey, R., Kelly, M., Mandel, R.J., Nguyen, M., Trono, D., and Naldini, L. (1998). A third-generation lentivirus vector with a conditional packaging system. Journal of virology *72*, 8463-8471.

Eshhar, Z., Waks, T., Bendavid, A., and Schindler, D.G. (2001). Functional expression of chimeric receptor genes in human T cells. Journal of Immunological Methods *248*, 67-76.

Eyquem, J., Mansilla-Soto, J., Giavridis, T., van der Stegen, S.J.C., Hamieh, M., Cunanan, K.M., Odak, A., Gönen, M., and Sadelain, M. (2017). Targeting a CAR to the TRAC locus with CRISPR/Cas9 enhances tumour rejection. Nature *543*, 113-117.

Farber, D.L., Yudanin, N.A., and Restifo, N.P. (2014). Human memory T cells. Generation, compartmentalization and homeostasis. Nature reviews. Immunology *14*, 24-35.

Farkona, S., Diamandis, E.P., and Blasutig, I.M. (2016). Cancer immunotherapy. The beginning of the end of cancer? BMC medicine *14*, 73.

Finkelshtein, D., Werman, A., Novick, D., Barak, S., and Rubinstein, M. (2013). LDL receptor and its family members serve as the cellular receptors for vesicular stomatitis virus. Proc. Natl. Acad. Sci. U.S.A. *110*, 7306-7311.

Finney, H.M., Akbar, A.N., and Lawson, A.D.G. (2004). Activation of Resting Human Primary T Cells with Chimeric Receptors. Costimulation from CD28, Inducible Costimulator, CD134, and CD137 in Series with Signals from the TCR Chain. The Journal of Immunology *172*, 104-113.

Frecha, C., Costa, C., Nègre, D., Gauthier, E., Russell, S.J., Cosset, F.-L., and Verhoeyen, E. (2008). Stable transduction of quiescent T cells without induction of cycle progression by a novel lentiviral vector pseudotyped with measles virus glycoproteins. Blood *112*, 4843-4852.

Funke, S., Maisner, A., Mühlebach, M.D., Koehl, U., Grez, M., Cattaneo, R., Cichutek, K., and Buchholz, C.J. (2008). Targeted cell entry of lentiviral vectors. Mol. Ther. *16*, 1427-1436.

Garrido, F., Aptsiauri, N., Doorduijn, E.M., Garcia Lora, A.M., and van Hall, T. (2016). The urgent need to recover MHC class I in cancers for effective immunotherapy. Current opinion in immunology *39*, 44-51.

Gattinoni, L., Klebanoff, C.A., and Restifo, N.P. (2012). Paths to stemness. Building the ultimate antitumour T cell. Nature reviews. Cancer *12*, 671-684.

Gattinoni, L., Lugli, E., Ji, Y., Pos, Z., Paulos, C.M., Quigley, M.F., Almeida, J.R., Gostick, E., Yu, Z., and Carpenito, C., et al. (2011). A human memory T cell subset with stem cell-like properties. Nature medicine *17*, 1290-1297.

Gee, A.P. (2015). Manufacturing genetically modified T cells for clinical trials. Cancer gene therapy *22*, 67-71.

Girard-Gagnepain, A., Amirache, F., Costa, C., Levy, C., Frecha, C., Fusil, F., Negre, D., Lavillette, D., Cosset, F.-L., and Verhoeyen, E. (2014). Baboon envelope pseudotyped LVs outperform VSV-G-LVs for gene transfer into early-cytokine-stimulated and resting HSCs. Blood *124*, 1221-1231.

Glienke, W., Esser, R., Priesner, C., Suerth, J.D., Schambach, A., Wels, W.S., Grez, M., Kloess, S., Arseniev, L., and Koehl, U. (2015). Advantages and applications of CAR-expressing natural killer cells. Frontiers in pharmacology *6*, 21.

Golubovskaya, V., and Wu, L. (2016). Different Subsets of T Cells, Memory, Effector Functions, and CAR-T Immunotherapy. Cancers *8*, 36.

Gross, G., Waks, T., and Eshhar, Z. (1989). Expression of immunoglobulin-T-cell receptor chimeric molecules as functional receptors with antibody-type specificity. Proc. Natl. Acad. Sci. U.S.A. *86*, 10024-10028.

Grupp, S.A., Kalos, M., Barrett, D., Aplenc, R., Porter, D.L., Rheingold, S.R., Teachey, D.T., Chew, A., Hauck, B., and Wright, J.F., et al. (2013). Chimeric antigen receptor-modified T cells for acute lymphoid leukemia. The New England journal of medicine *368*, 1509-1518.

Hammarlund, E., Lewis, M.W., Hansen, S.G., Strelow, L.I., Nelson, J.A., Sexton, G.J., Hanifin, J.M., and Slifka, M.K. (2003). Duration of antiviral immunity after smallpox vaccination. Nature medicine *9*, 1131-1137.

Hammill, J.A., VanSeggelen, H., Helsen, C.W., Denisova, G.F., Evelegh, C., Tantalo, D.G.M., Bassett, J.D., and Bramson, J.L. (2015). Designed ankyrin repeat proteins are

effective targeting elements for chimeric antigen receptors. Journal for immunotherapy of cancer *3*, 55.

Haring, J.S., Badovinac, V.P., and Harty, J.T. (2006). Inflaming the CD8+ T cell response. Immunity *25*, 19-29.

Hartmann, J., Schüßler-Lenz, M., Bondanza, A., and Buchholz, C.J. (2017). Clinical development of CAR T cells-challenges and opportunities in translating innovative treatment concepts. EMBO molecular medicine *9*, 1183-1197.

Hinrichs, C.S., and Rosenberg, S.A. (2014). Exploiting the curative potential of adoptive T-cell therapy for cancer. Immunological reviews *257*, 56-71.

Hombach, A., Hombach, A.A., and Abken, H. (2010). Adoptive immunotherapy with genetically engineered T cells. Modification of the IgG1 Fc 'spacer' domain in the extracellular moiety of chimeric antigen receptors avoids 'off-target' activation and unintended initiation of an innate immune response. Gene Ther *17*, 1206-1213.

Hombach, A.A., Schildgen, V., Heuser, C., Finnern, R., Gilham, D.E., and Abken, H. (2007). T Cell Activation by Antibody-Like Immunoreceptors. The Position of the Binding Epitope within the Target Molecule Determines the Efficiency of Activation of Redirected T Cells. The Journal of Immunology *178*, 4650-4657.

Hudecek, M., Sommermeyer, D., Kosasih, P.L., Silva-Benedict, A., Liu, L., Rader, C., Jensen, M.C., and Riddell, S.R. (2015). The nonsignaling extracellular spacer domain of chimeric antigen receptors is decisive for in vivo antitumor activity. Cancer immunology research *3*, 125-135.

Hughes, M.S., Yu, Y.Y.L., Dudley, M.E., Zheng, Z., Robbins, P.F., Li, Y., Wunderlich, J., Hawley, R.G., Moayeri, M., and Rosenberg, S.A., et al. (2005). Transfer of a TCR Gene Derived from a Patient with a Marked Antitumor Response Conveys Highly Activated T-Cell Effector Functions. Human gene therapy *16*, 457-472.

Imai, C., Mihara, K., Andreansky, M., Nicholson, I.C., Pui, C.-H., Geiger, T.L., and Campana, D. (2004). Chimeric receptors with 4-1BB signaling capacity provoke potent cytotoxicity against acute lymphoblastic leukemia. Leukemia *18*, 676-684.

Irving, B.A., and Weiss, A. (1991). The cytoplasmatic domain of the T cell receptor zeta chain is sufficient to couple to receptor-assocaited signal transduction pathways. Cell *64*, 891-901.

Ishikawa, F., Yasukawa, M., Lyons, B., Yoshida, S., Miyamoto, T., Yoshimoto, G., Watanabe, T., Akashi, K., Shultz, L.D., and Harada, M. (2005). Development of functional human blood and immune systems in NOD/SCID/IL2 receptor {gamma} chain(null) mice. Blood *106*, 1565-1573.

Ito, R., Katano, I., Kawai, K., Hirata, H., Ogura, T., Kamisako, T., Eto, T., and Ito, M. (2009). Highly sensitive model for xenogenic GVHD using severe immunodeficient NOG mice. Transplantation *87*, 1654-1658.

Iwashima, M., Irving, B.A., van Oers, Nicolai S C, Chan, A.C., and Weiss, A. (1994). Sequential Interactions of the TCR with Two Distinct Cytoplasmic Tyrosine Kinases. Science (New York, N.Y.) *263*, 1136-1139.

Jensen, M.C., Popplewell, L., Cooper, L.J., DiGiusto, D., Kalos, M., Ostberg, J.R., and Forman, S.J. (2010). Antitransgene rejection responses contribute to attenuated persistence of adoptively transferred CD20/CD19-specific chimeric antigen receptor redirected T cells in humans. Biology of blood and marrow transplantation : journal of the American Society for Blood and Marrow Transplantation *16*, 1245-1256.

Jones, B.S., Lamb, L.S., Goldman, F., and Di Stasi, A. (2014). Improving the safety of cell therapy products by suicide gene transfer. Frontiers in pharmacology *5*, 254.

Jonnalagadda, M., Mardiros, A., Urak, R., Wang, X., Hoffman, L.J., Bernanke, A., Chang, W.-C., Bretzlaff, W., Starr, R., and Priceman, S., et al. (2015). Chimeric antigen receptors with mutated IgG4 Fc spacer avoid fc receptor binding and improve T cell persistence and antitumor efficacy. Molecular therapy : the journal of the American Society of Gene Therapy *23*, 757-768.

June, C.H., O'Connor, R.S., Kawalekar, O.U., Ghassemi, S., and Milone, M.C. (2018). CAR T cell immunotherapy for human cancer. Science (New York, N.Y.) *359*, 1361-1365.

Kaech, S.M., Wherry, E.J., and Ahmed, R. (2002). Effector and memory T-cell differentiation. Implications for vaccine development. Nature reviews. Immunology *2*, 251-262.

Kafri, T., Blömer, U., Peterson, D.A., Gage, F.H., and Verma, I.M. (1997). Sustained expression of genes delivered directly into liver and muscle by lentiviral vectors. Nature genetics *17*, 314-317.

Kahlon, K.S., Brown, C., Cooper, L.J.N., Raubitschek, A., Forman, S.J., and Jensen, M.C. (2004). Specific Recognition and Killing of Glioblastoma Multiforme by Interleukin 13-Zetakine Redirected Cytolytic T cells. Canccer Research *64*, 9160-9166.

Kaiser, A.D., Assenmacher, M., Schröder, B., Meyer, M., Orentas, R., Bethke, U., and Dropulic, B. (2015). Towards a commercial process for the manufacture of genetically modified T cells for therapy. Cancer gene therapy *22*, 72-78.

Kalos, M., Levine, B.L., Porter, D.L., Katz, S., Grupp, S.A., Bagg, A., and June, C.H. (2011). T cells with chimeric antigen receptors have potent antitumor effects and can establish memory in patients with advanced leukemia. Sci Transl Med *3*, 95ra73.

Katayama, C.D., Eidelman, F.J., Duncan, A., Hooshmand, F., and Hedrick, S.M. (1995). Predicted complementarity determining regions of the T cell antigen receptor determine antigen specificity. The EMBO Journal *14*, 927-938.

Kaufmann, K.B., Büning, H., Galy, A., Schambach, A., and Grez, M. (2013). Gene therapy on the move. EMBO molecular medicine *5*, 1642-1661.

King, M., Pearson, T., Shultz, L.D., Leif, J., Bottino, R., Trucco, M., Atkinson, M.A., Wasserfall, C., Herold, K.C., and Woodland, R.T., et al. (2008). A new Hu-PBL model for the study of human islet alloreactivity based on NOD-scid mice bearing a targeted mutation in the IL-2 receptor gamma chain gene. Clin. Immunol. *126*, 303-314.

King, M.A., Covassin, L., Brehm, M.A., Racki, W., Pearson, T., Leif, J., Laning, J., Fodor, W., Foreman, O., and Burzenski, L., et al. (2009). Human peripheral blood leucocyte non-obese diabetic-severe combined immunodeficiency interleukin-2 receptor gamma chain gene mouse model of xenogeneic graft-versus-host-like disease and the role of host major histocompatibility complex. Clinical and experimental immunology *157*, 104-118.

Klebanoff, C.A., Finkelstein, S.E., Surman, D.R., Lichtman, M.K., Gattinoni, L., Theoret, M.R., Grewai, N., Spiess, P.J., Antony, P.A., and Palmer, D.C., et al. (2004). IL-15 enhances the in vivo antitumor activity of tumor-reactive CD8+ T Cells. Proc. Biol. Sci. *101*, 1969-1974.

Kneissl, S., Zhou, Q., Schwenkert, M., Cosset, F.-L., Verhoeyen, E., and Buchholz, C.J. (2013). CD19 and CD20 targeted vectors induce minimal activation of resting B lymphocytes. PloS one *8*, e79047.

Knipe, D.M. and Howley, P.M. (2007). Fields' Virology. 5th ed. (Philadelphia, PA: Lippincott Williams & Wilkins).

Kobinger, G.P., Weiner, D.J., Yu, Q.C., and Wilson, J.M. (2001). Filovirus-pseudotyped lentiviral vector can efficiently and stably transduce airway epithelia in vivo. Nat Biotechnol *19*, 225-230.

Kochenderfer, J.N., Dudley, M.E., Feldman, S.A., Wilson, W.H., Spaner, D.E., Maric, I., Stetler-Stevenson, M., Phan, G.Q., Hughes, M.S., and Sherry, R.M., et al. (2012). B-cell depletion and remissions of malignancy along with cytokine-associated toxicity in a clinical trial of anti-CD19 chimeric-antigen-receptor-transduced T cells. Blood *119*, 2709-2720.

Kochenderfer, J.N., Dudley, M.E., Kassim, S.H., Somerville, R.P.T., Carpenter, R.O., Stetler-Stevenson, M., Yang, J.C., Phan, G.Q., Hughes, M.S., and Sherry, R.M., et al. (2015). Chemotherapy-refractory diffuse large B-cell lymphoma and indolent B-cell malignancies can be effectively treated with autologous T cells expressing an anti-CD19 chimeric antigen receptor. Journal of clinical oncology : official journal of the American Society of Clinical Oncology *33*, 540-549.

Kolb, H.-J. (2008). Graft-versus-leukemia effects of transplantation and donor lymphocytes. Blood *112*, 4371-4383.

Kowolik, C.M., Topp, M.S., Gonzalez, S., Pfeiffer, T., Olivares, S., Gonzalez, N., Smith, D.D., Forman, S.J., Jensen, M.C., and Cooper, Laurence J N (2006). CD28 costimulation provided through a CD19-specific chimeric antigen receptor enhances in vivo persistence and antitumor efficacy of adoptively transferred T cells. Cancer research *66*, 10995-11004.

Kuwana, Y., Asakura, Y., Utsunomiya, N., Nakanishi, M., Arata, Y., Itoh, S., Nagase, F., and Kurosawa, Y. (1987). Expression of chimeric receptor composed of immunoglobulin-derived V resions and T-cell receptor-derived C regions. Biochemical and biophysical research communications *149*, 960-968.

Lau, L.L., Jamieson, B.D., Somaasundaram, T., and Ahmed, R. (1994). Cytotoxic T-cell memory without antigen. Nature *369*, 648-652.

Lee, D.W., Gardner, R., Porter, D.L., Louis, C.U., Ahmed, N., Jensen, M., Grupp, S.A., and Mackall, C.L. (2014). Current concepts in the diagnosis and management of cytokine release syndrome. Blood *124*, 188-195.

Lee, D.W., Kochenderfer, J.N., Stetler-Stevenson, M., Cui, Y.K., Delbrook, C., Feldman, S.A., Fry, T.J., Orentas, R., Sabatino, M., and Shah, N.N., et al. (2015). T cells expressing CD19 chimeric antigen receptors for acute lymphoblastic leukaemia in children and young adults. A phase 1 dose-escalation trial. The Lancet *385*, 517-528.

Lei, Y., Joo, K.-I., and Wang, P. (2009). Engineering fusogenic molecules to achieve targeted transduction of enveloped lentiviral vectors. Journal of biological engineering *3*, 3-8.

Letourneur, F., and Klausner, R.D. (1991). T-cell and basophil activaiton through the cytoplasmic tail of T-cell-receptor zeta family proteins. Immunology *88*, 8905-8909.

Levine, B.L., Miskin, J., Wonnacott, K., and Keir, C. (2017). Global Manufacturing of CAR T Cell Therapy. Molecular therapy. Methods & clinical development *4*, 92-101.

Liu, L., Sommermeyer, D., Cabanov, A., Kosasih, P., Hill, T., and Riddell, S.R. (2016). Inclusion of Strep-tag II in design of antigen receptors for T-cell immunotherapy. Nat Biotechnol *34*, 430-434.

Long, A.H., Haso, W.M., Shern, J.F., Wanhainen, K.M., Murgai, M., Ingaramo, M., Smith, J.P., Walker, A.J., Kohler, M.E., and Venkateshwara, V.R., et al. (2015). 4-1BB costimulation ameliorates T cell exhaustion induced by tonic signaling of chimeric antigen receptors. Nature medicine *21*, 581-590.

Lugli, E., Dominguez, M.H., Gattinoni, L., Chattopadhyay, P.K., Bolton, D.L., Song, K., Klatt, N.R., Brenchley, J.M., Vaccari, M., and Gostick, E., et al. (2013). Superior T memory stem cell persistence supports long-lived T cell memory. The Journal of clinical investigation *123*, 594-599.

Maude, S.L., Frey, N., Shaw, P.A., Aplenc, R., Barrett, D.M., Bunin, N.J., Chew, A., Gonzalez, V.E., Zheng, Z., and Lacey, S.F., et al. (2014). Chimeric antigen receptor T cells for sustained remissions in leukemia. The New England journal of medicine *371*, 1507-1517.

Merten, C.A., Stitz, J., Braun, G., Poeschla, E.M., Cichutek, K., and Buchholz, C.J. (2005). Directed evolution of retrovirus envelope protein cytoplasmic tails guided by functional incorporation into lentivirus particles. Journal of virology *79*, 834-840.

Meuer, S.C., Fitzgerald, K.A., Hussey, R.E., Hodgon James C, Schlossman, S.F., and Reinherz, E.L. (1983). Clonotypic structures involved in antigen-soecific human T cell function. J Exp Med *157*, 705-719.

Milone, M.C., Fish, J.D., Carpenito, C., Carroll, R.G., Binder, G.K., Teachey, D., Samanta, M., Lakhal, M., Gloss, B., and Danet-Desnoyers, G., et al. (2009). Chimeric receptors containing CD137 signal transduction domains mediate enhanced survival of T cells and increased antileukemic efficacy in vivo. Mol. Ther. *17*, 1453-1464.

Minguet, S., Swamy, M., Alarcón, B., Luescher, I.F., and Schamel, W.W.A. (2007). Full activation of the T cell receptor requires both clustering and conformational changes at CD3. Immunity *26*, 43-54.

Mitomo, K., Griesenbach, U., Inoue, M., Somerton, L., Meng, C., Akiba, E., Tabata, T., Ueda, Y., Frankel, G.M., and Farley, R., et al. (2010). Toward gene therapy for cystic fibrosis using a lentivirus pseudotyped with Sendai virus envelopes. Mol. Ther. *18*, 1173-1182.

Miyoshi, H., Blömer, U., Takahashi, M., Gage, F.H., and Verma, I.M. (1998). Development of a self-inactivating lentivirus vector. Journal of virology *72*, 8150-8157.

Miyoshi, H., Takahashi, M., Gage, F.H., and Verma, I.M. (1997). Stable and efficient gene transfer into the retina using an HIV-based lentiviral vector. Proceedings of the National Academy of Sciences *94*, 10319-10323.

Mora, J.R., and Andrian, U.H. von (2006). T-cell homing specificity and plasticity: new concepts and future challenges. Trends in immunology *27*, 235-243.

Morgan, R.A., Dudley, M.E., Wunderlich, J.R., Hughes, M.S., Yang, J.C., Sherry, R.M., Royal, R.E., Topalian, S.L., Kammula, U.S., and Restifo, N.P., et al. (2006). Cancer Regression in Patients after Transfer of Genetically Engineered Lymphocytes. Science (New York, N.Y.) *314*, 126-129.

Morgan, R.A., Yang, J.C., Kitano, M., Dudley, M.E., Laurencot, C.M., and Rosenberg, S.A. (2010). Case report of a serious adverse event following the administration of T cells transduced with a chimeric antigen receptor recognizing ERBB2. Molecular therapy : the journal of the American Society of Gene Therapy *18*, 843-851.

Moritz, D., and Groner, B. (1995). A spacer region between the single chain antibody- and the CD3 zeta-chain domain of chimeric T cell receptor components is required for efficient ligand binding and signaling actvity. Gene Ther *2*, 539-546.

Murphy, K., Travers, P. and Walport, Mark and Janeway, Charles (2012). Janeway's Immunobiology. Principles of innate and adaptive immunity (New York: Garland Science).

Naldini, L., Blömer, U., Gallay, P., Ory, D., Mulligan, R., Gage, F.H., Verma, I.M., and Trono, D. (1996). In vivo gene delivery and stable transduction of nondividing cells by a lentiviral vector. Science (New York, N.Y.) *272*, 263-267.

Naldini, L., Trono, D., and Verma, I.M. (2016). Lentiviral vectors, two decades later. Science (New York, N.Y.) *353*, 1101-1102.

Nayak, S., and Herzog, R.W. (2010). Progress and prospects. Immune responses to viral vectors. Gene Ther *17*, 295-304.

Nicholson, I.C., Lenton, K.A., Little, D.J., Decorso, T., Lee, F.T., Scott, A.M., Zola, H., and Hohmann, A.W. (1997). Construction and characterisation of a functional CD19 specific single chain Fv fragment for immunotherapy of B lineage leukaemia and lymphoma. Mol. Immunol. *34*, 1157-1165.

Oelsner, S., Friede, M.E., Zhang, C., Wagner, J., Badura, S., Bader, P., Ullrich, E., Ottmann, O.G., Klingemann, H., and Tonn, T., et al. (2017). Continuously expanding CAR NK-92 cells display selective cytotoxicity against B-cell leukemia and lymphoma. Cytotherapy *19*, 235-249.

Oiseth, S.J., and Aziz, M.S. (2017). Cancer immunotherapy. A brief review of the history, possibilities, and challenges ahead. JCMT *3*, 250.

Pearson, T., Greiner, D.L., and Shultz, L.D. (2008). Creation of "humanized" mice to study human immunity. Current protocols in immunology / edited by John E. Coligan … [et al.] *Chapter 15*, 15.

Pfeiffer, A., Thalheimer, F.B., Hartmann, S., Bender, R.R., Danish, S., Costa, C., Wels, W.S., Modlich, U., Stripecke, R., and Verhoeyen, E., et al. (submitted). In vivo generation of human CD19-CAR T cells results in B cell depletion and signs of cytokine release syndrome. EMBO molecular medicine.

Plückthun, A. (2015). Designed ankyrin repeat proteins (DARPins). Binding proteins for research, diagnostics, and therapy. Annual review of pharmacology and toxicology *55*, 489-511.

Pluta, K., and Kacprzak, M.M. (2009). Use of HIV as a gene transfer vector. Acta Biochimica Polonica *56*, 531-595.

Podack, E.R., and Kupfer, A. (1991). T-cell effector functions. Mechanisms for delivery of cytotoxicity and help. Annual review of cell biology *7*, 479-504.

Porter, D.L., Levine, B.L., Kalos, M., Bagg, A., and June, C.H. (2011). Chimeric antigen receptor-modified T cells in chronic lymphoid leukemia. The New England journal of medicine *365*, 725-733.

Presotto, D., Erdes, E., Duong, M.N., Allard, M., Regamey, P.-O., Quadroni, M., Doucey, M.-A., Rufer, N., and Hebeisen, M. (2017). Fine-Tuning of Optimal TCR Signaling in Tumor-Redirected CD8 T Cells by Distinct TCR Affinity-Mediated Mechanisms. Frontiers in immunology *8*, 1564.

Pulè, M.A., Straathof, K.C., Dotti, G., Heslop, H.E., Rooney, C.M., and Brenner, M.K. (2005). A chimeric T cell antigen receptor that augments cytokine release and supports clonal expansion of primary human T cells. Molecular Therapy *12*, 933-941.

Reinherz, E.L. (2014). Revisiting the Discovery of the αβ TCR Complex and Its Co-Receptors. Frontiers in immunology *5*, 583.

Robbins, P.F., Morgan, R.A., Feldman, S.A., Yang, J.C., Sherry, R.M., Dudley, M.E., Wunderlich, J.R., Nahvi, A.V., Helman, L.J., and Mackall, C.L., et al. (2011). Tumor regression in patients with metastatic synovial cell sarcoma and melanoma using genetically engineered lymphocytes reactive with NY-ESO-1. Journal of clinical oncology : official journal of the American Society of Clinical Oncology *29*, 917-924.

Roberts, Z.J., Better, M., Bot, A., Roberts, M.R., and Ribas, A. (2017). Axicabtagene ciloleucel, a first-in-class CAR T cell therapy for aggressive NHL. Leukemia & lymphoma *23*, 1-12.

Rosenberg, S.A., Restifo, N.P., Yang, J.C., Morgan, R.A., and Dudley, M.E. (2008). Adoptive cell transfer. A clinical path to effective cancer immunotherapy. Nature reviews. Cancer *8*, 299-308.

Sabatino, M., Hu, J., Sommariva, M., Gautam, S., Fellowes, V., Hocker, J.D., Dougherty, S., Qin, H., Klebanoff, C.A., and Fry, T.J., et al. (2016). Generation of clinical-grade CD19-specific CAR-modified CD8+ memory stem cells for the treatment of human B-cell malignancies. Blood *128*, 519-528.

Sallusto, F., Geginat, J., and Lanzavecchia, A. (2004). Central memory and effector memory T cell subsets. Function, generation, and maintenance. Annual review of immunology *22*, 745-763.

Savignac, M., Mellström, B., and Naranjo, J.R. (2007). Calcium-dependent transcription of cytokine genes in T lymphocytes. Pflugers Archiv : European journal of physiology *454*, 523-533.

Schluns, K.S., Kieper, W.C., Jameson, S.C., and Lefrançois, L. (2000). Interleukin-7 mediates the homeostasis of naïve and memory CD8 T cells in vivo. Nature immunology *1*, 426-432.

Schmidt, M., Hoffmann, G., Wissler, M., Lemke, N., Müssig, A., Glimm, H., Williams, D.A., Ragg, S., Hesemann, C.U., and Kalle, C. von (2001). Detection and direct genomic sequencing of multiple rare unknown flanking DNA in highly complex samples. Human gene therapy *12*, 743-749.

Schroeder, M.A., and DiPersio, J.F. (2011). Mouse models of graft-versus-host disease. Advances and limitations. Disease models & mechanisms *4*, 318-333.

Serfling, E., Berberich-Siebelt, F., Chuvpilo, S., Jankevics, E., Klein-Hessling, S., Twardzik, T., and Avots, A. (2000). The role of NF-AT transcription factors in T cell activation and differentiation. Biochimica et Biophysica Acta *1498*, 1-18.

Siegler, E., Li, S., Kim, Y.J., and and Wang, P. (2017). Designed Ankyrin Repeat Proteins as Her2 Targeting Domains in Chimeric Antigen Receptor-Engineered T Cells. Human gene therapy *28*, 726-736.

Siegler, E.L., and Wang, P. (2018). Preclinical models in chimeric antigen receptor-engineered T cell therapy. Human gene therapy *29*, 534-546.

Smith, T.T., Stephan, S.B., Moffett, H.F., McKnight, L.E., Ji, W., Reiman, D., Bonagofski, E., Wohlfahrt, M.E., Pillai, S.P.S., and Stephan, M.T. (2017). In situ programming of leukaemia-specific T cells using synthetic DNA nanocarriers. Nature nanotechnology *12*, 813-820.

Smith-Garvin, J.E., Koretzky, G.A., and Jordan, M.S. (2009). T cell activation. Annual review of immunology *27*, 591-619.

Sommermeyer, D., Hudecek, M., Kosasih, P.L., Gogishvili, T., Maloney, D.G., Turtle, C.J., and Riddell, S.R. (2015). Chimeric antigen receptor-modified T cells derived from defined CD8(+) and CD4(+) subsets confer superior antitumor reactivity in vivo. Leukemia *30*, 492-500.

Stumpp, M.T., and Amstutz, P. (2007). DARPins: a true alterniative to antibodies. curr opin drug discov Devel. *10*, 153-159.

Till, B.G., Jensen, M.C., Wang, J., Qian, X., Gopal, A.K., Maloney, D.G., Lindgren, C.G., Lin, Y., Pagel, J.M., and Budde, L.E., et al. (2012). CD20-specific adoptive

immunotherapy for lymphoma using a chimeric antigen receptor with both CD28 and 4-1BB domains. Pilot clinical trial results. Blood *119*, 3940-3950.

Turtle, C.J., Hanafi, L.-A., Berger, C., Gooley, T.A., Cherian, S., Hudecek, M., Sommermeyer, D., Melville, K., Pender, B., and Budiarto, T.M., et al. (2016). CD19 CAR-T cells of defined CD4+:CD8+ composition in adult B cell ALL patients. The Journal of clinical investigation *126*, 2123-2138.

van den Broek, T., Borghans, J.A.M., and van Wijk, F. (2018). The full spectrum of human naive T cells. Nature reviews. Immunology *18*, 363-373.

van Rijn, R.S., Simonetti, E.R., Hagenbeek, A., Hogenes, M.C.H., Weger, R.A. de, Canninga-van Dijk, M.R., Weijer, K., Spits, H., Storm, G., and van Bloois, L., et al. (2003). A new xenograft model for graft-versus-host disease by intravenous transfer of human peripheral blood mononuclear cells in RAG2-/- gammac-/- double-mutant mice. Blood *102*, 2522-2531.

van Stipdonk, M.J., Lemmens, E.E., and Schoenberger, S.P. (2001). Naïve CTLs require a single brief period of antigenic stimulation for clonal expansion and differentiation. Nature immunology *2*, 423-429.

Verhoeyen, E., Dardalhon, V., Ducrey-Rundquist, O., Trono, D., Taylor, N., and Cosset, F.-L. (2003). IL-7 surface-engineered lentiviral vectors promote survival and efficient gene transfer in resting primary T lymphocytes. Blood *101*, 2167-2174.

Wang, J.-h., and Reinherz, E.L. (2012). The structural basis of αβ T-lineage immune recognition. TCR docking topologies, mechanotransduction, and co-receptor function. Immunological reviews *250*, 102-119.

Wang, X., Naranjo, A., Brown, C.E., Bautista, C., Wong, C.W., Chang, W.-C., Aguilar, B., Ostberg, J.R., Riddell, S.R., and Forman, S.J., et al. (2012). Phenotypic and functional attributes of lentivirus-modified CD19-specific human CD8+ central memory T cells manufactured at clinical scale. Journal of immunotherapy (Hagerstown, Md. : 1997) *35*, 689-701.

Wang, X., and Rivière, I. (2015). Manufacture of tumor- and virus-specific T lymphocytes for adoptive cell therapies. Cancer gene therapy *22*, 85-94.

Wang, X., and Rivière, I. (2016). Clinical manufacturing of CAR T cells. Foundation of a promising therapy. Molecular therapy oncolytics *3*, 16015.

Weiss, A., and Stobo, J.D. (1984). Requirement for the coexpression of T3 and the T cell antigen receptor on a malignant human T cell line. J Exp Med *160*, 1284-1299.

Wu, C.-Y., Roybal, K.T., Puchner, E.M., Onuffer, J., and Lim, W.A. (2015). Remote control of therapeutic T cells through a small molecule-gated chimeric receptor. Science (New York, N.Y.) *350*, aab4077.

Xu, Y., Zhang, M., Ramos, C.A., Durett, A., Liu, E., Dakhova, O., Liu, H., Creighton, C.J., Gee, A.P., and Heslop, H.E., et al. (2014). Closely related T-memory stem cells correlate with in vivo expansion of CAR.CD19-T cells and are preserved by IL-7 and IL-15. Blood *123*, 3750-3759.

Yee, C. (2013). Adoptive T-cell therapy for cancer. Boutique therapy or treatment modality? Clinical cancer research : an official journal of the American Association for Cancer Research *19*, 4550-4552.

Zhao, Y., Wang, Q.J., Yang, S., Kochenderfer, J.N., Zheng, Z., Zhong, X., Sadelain, M., Eshhar, Z., Rosenberg, S.A., and Morgan, R.A. (2009). A herceptin-based chimeric antigen receptor with modified signaling domains leads to enhanced survival of transduced T lymphocytes and antitumor activity. Journal of immunology (Baltimore, Md. : 1950) *183*, 5563-5574.

Zhou, Q., Schneider, I.C., Edes, I., Honegger, A., Bach, P., Schönfeld, K., Schambach, A., Wels, W.S., Kneissl, S., and Uckert, W., et al. (2012). T-cell receptor gene transfer exclusively to human CD8(+) cells enhances tumor cell killing. Blood *120*, 4334-4342.

Zhou, Q., Uhlig, K.M., Muth, A., Kimpel, J., Lévy, C., Münch, R.C., Seifried, J., Pfeiffer, A., Trkola, A., and Coulibaly, C., et al. (2015). Exclusive Transduction of Human CD4+ T Cells upon Systemic Delivery of CD4-Targeted Lentiviral Vectors. J. Immunol. *195*, 2493-2501.

Zufferey, R., Nagy, D., Mandel, R.J., and Naldini, Luigi and Trono, Didier (1997). Multiply attenuated lentiviral vector achieves efficient gene delivery in vivo. Nat Biotechnol *15*, 871-875.

6 Abbreviations

Δ	delta
°C	degree celcius
µg	microgram
µl	microliter
µm	micrometer
µM	micromolar
ALL	acute lymphoblastic leukemia
APC	antigen presenting cell
ASCO	american society of clinical oncology
BaEV	baboon endogenous virus
BFP	blue fluorescent protein
bp	base pairs
CAR	chimeric antigen receptor
CCR7	C-C chemokine receptor 7
CD	cluster of differentiation
CD8-LV	CD8-targeted lentiviral vector
CFSE	carboxyfluorescein succinimidyl ester
CLL	chronic lymphocytic leukemia
CRS	cytokine release syndrome
DARPins	designed ankyrin repeat proteins
DC	dendritic cell
DLBL	diffuse large B-cell lymphoma
DMEM	dulbecco's modified eagle medium
DMSO	dimethyl sulfoxide
DNA	deoxyribonucleic acid
dNTP	deoxyribonucleoside triphosphate
E.coli	Escherichia coli
e.g.	exempli gratia, for example
EDTA	ethylenediaminetetraacetic acid
EF1α	elongation factor 1 alpha
et al.	and others
F	fusion protein
FCS	fetal calf serum
FDA	food and drug administration
FoxP3	forkhead box P3

g ....gravity force
G ....glycoprotein
ɣ ....gamma
gag ....group-specific antigen
gDNA...genomic DNA
GFP ....green fluorescent protein
GMP .... good manufacturing practice
GvHD...graft-versus-host disease
Gy..gray
h ....hour
H ....hemagglutinin
HEK-293T..human embryonic kidney 293T
HEPES ....4-(2-hydroxyethyl)-1-piperazineethanesulfonic acid
HIV-1 .... human immunodeficiency virus-1
HLA ....human leukocyte antigen
HSC..hematopoietic stem cell
i.v..intravenously
IFN-ɣ .... interferon gamma
Ig ....Immunoglobulin
IL-2 ....interleukin-2
IRES ....internal ribosomal entry site
ITAM...immunoreceptor tyrosine-based activation motif
IVC ....individually ventilated cage
kb...kilobase
LB ....lysogeny broth
LDL.. low density lipoprotein
LED .... light-emitting diode
LM-PCR... ligation-mediated PCR
LTR..long terminal repeat
luc..luciferase
LV .... lentiviral vector
MFI .... mean fluorescence intensity
MHC ....major histocompatibility complex
min.. minutes
miRNA ....micro RNA
ml..mililiter
mM ....milimolar

MOI.. multiplicity of infection

MV .... measles virus

ng .... nanogram

NiV... Nipah virus

NK cell .... natural killer cell

ns.. not significant

NSG... NOD.Cg.PrkdcscidIL2rgtmWjl/SzJ

p/sec/cm²/sr .... photons/seconds/square centimeter/steradian

PBMC .... peripheral blood mononuclear cells

PBS .... phosphate-buffered saline

PCR... polymerase chain reaction

PE.. phycoerythrin

PEI.. polyethylenimine

pol.. DNA-polymerase

qPCR.. quantitative real-time PCR

r/r .... relapsed/refractory

rpm .... rounds per minute

RT... room temperature

s .... seconds

scFv.. single chain variable fragment

SD .... standard deviation

SEM... standard error of the mean

SFFV .... spleen focus forming virus

SIN-LV... self-inactivating lentiviral vector

t.u./ml... transducing units per ml

T_{CM}.. central memory T cell

TCR .... T cell receptor

T_{Eff} .... effector T cell

T_{EM}.. effector memory T cell

TIL .... tumor infiltrating lymphocyte

TM .... transmembrane domain

T_N .... naïve T cell

TNF-α .... tumor necrosis factor alpha

T_{reg}... regulatory T cell

T_{SCM} .... stem cell-like memory T cell

U .... units

U.S. .... united states

V .... *volt*

VCN .... *vector copy number*

VSV .... *vesicular stomatitis virus*

w/o .... *without*

w/v .... *weight per volume*

WPRE .... *woodchuck hepatitis virus posttranscriptional regulatory element*

α .... *alpha or anti*

7   List of Publications

Publications

In vivo generation of human CD19-CAR T cells results in B cell depletion and signs of cytokine release syndrome

Pfeiffer A*, Thalheimer F*, Hartmann S, Bender RR, Danish S, Costa C, Wels WS, Modlich U, Stripecke R, Verhoeyen E, Buchholz CJ

EMBO Mol Med, in revision, 2018 June

* shared first authorship

CD30-targeted oncolytic viruses as novel therapeutic approach against classical Hodgkin lymphoma

Hanauer JDS, Rengstl B, Kleinlützum D, Reul J, **Pfeiffer A**, Friedel T, Schneider IC, Newrzela S, Hansmann ML, Buchholz CJ, Muik A

Oncotarget, 2018 Jan, *9*, 12971-12981

Exclusive transduction of human CD4+ T cells upon systematic delivery of CD4-targeted lentiviral vectors

Zhou Q, Uhlig KM, Muth A, Kimpel J, Lévy C, Münch RC, Seifried J, **Pfeiffer A,** Trkola A, Coulibaly C, von Laer D, Wels WS, Hartwig UF, Verhoeyen E, Buchholz CJ

J Immunol, 2015 Sep, *195*, 2493-501

Oral presentations at conferences

Towards *in vivo* delivery of chimeric antigen receptors

Anett Pfeiffer, Ruben R. Bender, Qi Zhou, Winfried S. Wels and Christian J. Buchholz

7th UCT Science Day, 2016 Oct

Towards *in vivo* delivery of chimeric antigen receptors

Anett Pfeiffer, Ruben R. Bender, Qi Zhou, Winfried S. Wels and Christian J. Buchholz

22nd Annual Meeting of the German Society for Gene Therapy, 2016 Sep

Towards *in vivo* delivery of chimeric antigen receptors

Anett Pfeiffer, Ruben R. Bender, Qi Zhou, Winfried S. Wels and Christian J. Buchholz

14th Annual Cancer Immunotherapy (CIMT) Meeting, 2016 May

Receptor-targeted viral vectors for immunotherapy

Anett Pfeiffer, Ruben R. Bender, Katharina Uhlig, Winfried S. Wels, Christian J. Buchholz and Qi Zhou

Summer School of the LOEWE CGT, 2015 Oct

Poster presentations at conferences

In vivo generation of CAR T cells mediated by a CD8-targeted lentiviral vector

Anett Pfeiffer, F. Thalheimer, Ruben R. Bender, Winfried S. Wels and Christian J. Buchholz

Annual PEI Retreat, 2018 Jan

In vivo generation of antigen-reactive T cells for immunotherapy

Anett Pfeiffer, Inan Edes, Irene C. Schneider, Qi Zhou, Ruben R. Bender, Veit R. Buchholz, Winfried S. Wels, Dirk H. Busch, Wolfgang Uckert, Christian J. Buchholz

25th Annual Meeting of the European Society for Gene and Cell Therapy, 2017 Oct

In vivo generation of CAR T cells mediated by a CD8-targeted lentiviral vector

Anett Pfeiffer, F. Thalheimer, Ruben R. Bender, Winfried Wels and Christian J. Buchholz

3rd CRI-CIMT-EATI-AACR International Cancer Immunotherapy Conference, 2017 Sep

Towards *in vivo* delivery of chimeric antigen receptors

Anett Pfeiffer, Ruben R. Bender, Qi Zhou, Winfried Wels and Christian J. Buchholz

Annual PEI Retreat, 2017 Jan

Towards *in vivo* delivery of chimeric antigen receptors

Anett Pfeiffer, Ruben R. Bender, Qi Zhou, Winfried Wels and Christian J. Buchholz

14th Annual Cancer Immunotherapy (CIMT) Meeting, 2016 May

Receptor-targeted viral vectors for immunotherapy

Anett Pfeiffer, Qi Zhou, Ruben R. Bender, Katharina Uhlig, Winfried Wels, Christian J. Buchholz

Annual PEI Retreat, 2016 Feb

8 Curriculum Vitae

Persönliche Information

Name:	Anett Pfeiffer
Geburtsdatum:	17.04.1989
Geburtsort:	Görlitz

Wissenschaftlicher Werdegang

06/2018	Abgabe der Doktorarbeit am Fachbereich Biologie der Technischen Universität Darmstadt Title: CD8 Receptor-Targeted Lentiviral Vectors – an Approach for the *in vivo* Generation of Chimeric Antigen Receptor (CAR) T Cells
05/2014 - 02/2018	Promotionsstudentin in der Arbeitsgruppe "Molekulare Biotechnologie und Gentherapie" am Paul-Ehrlich-Institut in Langen
10/2011 - 12/2013	Master of Science in Molecular Life Science an der Universität zu Lübeck
10/2008 - 10/2011	Bachelor of Science in Molecular Life Science an der Universität zu Lübeck
10/2001 - 08/2008	Allgemeine Hochschulreife am Einstein-Gymnasium in Neuenhagen

9 Danksagung

Mein besonderer Dank gilt Herrn Prof. Dr. Christian Buchholz, für die Möglichkeit meine Doktorarbeit in seiner Arbeitsgruppe durchführen zu können und für die Vergabe dieses spannenden und interessanten Themas. Seine Betreuung, viele nützliche Ratschläge und die stete Diskussionsbereitschaft haben maßgeblich zur Entstehung dieser Arbeit beigetragen.

Für die freundliche und unkomplizierte Betreuung seitens der TU Darmstadt möchte ich mich bei Frau Prof. Dr. Süß bedanken und bei Herrn Prof. Dr. Löwer, der die Aufgabe des Zweitgutachters übernimmt.

Bei Frau Prof. Dr. Dr. Ute Modlich und Franziska Schenk möchte ich mich herzlich für die Zusammenarbeit rund um das Thema lentivirale Integration bedanken. Die zahlreichen Tipps und Diskussionen waren sehr hilfreich für mich.

Ein großes Dankeschön geht an alle Mitglieder der Arbeitsgruppe Molekulare Biotechnologie und Gentherapie. Vielen Dank Ruben, Patricia, Johanna, Julia H., Annika, Laura, Tatjana, Frederic, Jessi, Janina, Dina, Alex, Anke, Sarah, Robert, Irene, Thorsten, Qi, Tobi, Julia B., Ruth und Gundi. Die tolle Arbeitsatmosphäre, ständige Hilfsbereitschaft und unzähligen Diskussionen waren eine riesige Unterstützung. Die Zeit im Labor und auch außerhalb hat mir sehr viel Freude gemacht.

Bei meiner Familie und meinen Freunden möchte ich mich für ihre Unterstützung und ihr Verständnis bedanken, das sie mir während dieser Zeit entgegengebracht haben.
Ganz besonders bedanken möchte ich mich bei meinen Eltern für ihre uneingeschränkte und bedingungslose Unterstützung zu jeder Zeit. Ohne euch wäre diese Arbeit nicht möglich gewesen.

Christoph, ich bin dir unglaublich dankbar, dass du mich während dieser Zeit so verständnisvoll unterstützt hast. Ich bin sehr glücklich, dass du an meiner Seite bist!

10 Ehrenwörtliche Erklärung

Ich erkläre hiermit ehrenwörtlich, dass ich die vorliegende Arbeit entsprechend den Regeln guter wissenschaftlicher Praxis selbstständig und ohne unzulässige Hilfe Dritter angefertigt habe.

Sämtliche aus fremden Quellen direkt oder indirekt übernommenen Gedanken sowie sämtliche von Anderen direkt oder indirekt übernommenen Daten, Techniken und Materialien sind als solche kenntlich gemacht. Die Arbeit wurde bisher bei keiner anderen Hochschule zu Prüfungszwecken eingereicht.

Frankfurt am Main, den

…………………………………………………..

Anett Pfeiffer